Glued-In Rods for Timber Structures - Development of a Calculation Model

Gustafsson, Per-Johan; Serrano, Erik

2001

Document Version:
Publisher's PDF, also known as Version of record

LUND UNIVERSITY

GLUED-IN RODS FOR TIMBER STRUCTURES
Development of a Calculation Model

PER JOHAN GUSTAFSSON and ERIK SERRANO

Structural Mechanics

Structural Mechanics

ISRN LUTVDG/TVSM--01/3056--SE (1-96)
ISSN 0281-6679

GLUED-IN RODS FOR TIMBER STRUCTURES - Development of a Calculation Model

PER JOHAN GUSTAFSSON
and ERIK SERRANO

Printed by KFS i Lund AB, Lund, Sweden, December 2002.

For information, address:
Division of Structural Mechanics, LTH, Lund University, Box 118, SE-221 00 Lund, Sweden.
Homepage: http://www.byggmek.lth.se

Acknowledgements

This report is the final report for Work Package 1 “Development of a Calculation Model” of the research project, “GIROD-Glued-in Rods for Timber Structures”, which has been running since 1998. The project has been a co-operation between several institutes in Sweden, Germany and the UK, and has been financially supported by the European Commission (DG XII) through grant no. (SMT4–CT97–2199). For the work carried out by project partner Lund University, financial support has been obtained also from the Swedish Council for Building Research through grants no 960635-5 and 960633-4. Apart from Structural Mechanics at Lund University, the participating institutes have been: the Swedish National Testing and Research Institute (SP), also responsible for the coordination of the project, the Otto-Graf Institute at the University of Stuttgart, Germany, the University of Karlsruhe, Germany and TRADA Technology, UK. The financial support and the kind co-operation of all the involved partners are gratefully acknowledged.

Lund, May 2001

Per Johan Gustafsson Erik Serrano

Summary

This report relates to GIROD WP1 – "Development of a calculation model". WP1 consists of four sub-WPs: 1.1 "Theoretical work", 1.2 "Bond line tests", 1.3 "Tests for calibration" and 1.4 "Calibration of model".

In WP1.1 theoretical models for rational prediction of pull out strength have been developed. The models include a very simple ideal plastic model, a linear elastic fracture mechanics model, a bar shear lag fracture model, a Timoshenko beam shear lag fracture model and a 3D non-linear finite element fracture model. Several simulations have been made by the finite element model in order to investigate the effect of various geometry and material parameters on the pull out strength. The theoretical formats developed in WP1.1 has been further studied and evaluated in WP1.4 by means of test results.

In WP1.2, the bond line properties for three different adhesives, a fibre reinforced phenol-resorcinol, PRF, a 2-component polyurethane, PUR, and an epoxy, EPX, have been determined by tests of small specimens in pure shear. Specimens with a very small bond area were tested in order to ensure as uniform stress as possible. The load versus deformation response of the bond line is recorded. An initially chosen test set-up was used for a large amount (approximately 30) of pre-tests. The mean strength of the adhesives was lower than expected (less than 6 MPa) and the test response was often unstable for the PUR and EPX. The PRF adhesive failed due to crushing of the threads in the adhesive, while the PUR and EPX adhesives failed in the wood/adhesive interface region with a large amount of wood fibres left on the adhesive. Due to the unstable response, these results were not suitable for evaluation, and a second test set-up was designed. A few (12) pre-test with the PRF-adhesive were performed with this second test set-up, producing useful results. Using a slightly modified version of the second test set-up, the main test series was performed with a total of 61 successful tests. The mean *strength* was found to be 7.1 MPa for the PRF, 10.5 MPa for the PUR and 13.1 MPa for the EPX adhesive at 0º load to grain angle. The *density of the wood* was measured and it was found that it had no significant influence on the strength for the PUR adhesive. A small effect was found for the EPX and PRF bonded specimens. The mean *work to failure* was found to be 11.8, 9.6 and 22.0 kJ/m^2 for the PRF, PUR and EPX adhesives respectively. A method for evaluation of the *effective fracture* energy from the tests has been proposed. The method is based on evaluating the initial slope of the descending stress–displacement curve, rather than the conventional calculation of the area below the curve. This initial, negative, slope of the descending part of the stress-displacement curve, which can be used as a measure of the brittleness of the bondline, was evaluated for the three adhesives. It was found that the EPX and the PUR were the more brittle ones and that the PRF was more ductile. The *load to grain angle* was found to have a major influence on both the strength and the ductility. At 0º the average shear strength was 13.1 MPa and the alternate load to grain angles resulted in shear strengths of 12.8, 10.7 and 7.1 MPa for 22.5º, 45º and 90º respectively. The more ductile behaviour of the cross grain specimens is explained in part by a propagating (in the circumferential direction) failure mode.

In WP1.3 a large number of full-scale short term ramp load tests of glued-in rods have been made. Three glues have been tested (PRF, PUR and EPX), various joint geometries (rod length, rod diameter, wood cross section dimensions and angle between rod and grain direction of the wood) and densities of the wood. The specimens were conditioned at 65% relative humidity before testing. Each test series comprised 7 nominally equal tests. The failure mode observed in these tests was pull out of the rod, i.e. not splitting of the wood. The testing work is finished. A more detailed presentation of the test results than given in this report is compiled by project partner FMPA.

In WP1.4 strength design methods for the basic short term constant climate pull-out strength of glued-in rods are proposed. A basic proposal discussed in greater detail has been used in WP8. For

adhesives that don't shrink significantly and have some bond to the rod (epoxy and PUR) a design equation that is simple and based on rational mechanics has been developed. For other adhesives empirical strength design by tests is proposed. The basic design equation has been verified by short time ramp load test results obtained within WP1.3 and WP7. In WP1.4 there are moreover FE-results, showing the non-linear fracture mechanics prediction of the performance of full scale joints tested in WP1.3, as obtained using basic material property data from WP 1.2. The FE-results also comprise verification analysis of the small specimen test method.

Table of Contents

1 ACRONYMS, ABBREVIATIONS AND SYMBOLS

COV	coefficient of variation
EP,EPX	epoxy
FRP	glass fibre reinforced polyester
PR,PRF	fibre reinforced phenol-resorcinol adhesive
PU,PUR	polyurethane
RH	relative humidity
Θ	beam cross section inclination
ϕ	rod diameter
γ	engineering shear strain
δ	displacement (slip) across bondline
ε	normal strain
λ	slenderness ratio of rod, l/d
ν	Poisson's ratio
σ	normal stress, peel stress
τ	shear stress
φ	mixed mode angle
ω	stiffness ratio of joint
A	cross sectional area
C	constant
E	Young's modulus
G	shear modulus
G_f	fracture energy
I	area moment of inertia
M	bending moment
N	normal force
P	external force
Q	distributed load (body force)
S	stiffness ratio of joint
T	stiffness ratio of joint
V	shear force
b	width
d	rod diameter
e	eccentricity
e	base of natural logarithm, 2.71828…
k	root to characteristic equation
l	length
m	distributed bending moment, exponent
n	exponent
p	exponent
r	radius
t	bondline thickness
u	axial displacement
v	radial displacement
x	axial coordinate
y	radial coordinate

2 INTRODUCTION

2.1 Present state of the project

2.1.1 Work content

The objective of WP1 is to establish a calculation model for the basic pull-out strength, that can be used as a basis for establishing design rules for glued-in rods in Eurocode 5, and for creating a better understanding of the mechanical behaviour of glued in rods.

WP1 is organised in four parts: WP1.1, WP1.2, WP1.3 and WP1.4. In the below, the work content of the four parts is described.

WP1.1 is theoretical work. An analytical equation for the strength of glued-in rods derived from Volkersen's theory and fracture mechanics will be used as the starting point for the work. The model includes the factors that are estimated to be the most important for the load capacity of glued-in rods loaded in tension: length and diameter of the rod, the shear strength and the fracture energy of the bond line, and the stiffness of the two adherent materials. The model is, however, one-dimensional, assuming pure shear in the bond-line and only axial deformation in the adherents. Therefore modifications and extension may be required. Finite element analysis will be carried out using a non-linear mixed mode fracture mechanics model of bond-lines. By FE-analysis several parameters studies for the influence on load bearing capacity of type of loading, geometry and material properties will be carried out

In WP1.2, bond line properties will be determined by tests of small specimens in pure shear. Specimens with a very small bond area are tested in order to ensure as uniform stress as possible. The local load versus deformation response of the bond line is recorded. A criterion for such a test to be successful is that is has to be stable i.e. it is required that the complete descending branch of the stress-displacement curve can be recorded. From this recording, strength and fracture energy can be evaluated.

WP1.3 is full scale testing of glued-in rods. The object of the testing is to enable verification and calibration of the model. According to a preliminary testing plan 22 types of glued in rods shall be tested, the testing of each type including 7 nominally equal tests.

WP1.4 is calibration and verification of the theoretical models. The analytical model and the FE-model from WP1.1 will be verified by means of the test results obtained in WP1.2 and WP1.3. As a part of this work, FE-analysis of the test specimen of WP1.2 and the glued–in rods tested in WP1.3 will also be made.

2.1.2 Current status

The study of glued-in rods in project SMT4-CT97-2199 has been completed.

2.2 Time schedule – deviations from work plan

There was no significant deviation between the work plan for WP1 and the work carried out.

3 RESULTS OF THE WORK CARRIED OUT – WP1.1

3.1 Introduction

WP1.1 comprises theoretical work for the development of the format of a rational strength calculation model. This work has, in accordance with the planed work, comprised analytical work and numerical calculations. The analytical work is to large extent based on concepts of fracture mechanics and developments of the so-called Volkersen theory for stress analysis of lap joints. The numerical calculations were made by the finite element method, using a 3D geometry model and a mixed mode material model for non-linear gradual fracture of the bond surface. By the numerical calculations the sensitivity in load capacity to various geometry and material parameters were studied.

3.2 Overview of strength calculation models

First, two main groups of strength calculation models can be identified: empirical models and rational models. In empirical models some arbitrary equation with one or more free parameters is assumed. The numerical values of the parameters are then determined by fit to experimental strength test data.

The discussion here will focus on rational, theoretical models. In such models a strength equation or calculation algorithm is developed by means of fundamentals such equilibrium, geometrical compatibility of deformations and some mathematical description of the performance of the materials. The free parameters may be identified as parameters that define geometry, loading conditions and material properties. The numerical values of the material parameters may be obtained by separate and independent material property tests or by fitting of theoretical strength equation to experimental strength test data.

In Table 1 an overview of the models dealt with here is given. In the table the simplest models are indicated first. Models 1 and 2 are both special cases of model 3. Model 3 and thereby also models 1 and 2 are special cases of model 4. In the below, first model 3 will be derived and then models 1 and 2 identified by assuming a very ductile adhesive performance and a very brittle adhesive performance, respectively. Models 3 and 4 are then discussed.

Table 1. Over-view of models dealt with.

Nr	Name	Geometry	Confinement to displacement field	Properties of bond layer
1	Ideal plastic model	Bar (the rod) in cylinder (the wood)	Rod and wood modelled as bars and adhesive as a shear lag layer.	Ductile, ideal plastic shear layer. Parameter: local strength, τ_f [e.g. in MPa]
2	Linear elastic fracture mechanics	Bar (the rod) in cylinder (the wood)	Rod and wood modelled as bars and adhesive as a shear lag layer	Brittle, shear layer with negligible deformation. Parameter: fracture energy, G_f [e.g. in J/m^2]
3	Bar shear lag fracture model	Bar (the rod) in cylinder (the wood)	Rod and wood modelled as bars and adhesive as a shear lag layer	Linear elastic shear layer with local strength defined by τ_f and local deformation capacity defined from the fracture energy, G_f.
4	Shear beam shear lag fracture model	Bar (the rod) in cylinder (the wood)	Rod modelled as a bar, wood as a beam, taking into account shear deformation and zero bending, and adhesive as a shear lag layer	Linear elastic shear layer with local strength defined by τ_f and local deformation capacity defined from the fracture energy, G_f
5	FEM non-linear fracture model	Arbitrary 3D: bar (the rod) in box (the wood)	Strains in the adhesive layer taken as the mean strains across the thickness of the layer	Non-linear performance with shear and normal stress both determined from the shear and normal deformations

3.3 Bar shear lag fracture model

3.3.1 Introduction and notations

This model may be regarded as a combination of the so-called Volkersen model and fracture mechanics [5]. The model is here dealt with for application to axi-symmetric geometry and to general cases of loading, including distributed loading along the joint and to loading that reflects the effect of strains due to variation in temperature or moisture content. The rod and the wood are assumed to perform as bars, indicated by 1 and 2, respectively, and the bond layer as a shear lag layer indicated by 3. The elastic stiffnesses are denoted E_1, E_2 and G_3. The size of the cross section of part 1 is A_1 and of part 2 A_2. The size of the bond area is $2\pi rl$. Other symbols are defined in Figure 1. Q indicates distributed external load acting on the wood adherent. The dimension of Q is force per volume, the load is acting in the x-direction and may in a general case vary with x. N indicates cross section normal force.

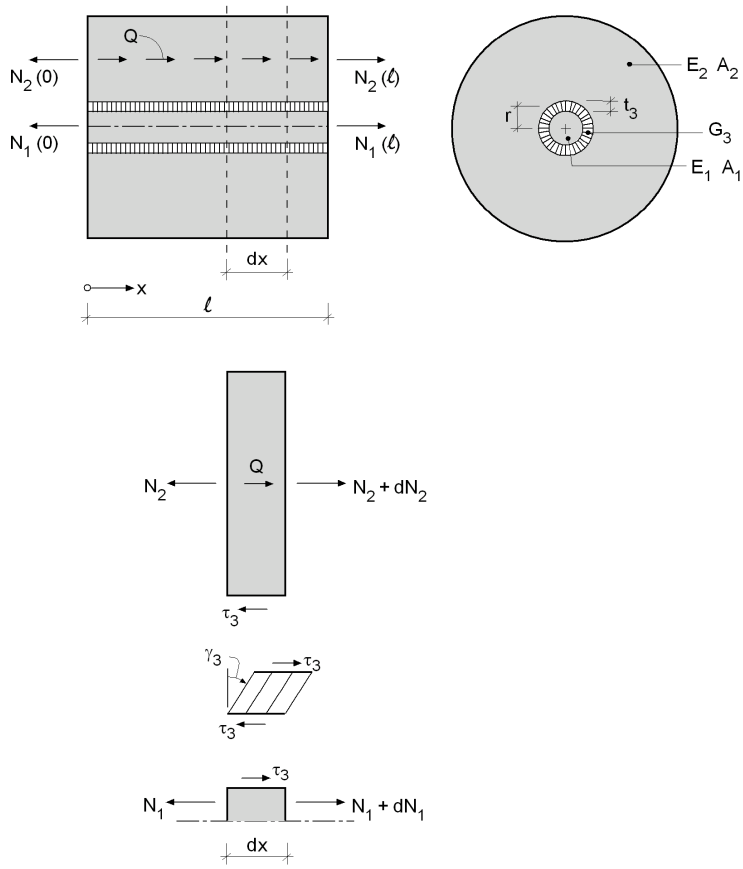

Figure 1. Geometry and notations used in bar shear lag analysis.

3.3.2 Governing differential equation and general solution

Equilibrium of lengths dx of part 1 and 2 gives

$$dN_1+2\pi r dx\tau_3 = 0 \tag{1}$$

$$dN_2-2\pi r dx\tau_3 - QA_2 dx = 0 \tag{2}$$

Compatibility of deformations gives

$$u_2-u_1=t_3\gamma_3 \tag{3}$$

where u indicates displacement and γ shear strain. Since normal strain is defined by $\varepsilon_i=du_i/dx$, eq (3) entails

$$\varepsilon_2 - \varepsilon_1=t_3\gamma'_3 \tag{4}$$

Relations between strain and stress are given by the elastic parameters

$$\gamma_{3=}\tau_3/G_3 \quad (5)$$

$$\varepsilon_1=\sigma_1/E_1=N_1/(E_1A_1) \quad (6)$$

$$\varepsilon_2=\sigma_2/E_2=N_2/(E_2A_2) \quad (7)$$

Differentiating eq (5), and then substituting eq (5), (6) and (7) into eq (4) give

$$N_2/(E_2A_2) - N_1/(E_1A_1) = t_3\tau'_3/G_3 \quad (8)$$

Differentiating this equation and with $N_i'=dN_i/dx$ from the equations of equilibrium, (1) and (2), a differential equation which governs the shear stress distribution along the rod, $\tau_3(x)$, is obtained:

$$\tau_3'' - \omega^2\tau_3 = -QG_3/(t_3E_2) \quad (10)$$

where

$$\omega^2 = (G_3/t_3)\ (2\pi r)\ (1/(E_2A_2) + 1/(E_1A_1)) \quad (11)$$

The general solution of eq (10) is

$$\tau_3 = C_1\cosh(\omega x) + C_2\sinh(\omega x) + \tau_{3p} \quad (12)$$

For constant distributed load $Q(x)=Q_0$ a particular solution is

$$\tau_{3p}(x) = Q_0\ G_3/(t_3E_2\omega^2) \quad (13)$$

For the common case Q(x)=0 the particular solution is $\tau_{3p}(x)=0$.

3.3.3 Determination of constants from boundary conditions

To determine the constants C_1 and C_2 knowledge about $N_1(0)$, $N_2(0)$, $N_1(l)$ and $N_2(l)$ shall be utilised. Differentiation of eq (12) and then substitution of τ'_3 into eq (8) yields

$$N_2/(E_2A_2) - N_1/(E_1A_1) = (t_3/G_3)\ \omega\ (C_1\sinh(\omega x) + C_2\cosh(\omega x)) \quad (14)$$

provided that Q(x) is constant. Eq (14) is valid for all x, and in particular for x=0 and x=l are found:

$$N_2(0)/(E_2A_2) - N_1(0)/(E_1A_1) = (t_3/G_3)\ \omega\ (0 + C_2) \quad (15)$$

$$N_2(l)/(E_2A_2) - N_1(l)/(E_1A_1) = (t_3/G_3)\ \omega\ (C_1\sinh(\omega l) + C_2\cosh(\omega l)) \quad (16)$$

3.3.4 Shear stress distribution equations for five loading conditions

From eq (15) and (16) constants C_1 and C_2 can be determined for arbitrary boundary conditions. Here the constants shall be given for five basic load cases. These cases may then be superposed into many other cases.

The first case, 1, "pull-pull" relates to the conditions $N_1(0)=N_2(l)=P$, $N_2(0)=N_1(l)=0$ and $Q_0=0$. For these conditions are found constants C_1 and C_2 which substituted into eq (12) give

$$\tau_3 = P\, G_3/(t_3 \omega\, E_1A_1)\, \{[\cosh(\omega l) + E_1A_1/(E_2A_2)]\, \cosh(\omega x)/\sinh(\omega l) - \sinh(\omega x)\} \quad (17)$$

The second case, 2, "pull-compression" relates to the conditions $N_1(0)=-N_2(0)=P$, $N_2(l)=N_1(l)=0$ and $Q_0=0$. For these conditions are found constants C_1 and C_2 which substituted into eq (12) give

$$\tau_3 = P\, G_3/(t_3 \omega\, E_1A_1)\, [1 + E_1A_1/(E_2A_2)]\, [\cosh(\omega x)/\tanh(\omega l) - \sinh(\omega x)] \quad (18)$$

The third case, 3, "pull of rod" relates to the conditions $N_1(0)=N_1(l)=P$, $N_2(0)=N_2(l)=0$ and $Q_0=0$. For these conditions are found constants C_1 and C_2 which substituted into eq (12) give

$$\tau_3 = P\, G_3/(t_3 \omega\, E_1A_1)\, [\cosh(\omega x)\, (\cosh(\omega l)-1)/\sinh(\omega l) + \sinh(\omega x)] \quad (19)$$

This third case may be used for analyses of the shear stress along the bond line in the case of internal straining of the rod, e.g. due to increased temperature in the rod. Denoting the free strain of the rod by ε_0, eq (19) gives the shear stress distribution by

$$P = \varepsilon_0 E_1A_1 \quad (20)$$

The fourth case, 4, "pull of wood" refers to $N_2(0)=N_2(l)=P$, $N_1(0)=N_1(l)=0$ and $Q_0=0$. For these conditions are found constants C_1 and C_2 which substituted into eq (12) give

$$\tau_3 = -\, P\, G_3/(t_3 \omega\, E_1A_1)\, (E_1A_1/E_2A_2)\, [\cosh(\omega x)\, (\cosh(\omega l)-1)/\sinh(\omega l) - \sinh(\omega x)] \quad (21)$$

This forth case may be used for analyses of the shear stress along the bond line in the case of internal straining of the wood, e.g. due to increased moisture content. Denoting the free strain in wood by ε_0, eq (21) gives the shear stress distribution by

$$P = \varepsilon_0 E_2A_2 \quad (22)$$

The fifth case, 5, is denoted "pull-distributed". It refers to uniform volume loading of the wood in the x-direction of magnitude $Q_0=P/(A_2l)$ and a counteracting pull of the rod, P, at x=0. In this case $N_1(0)=P$, $N_1(l)=N_2(0)=N_2(l)=0$ and $Q_0=\text{constant}=P/(A_2l)$. Solving eq(15) and (16) for C_1 and C_2, and then substitution into eq (11) with the particular solution from eq (12) gives

$$\tau_3 = P\, G_3/(t_3 \omega\, E_1A_1)\, [\cosh(\omega x)\, \cosh(\omega l)/\sinh(\omega l) - \sinh(\omega x) + E_1A_1/(E_2A_2 \omega l)\,] \quad (23)$$

The fifth loading case is primarily intended for use, in combination with other loading, when analysing rods glued perpendicular into a beam.

In Figure 2 the shear stress distributions corresponding to the five loads are shown for one example of parameter values: P=10000 N, E_1=200000 N/mm^2, E_2=10000 N/mm^2, G_3=100 N/mm^2, r=8 mm, A_1=200 mm^2, A_2=10000 mm^2, t_3=0.5 mm and l=160 mm.

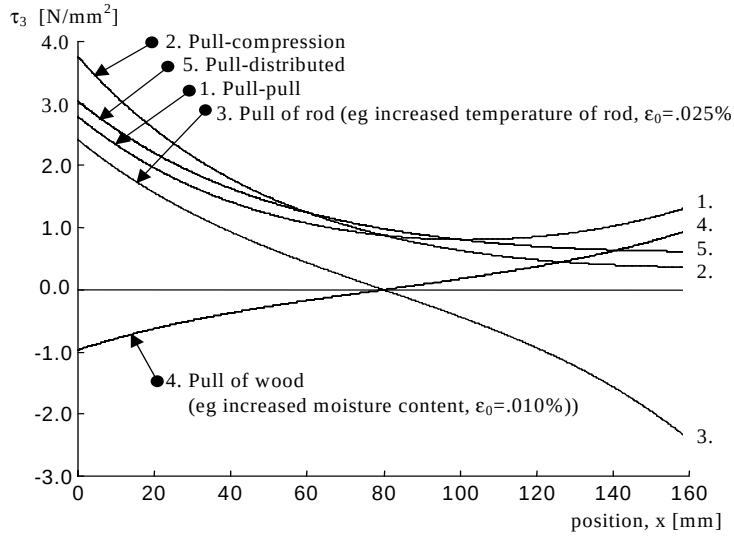

Figure 2. Shear stress distribution along rod for different loading

3.3.5 Interpretation of shear layer stiffness before strength analysis

Before glued in rod strength analysis the shear layer stiffness, G_3/t_3, shall be interpreted in terms of the fracture energy and the strength of the layer. Since the layer is linear elastic, the fracture energy G_f, i.e. the work needed for separation of unit area, is

$$G_f = (1/2)\,\tau_f\,\delta_f = (1/2)\,\tau_f\,\tau_f/\,(G_3/t_3) \qquad (24)$$

Where τ_f is the local shear strength of the bond layer and δ_f the corresponding shear slip. The shear strength and the fracture energy of the layer shall be regarded as the basic bond parameters for the analysis of the pull out load carrying capacity of the glued in rods. In terms of these parameters the shear stiffness is, as determined by eq (24),

$$(G_3/t_3) = \tau_f^2/(2G_f) \qquad (25)$$

This shear stiffness, which is relevant for strength analysis, is commonly much less than the elastic stiffness of the adhesive layer, the ratio as a typical example being in the order of 1/100.

Substituting eq (25) into eq (11), the parameter ω^2 can be written as

$$\omega^2 = (\pi r\tau_f^2/G_f)\,(1/(E_2A_2) + 1/(E_1A_1)) \qquad (26)$$

3.3.6 Equations for the pull out strength

The criterion of failure may be defined as

$$\tau_{max} = \tau_f \tag{27}$$

where τ_{max} is the largest absolute value of the shear stress, τ_3. Although the criterion is formulated as a stress criterion, it is not a stress criterion in a conventional sense since τ_3 and thereby τ_{max} are effected by the material strength parameters τ_f and G_f through the relation of eq (25).

For load case 1, "pull-pull", $\tau_{max} = \tau(0)$ if $(E_2A_2)/(E_1A_1) > 1$, which probably is the case in almost all cases of practical interest. With $\tau_{max} = \tau(0)$ eq (17) together with eq (25) and (27) gives

$$P_f/(2\pi rl\,\tau_f) = (G_f\omega E_1A_1)/(\tau_f^2\pi rl)\,[\,\sinh(\omega l)/(\cosh(\omega l)+(E_1A_1)/(E_2A_2))\,] \tag{28}$$

where P_f is the predicted pull out load capacity of the glued in rod. $P_f/(2\pi rl\,\tau_f)$ is the ratio between the nominal shear stress at failure, $P_f/(2\pi rl)$, and the bond strength, τ_f.

For load case 2, "pull-compression", $\tau_{max} = \tau(0)$. With $\tau_{max} = \tau(0)$ eq (18) together with eq (25) and (27) gives

$$P_f/(2\pi rl\,\tau_f) = (G_f\omega E_1A_1)/(\tau_f^2\pi rl)\,[\tanh(\omega l)/(1+(E_1A_1)/(E_2A_2))\,] \tag{29}$$

For load case 3, "pull of rod ", $\tau_{max} = \tau(0) = -\tau(l)$. With $\tau_{max} = \tau(0)$ eq (19) together with eq (25) and (27) give

$$P_f/(2\pi rl\,\tau_f) = (G_f\omega E_1A_1)/(\tau_f^2\pi rl)\,[\,\sinh(\omega l)/(\cosh(\omega l)-1)\,] \tag{30}$$

For load case 4, "pull of wood", $\tau_{max} = -\tau(0) = \tau(l)$. With $\tau_{max} = -\tau(0)$ eq (21) together with eq (25) and (27) gives

$$P_f/(2\pi rl\,\tau_f) = (G_f\omega E_1A_1)/(\tau_f^2\pi rl)\,[(E_2A_2)/(E_1A_1)]\,[[\,\sinh(\omega l)/(\cosh(\omega l)-1)\,] \tag{31}$$

For load case 5, "pull-distributed", $\tau_{max} = \tau(0)$ at least if $(E_2A_2)/(E_1A_1) > 1$, which probably is the case in almost all cases of practical interest. With $\tau_{max} = \tau(0)$ eq (23) together with eq (25) and (27) gives

$$P_f/(2\pi rl\,\tau_f) = (G_f\omega E_1A_1)/(\tau_f^2\pi rl)\,/\,[\cosh(\omega l)/\sinh(\omega l)\,+(E_1A_1)/(E_2A_2\omega l)] \tag{32}$$

Figure 3 shows failure loads for one example of parameter values: E1=200000 N/mm^2, E_2=10000 N/mm^2, G_f=2 Nmm/mm^2, τ_f=8 N/mm^2, r=8 mm, A_1=200 mm^2 and A_2=10000 mm^2. The values of G_f and τ_f correspond to G_3=8 N/mm^2 if t_3=0.5 mm.

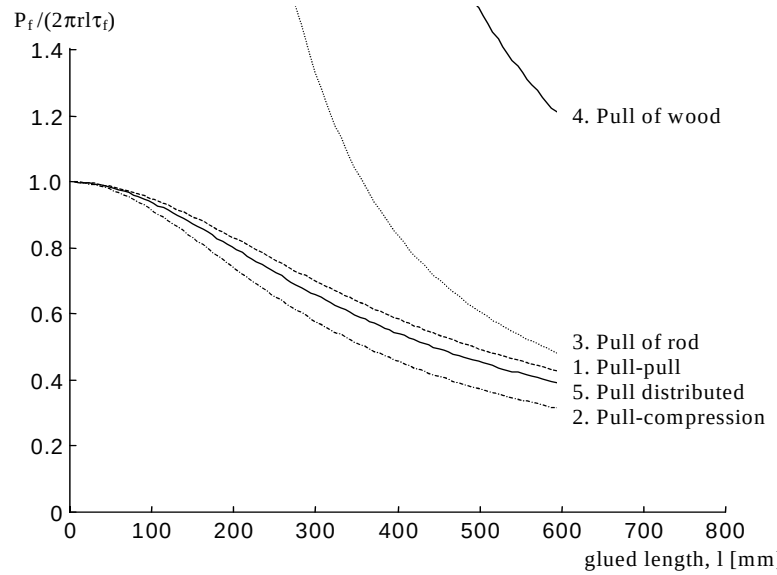

Figure 3. Failure load, P_f, vs. glued length, l, for different loads according to a bar shear lag fracture model.

3.4 Pull out strength according to ideal plastic model

In this simple model it is assumed that the adhesive layer has the ability to perform in an ideal plastic manner and carry a constant shear stress, τ_f , at any magnitude of the shear deformation of the bond layer. This means that the shear stress is constant along the rod at failure. The pull out strength of the rod may be obtained in a simple manner by equations of equilibrium or by letting $G_f$approach infinity in the above eq (28) – (32).

For load cases 1 (pull-pull), 2 (pull-compression) and 5 (pull distributed) is found

$$P_f/(2\pi rl\tau_f) = 1.0 \tag{33}$$

For load cases 3 (pull of the rod) and 4 (pull of the wood) is found

$$P_f/(2\pi rl\tau_f) \rightarrow \infty \tag{34}$$

Eq (34) means that failure of the bond layer can not be achieved by pulling the rod or the wood if the bond layer has large ductility. This result is consistent with a general theorem of the theory of ideal plasticity, according to which internal strains, e.g. due to temperature gradients, don't influence load carrying capacity.

3.5 Pull out strength according to linear elastic fracture mechanics

In this model the adhesive layer is assumed to perform in a brittle manner in the sense that failure is assumed to take place as start of crack propagation along the rod.

The load carrying fracture process region in front of the crack tip is assumed to be small as compared to the length of the rod. Equations for the pull out strength can be obtained by an equation for the balance between release of strain energy and dissipation of fracture energy as the

crack propagates. Alternatively the strength equations may by obtained from the above eq (28)-(32) by letting the dimensionless number ωl approach infinity. This corresponds to zero deformation capacity, $\tau_f(G_2/t_3)$, of the bond layer, see eq (25) and (26).

The same results is obtained for load cases 1 (pull-pull), 3 (pull of rod) and 5 (pull distributed). By letting ωl approach infinity, eq (28), (30) and (32) give

$$P_f/(2\pi rl\,\tau_f) = (G_f\omega E_1A_1)/(\tau_f^2\pi rl) \tag{35}$$

which also may be written as

$$P_f = 2\sqrt{\pi r G_f E_1 A_1}\ \sqrt{1+E_1A_1/(E_2A_2)} \tag{36}$$

or, if $A_1=\pi r^2$, as

$$P_f = 2\pi r\sqrt{E_1 G_f\, r}\ \sqrt{1+E_1A_1/(E_2A_2)} \tag{37}$$

For load case 2 (pull-compression) eq (29) gives

$$P_f/(2\pi rl\,\tau_f) = (G_f\omega E_1A_1)/(\tau_f^2\pi rl) \,/\, (1+E_1A_1/(E_2A_2)) \tag{38}$$

which, if $A_1=\pi r^2$, can by written as

$$P_f = 2\pi r\sqrt{E_1 G_f\, r}\ /\ \sqrt{1+E_1A_1/(E_2A_2)} \tag{39}$$

For load case 4 (pull of wood) eq (29) gives

$$P_f/(2\pi rl\,\tau_f) = (G_f\omega E_1A_1)/(\tau_f^2\pi rl)\ (E_2A_2/(E_1A_1)) \tag{40}$$

which, if $A_1=\pi r^2$, can by written as

$$P_f = 2\pi r\sqrt{E_1 G_f\, r}\ \sqrt{(E_2A_2/(E_1A_1))^2 + E_2A_2/(E_1A_1))} \tag{41}$$

Figure 4 shows failure loads as predicted by the linear elastic fracture mechanics equations versus glued length for one example of parameter values: E1=200000 N/mm^2, E_2=10000 N/mm^2, G_f=2 Nmm/mm^2, r=8 mm, A_1=200 mm^2 and A_2=10000 mm^2. To enable comparisons the results of the bar shear lag fracture model, see Figure 3, are also shown.

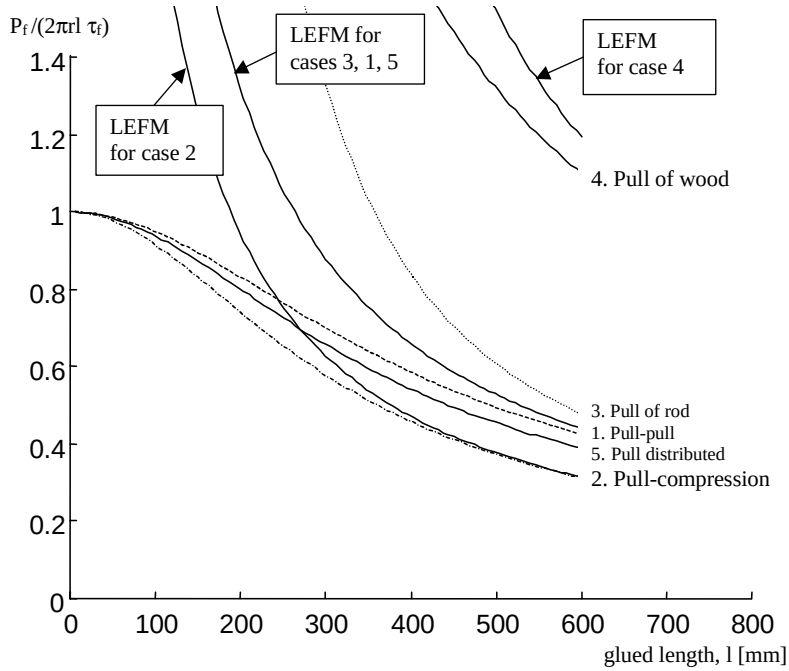

Figure 4. Pull out strength results of linear elastic fracture mechanics, LEFM. The curves from Figure 3 are also shown.

3.6 Timoshenko beam shear lag fracture model

3.6.1 Introduction

Major simplifications adopted in the lap joint model of Volkersen and in the bar shear lag fracture model dealt with in the above are that bending and shear deformations of the adherents are not taken into account. In the case of glued in rods, neglect of bending is probably a reasonable approximation due to the approximately axi-symmetric character of the geometry. The shear deformations in the wood might be of greater and significant importance, in particular if cross sectional dimension of the wood is of the same magnitude as the length of the rod. Moreover, the low shear stiffness of wood adds to the magnitude and possible significance of the shear deformations. In order to investigate if an analytical equation for glued rods can be developed and to study the effect of the shear deformations a theory where shear is taken into account in a similar way as in the Timoshenko beam theory will be discussed in the below.

3.6.2 Development of governing differential equation

In Figure 5 geometry, notations and positive directions are defined. To simplify the development and understanding of the model, a single lap joint with supports that prevent bending is studied at first. The results obtained for this single lap joint can then be applied to an axi-symmetric joint by making relevant substitutions. Material properties are as in the bar shear lag model with the addition of the elastic shear modulus G_2 of the wood. The rod is treated as a bar and the bond layer as an elastic shear lag layer, just as in the above analysis. The wooden part is modelled as a Timoshenko beam. Since equations of bending moment equilibrium will be needed, normal stress, σ_3, acting perpendicular to the adhesive layer must be included in the analysis. Normal strain perpendicular to the layer is however disregarded.

Bending curvature is prevented and the centre line of the wooden part is accordingly assumed to remain straight. The beam cross sections are in accordance with Timoshenko beam theory assumed to remain plane, but not, as in conventional beam theory, necessarily perpendicular to the centre line. Beam cross section inclination is denoted Θ. Since the beam remains straight

$$\Theta = -\gamma_2 \tag{42}$$

where the γ_2 is the shear strain in the wood material. The allowable displacement field of the wood is restricted by

$$u(x,y) = u(x,0) - y\,\Theta(x)\,, \quad v(x,y) = 0 \tag{43}$$

Comparing this with the bar theory, the unknown displacements are know defined by two functions, u(x,0) and Θ(x), instead of only by u(x,0).

To develop a governing differential equation, first equations for the wooden part are dealt with. Equilibrium in the x-direction of a part dx of the wood gives $N_2'-\tau_3 b=0$, which together with $N_2=A_2\sigma_0=E_2A_2\varepsilon_0= E_2A_2u_0'$ gives

$$E_2A_2u_0''-\tau_3 b=0 \tag{44}$$

with b dening the width, cf. Figure 5. Equilibrium in the y-direction of a part dx gives $V_2'-\sigma_3 b=0$, which together with $V_2=A_2\tau_2=G_2A_2\gamma_2= -G_2A_2\Theta$ gives

$$G_2A_2\Theta'+\sigma_3 b=0 \tag{45}$$

Moment equilibrium of a part dx gives $M_2'+V_2-e\tau_3 b=0$, which together with $M_2=E_2I_2\Theta'$ and $V_2= -G_2A_2\Theta$ gives

$$E_2I_2\Theta''-G_2A_2\Theta-e\tau_3 b=0 \tag{46}$$

For the rod, in analogy with the wood, the basic equations give

$$E_1A_1u_1''+\tau_3 b=0 \tag{47}$$

For the adhesive layer

$$\tau_3 = G_3\gamma_3 = G_3(u_2-u_1)/t_3 = G_3(u_0+e\Theta-u_1)/t_3 \tag{48-a}$$

By differentiating eq (48-a) twice and then taking u_0'' and u_1'' from eq (44) and (47), respectively, is found

$$\tau_3'' = G_3(\tau_3 b/(E_2A_2) + e\Theta''+ \tau_3 b/(E_1A_1))/t_3 \tag{48-b}$$

Eq (46) and (48-b) constitutes a system of two second order differential equations with Θ and τ_3 as the unknown functions. These equations are transformed to one fourth order differential

equation by a set of manipulations: first eq (46) is differentiated twice, then Θ'' and Θ'''' are substituted from eq (48-b), Θ'''' being obtained by differentiating eq (48-b) twice. This gives the governing differential equation

$$\tau_3'''' + S\tau_3'' + T\tau_3 = 0 \qquad (49)$$

where

$$S = -(G_3/t_3)\,(b/(E_2A_2)+b/(E_1A_1)+e^2b/(E_2I_2)) - G_2A_2/(E_2I_2) \qquad (50)$$

$$T = (G_3/t_3)\,(G_2A_2)/(E_2I_2)\,(b/(E_2A_2)+b/(E_1A_1)) \qquad (51)$$

The general solution to eq (49) is

$$\tau_3 = C_1 e^{k_1 x} + C_2 e^{k_2 x} + C_3 e^{k_3 x} + C_4 e^{k_4 x} \qquad (52)$$

where the constants C_1, C_2, C_3 and C_4 must be determined from boundary conditions. The coefficients k_1, k_2, k_3 and k_4 can be found by solving the characteristic equation

$$k^4 + S\,k^2 + T = 0 \qquad (53\text{-a})$$

which gives

$$k_1 = -k_3 = \sqrt{-S/2 + \sqrt{(S/2)^2 - T}} \quad , \quad k_2 = -k_4 = \sqrt{-S/2 - \sqrt{(S/2)^2 - T}} \qquad (53\text{-b})$$

By letting $G_2A_2 \rightarrow \infty$, i.e. for zero shear strain in the wood, eq (49) becomes equal to the homogenous part of eq (10). This reflects that the theory dealt with in section 3.3 can be regarded as a special case of the theory dealt with in this section

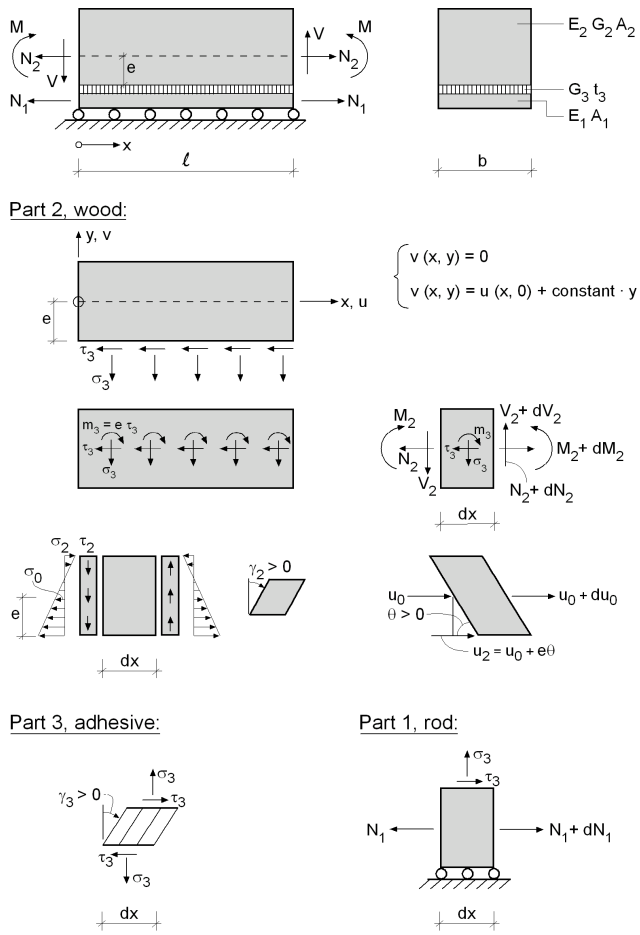

Figure 5. Geometry, notations and positive directions used in Timoshenko beam shear lag analysis.

3.6.3 Equations for determination of constants from boundary conditions

The boundary conditions are commonly known in terms of N_1 (or u_1'), N_2 (or u_2'), V_2 (or Θ) and/or M_2 (or Θ') at x=0 and at x=l, not directly in terms of τ_3. In the below conditions for τ_3 corresponding to various cross section conditions are given. Altogether there are 8 end cross section quantities. Since these must be such that global equilibrium of the joint in the x-direction is fulfilled, there are 7 quantities that may be assigned arbitrary values. There are, however, only 4 constants to be determined. This can be dealt with in two ways. Either certain linear combinations of end cross sectional quantities are assigned the desired values (obtained from the desired values of the individual quantities) or else 4 (at the most) individual quantities are assigned values and the remaining quantities obtained as a result of the calculations.

Knowing N_1, N_2 and M_2 (e.g. at x=0 and/or at x=l) the corresponding condition for τ_3 can be found by differentiating eq (48) and make the substitutions $u_0' = N_2/(E_2A_2)$, $\Theta' = M_2/(E_2I_2)$ and $u_1' = N_1/(E_1A_1)$, giving

$$\tau_3' = (G_3/t_3)\,(N_2/(E_2A_2) + M_2e/(E_2I_2) - N_1/(E_1A_1)) \qquad (54)$$

To obtain a condition for a known V_2, Θ'' from eq (46) can be substituted into eq (48). Use of $V_2 = -G_2A_2\Theta$ then gives

$$\tau_3'' - (G_3/t_3)\,(b/(E_2A_2) + e^2b/(E_2I_2) + b/(E_1A_1))\,\tau_3 = V_2\,(G_3/t_3)\,e/(E_2I_2) \qquad (55)$$

To get a separate condition for a given value of M_2, V_2 is replaced by $-G_2A_2\Theta$ in eq (55), then the equation is differentiated and $M_2=E_2I_2\Theta'$ utilised, giving

$$\tau_3''' - (G_3/t_3)\,(b/(E_2A_2) + e^2b/(E_2I_2) + b/(E_1A_1))\,\tau_3' = M_2\,(G_2A_2)(G_3/t_3)\,e/(E_2I_2)^2 \qquad (56)$$

To get a separate condition for loading by normal forces, M_2 from eq (56) may be substituted into eq (54), giving

$$\tau_3''' - [(G_2A_2)/(E_2I_2) + (G_3/t_3)\,(b/(E_2A_2) + e^2b/(E_2I_2) + b/(E_1A_1)]\,\tau_3' =$$

$$= (G_3/t_3)\,(G_2A_2)/(E_2I_2)\,(N_2/(E_2A_2) - N_1/(E_1A_1)) \qquad (57)$$

To get a set of equations for determination the constants C_1, C_2, C_3 and C_4 by use of eq (54), (55), (56) and/or (57), τ_3 and the derivatives of τ_3 are expressed by eq (52).

Having obtained the solution for $\tau_3(x)$, the above equations may also be used for calculation of $M_2(x)$, $V_2(x)$ and $\Theta(x)$. The normal forces $N_1(x)$ and $N_2(x)$ can be obtained by integration of $\tau_3(x)$. The stress $\sigma_3(x)$ can be calculated from $\Theta(x)$ by use of eq (45).

3.6.4 Determination of constants for one set of boundary conditions

The "pull-pull" loading case shall be studied in greater detail and the following conditions are chosen in this example: $N_1(0)=P$, $N_1(l)=0$, $N_2(0)=0$, $N_2(l)=P$, $M_2(0)=0$ and $V_2(l)=0$. The four first of these six conditions are really only two conditions, namely that $(N_2/(E_2A_2) - N_1/(E_1A_1))$ is $-P/(E_1A_1)$ at x=0 and $P/(E_2A_2)$ at x=l. It is sufficient to prescribe $(N_2/(E_2A_2) - N_1/(E_1A_1))$ since it is this difference that produces shear in the adhesive layer, not the absolute magnitude of normal forces.

The boundary conditions give a set of four equations. The first equation is eq (57) at x=0, the second is eq (56) at x=0, the third is eq (57) at x=l and the fourth is eq (55) at x=l. Using matrix notation, the equations may be written as

$$\mathbf{KC} = \mathbf{P} \qquad (58)$$

where the **C** vector contains the constants to be determined, i.e.

$$\mathbf{C} = [C_1\ C_2\ C_3\ C_4]^T \qquad (59)$$

The 4 by 4 coefficient matrix **K** is

$$\mathbf{K} = \begin{bmatrix} k_1^3 & k_2^3 & k_3^3 & k_4^3 \\ k_1^3 & k_2^3 & k_3^3 & k_4^3 \\ k_1^3 e^{k_1 l} & k_2^3 e^{k_2 l} & k_3^3 e^{k_3 l} & k_4^3 e^{k_4 l} \\ k_1^2 e^{k_1 l} & k_2^2 e^{k_2 l} & k_3^2 e^{k_3 l} & k_4^2 e^{k_4 l} \end{bmatrix} - \begin{bmatrix} D_N [& k_1 & k_2 & k_3 & k_4 &] \\ D_M [& k_1 & k_2 & k_3 & k_4 &] \\ D_N [& k_1 e^{k_1 l} & k_2 e^{k_2 l} & k_3 e^{k_3 l} & k_4 e^{k_4 l} &] \\ D_V [& e^{k_1 l} & e^{k_2 l} & e^{k_3 l} & e^{k_4 l} &] \end{bmatrix} \quad (60)$$

where

$$D_N = (G_3/t_3)\,(b/(E_2A_2) + e^2 b/(E_2I_2) + b/(E_1A_1)) + (G_2A_2)/(E_2I_2) \quad (61)$$

$$D_M = (G_3/t_3)\,(b/(E_2A_2) + e^2 b/(E_2I_2) + b/(E_1A_1)) \quad (62\text{-a})$$

$$D_V = (G_3/t_3)\,(b/(E_2A_2) + e^2 b/(E_2I_2) + b/(E_1A_1)) \quad (62\text{-b})$$

The **P** vector is

$$\mathbf{P} = \begin{bmatrix} F_N\,(-P/(E_1A_1)) & 0 & F_N\,(P/(E_2A_2)) & 0 \end{bmatrix}^T \quad (63)$$

where

$$F_N = (G_3/t_3)\,(G_2A_2)/(E_2I_2) \quad (64)$$

By principle it may be possible to solve eq (58) analytically and then get an explicit expression for the shear stress distribution along the rod. One may, however, expect such an expression to be lengthy. It is therefore more convenient to solve the equation after having inserted the numerical values of the parameters.

In the below numerical results are presented also for some other loading and end conditions than the one here discussed in greater detail. The method to determine the constants C_1, C_2, C_3 and C_4 is analogous for the various conditions, the only difference being the equations used in eq (58).

3.6.5 Substitution of parameters for axi-symmetric geometry

The above Timoshenko beam shear lag theory has basically been derived for a lap joint with rectangular cross section. For application to axi-symmetric joints:

$$b = 2\pi r, \quad (65)$$

$$e = (2/3)\,(r_{2y}^3 - r_{2i}^3)/(r_{2y}^2 - r_{2i}^2) - r_{2i}, \quad (66)$$

$$I_2 = (\pi/2)\,(r_{2y}^4 - r_{2i}^4) - (4\pi/9)\,(r_{2y}^3 - r_{2i}^3)^2 / (r_{2y}^2 - r_{2i}^2) \quad (67)$$

$$A_1 = \pi r_1^2, \quad (68)$$

and

$$A_2 = \pi(r_{2y}^2 - r_{2i}^2) \ , \qquad (69)$$

r_{2y} and r_{2i} denote the outer and inner radius of the wood part, r_1 the radius of the rod and r the distance from the centre to the shear layer. Commonly it may be a reasonable approximation to assume $r = r_1 = r_{2i}$.

3.6.6 Examples of shear stress distribution

In Figure 6 is the shear stress distribution corresponding to the "pull-pull" load shown for one example of parameter values: P=10000 N, E_1=200000 N/mm^2, E_2=10000 N/mm^2, G_3=100 N/mm^2, r=8 mm, A_1=200 mm^2, A_2=10000 mm^2, t_3=0.5 mm, l=160 mm and G_2=700 N/mm^2. Apart from the value of the new parameter, G_2, the numerical values used are the same as used when calculating the shear stress distributions shown in Figure 2. For comparison the result obtained for a high value of G_2, G_2=5000 N/mm^2, and the result obtained by the bar shear lag theory, corresponding to $G_2 \rightarrow \infty$, are also shown. G_2=5000 N/mm^2=$E_2/2$ corresponds to the shear stiffness of an isotropic material with zero Poisson's ratio.

Figure 7 illustrates the effect of end conditions. For the condition $V_2(0)=0$ is in general obtained $M_2(0)\neq 0$ as a result and for the condition $M_2(0)=0$ is in general obtained $V_2(0)\neq 0$. If G_2 is increased towards infinity the same result is obtained for the two conditions, coinciding also with the result of the bar shear lag model. $V_2(0)\neq 0$, which is estimated to be closer to reality than $M_2(0)\neq 0$, is a radial load acting on the wood at x=0. Such loading corresponds to concentrated tangential stress in the wood at x=0 and to concentrated normal stress acting across the bond layer at x=0. It might be possible to use a beam theory for calculating the stresses corresponding to $V_2(0)$.

Figure 8 shows the cross section inclination, θ, for the same conditions as illustrated in Figure 7. The bending moment in the wood is proportional to the slope of the θ-curve, θ', and the shear force is proportional the to magnitude of θ. Figure 9 and Figure 10 show the distributed radial load σ_3 as determined from θ' by eq (45). This load corresponds to tangential stresses in the wood and radial normal stress across the bond layer.

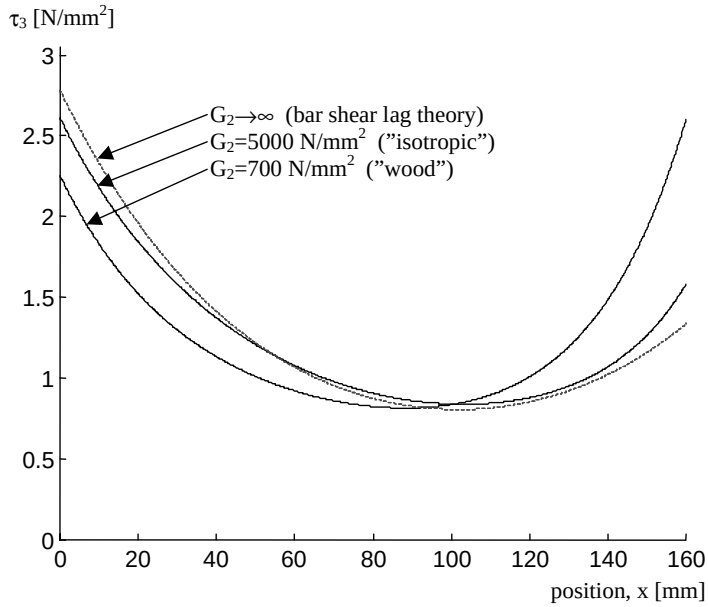

Figure 6. Shear stress distribution according to a Timoshenko shear lag theory at different shear stiffness of the wood.

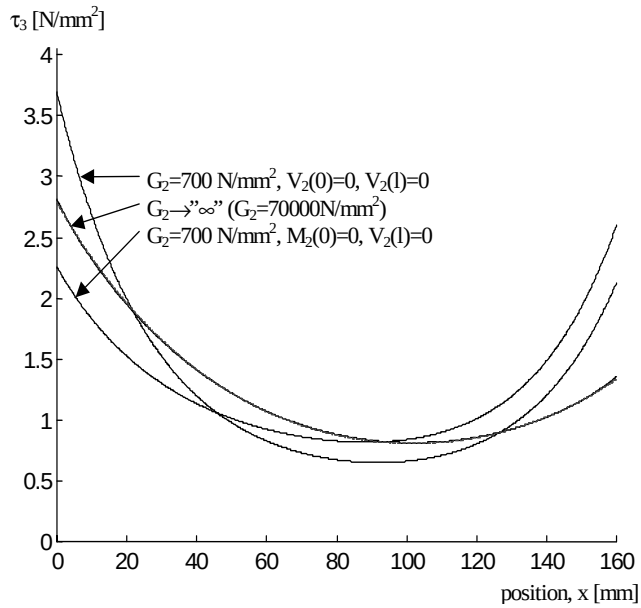

Figure 7. Shear stress distribution for different end conditions.

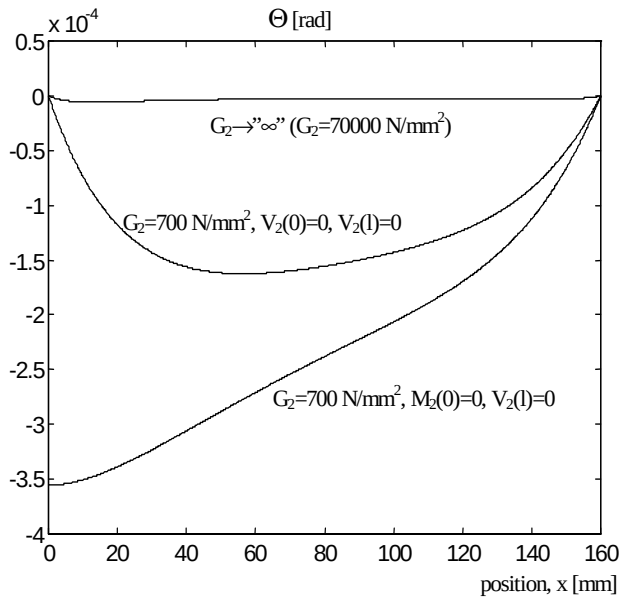

Figure 8. Wood cross section inclination, Θ (=-γ_2), according to a Timoshenko beam shear lag theory.

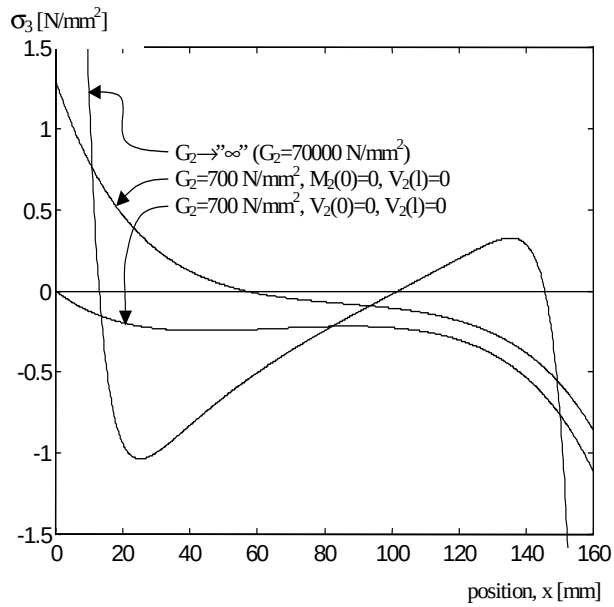

Figure 9. Stress σ_3. See Figure 10 for other scale.

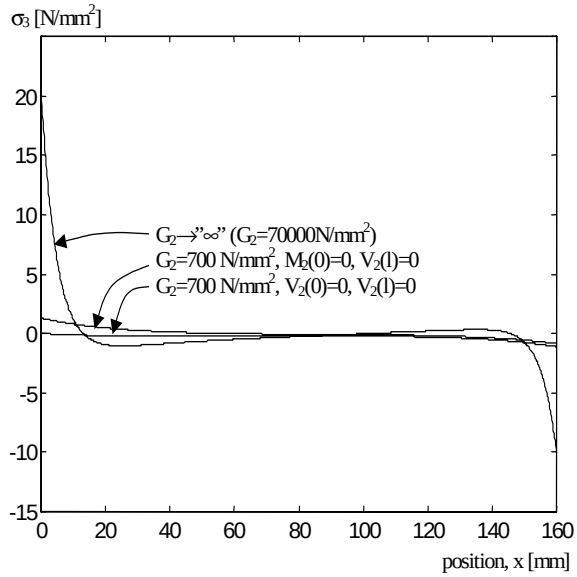

Figure 10. Stress σ_3. See Figure 9 for other scale.

3.6.7 Pull out strength

Knowing $\tau_3(x)$ from a calculation with (G_3/t_3) set equal to $\tau_f^2/(2G_f)$, the pull out strength is obtained from the criterion

$$|\tau_3(x)|_{max} = \tau_f \tag{70}$$

In Figures 11,12 and 13, some results are shown. Unless otherwise stated in the figure, the results were all obtained for the "pull-pull" kind of load and with the same set of parameter values as in previous strength calculations: E_1=200000 N/mm^2, E_2=10000 N/mm^2, G_f=2 Nmm/mm^2, τ_f=8 N/mm^2, r=8 mm, A_1=200 mm^2 and A_2=10000 mm^2. The values of G_f and τ_f corresponds to G_3=8 N/mm^2 if t_3=0.5 mm. In addition, especially for the present Timoshenko kind of modelling: G_2=700 N/mm2, $M_2(0)$=0 and $V_2(l)$=0.

Figure 11 shows that the results are not very different from those of the bar shear lag theory, shown by the curve indicated by $G_2 \to \infty$. The figure also shows that short rods, with a length less than about 170 mm, have an other decisive mode of failure than the longer rods, failure being initiated at x=l. The Timoshenko beam kind of theory predicts a somewhat higher strength than the bar kind of theory for the longer rods and a somewhat lower strength for the short rods.

Figure 12 shows the effect of the end-conditions. The results of the two conditions coincide as G_2 is increased towards infinity. Figure 13 gives an illustration of the strength at "pull-compression" load versus "pull-pull" load. Moreover Figure 13 shows how the fracture energy of the bond layer effects the pull out strength.

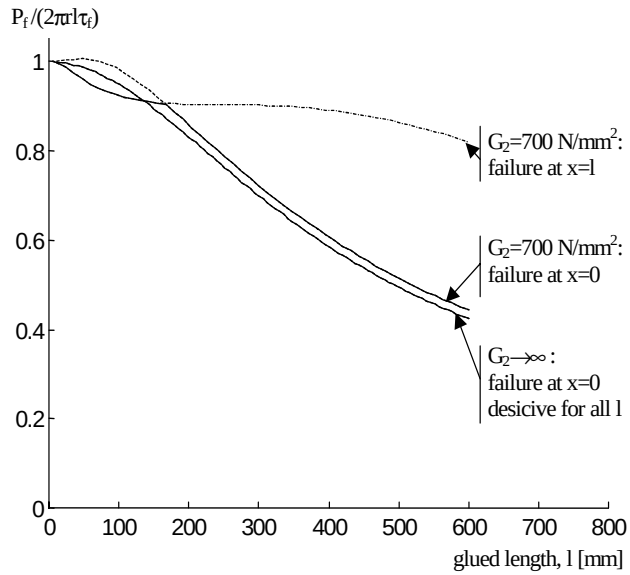

Figure 11. Pull out strength according to a Timoshenko beam fracture theory.

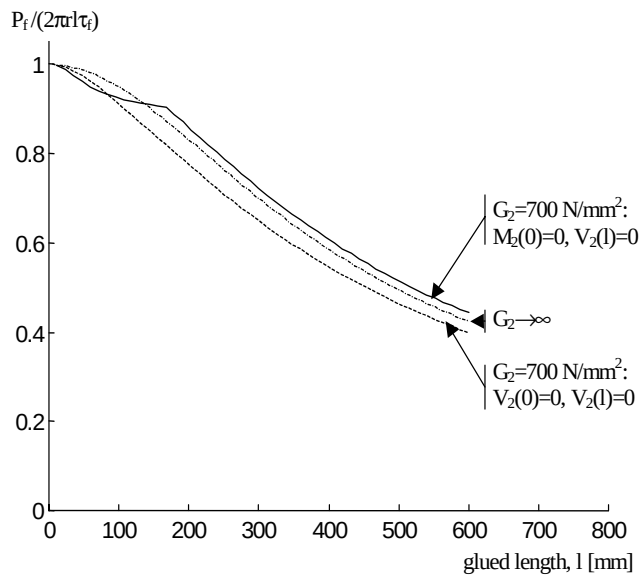

Figure 12. Effect of end conditions on pull out strength.

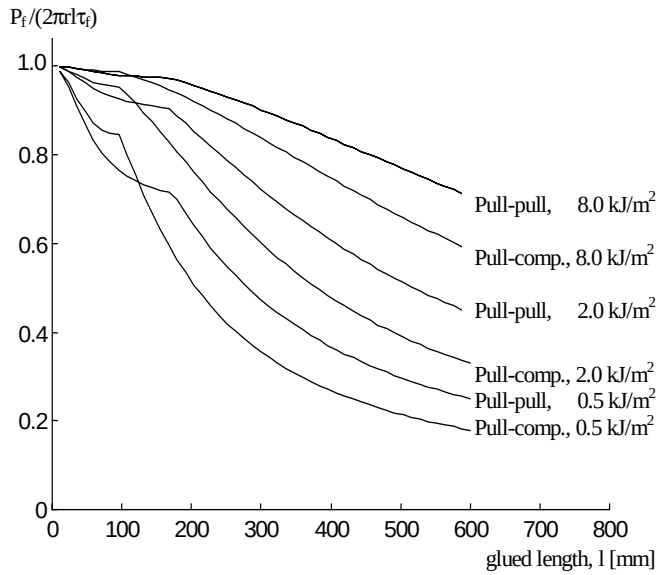

Figure 13. Pull out strength predictions for two kinds of loading and for various fracture energy values.

3.7 Finite element analysis

3.7.1 Introduction

Finite element simulations based on a non-linear fracture mechanics model have been performed. In the simulations the 3D geometry of glued in rod joints were taken into account as well as gradual fracture softening, or damage, of the bond layer. In order to study the effect of various parameters on the pull out strength of glued in rods several FE-calculations have been carried out. Three parameter studies, denoted I, II and III, have been made. The main objectives of these three studies were:

I. Analysis of the pull out strength with regard to the influence of various geometry and material property parameters. The loading case "pull-pull" was studied.

II. Analysis of the stresses in the wood and the effect on pullout strength of varying stiffness properties within the wood.

III. Analysis of the pull out strength at loading "pull-compression" versus the strength at "pull-pull". The effect of support arrangements was studied.

IV. Analysis of the pull out strength for different load-to-grain angles. Both pull-pull and three-point bending loading was examined.

3.7.2 Computational model: geometry, material and FE-mesh

All simulations were made by the general-purpose finite element code ABAQUS, [6]. In the model three materials are considered: wood, steel and bond layer. The wood is treated as an orthotropic linear elastic continuum, the steel as an isotropic linear elastic continuum and the bond layer as a layer in which the components of stress are non-linear functions of the relative shear and normal displacements across the layer. Figure 14 shows the geometry of the joints studied and defines various geometry parameters. Numerical values of parameters are indicated in the below sections.

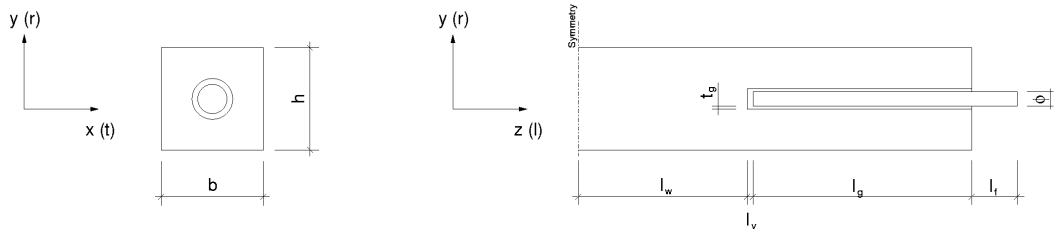

Figure 14. Geometry of joints and geometry parameters.

The threading of the rods is not taken into account in the geometry model. The effect of the threading on the axial stiffness of the rods can be taken into account by reducing the value of the modulus of elasticity of the steel. A rod with the nominal diameter ϕ=16 mm is taken as an example. From handbooks it is found that the effective cross section area of such a rod, if having metric threads with the coarse pitch, is 157 mm^2. This means that the modulus of elasticity of the steel could be reduced by the factor $157/(\pi\ 8^2)$=0.78 in order to correctly model the normal stiffness of the rod. No such reduction is made in the present calculations.

The steel was throughout the present calculations assumed to perform in an isotropic linear elastic manner, characterised by E_s=210000 N/mm^2 and ν=0.3.

The wood was throughout the present calculations assumed to perform in an orthotropic linear elastic manner. The notations and the numerical values of the nine parameters that define such a material are given in Table 2. The material directions were assumed to be constant within the specimen in studies I and II. These directions, l for longitudinal, r for radial and t for tangential, are indicated in Figure 14. In study II variations of the directions according to the orientation of the annual rings and the build up of glulam from laminations were considered.

Table 2. Stiffness parameters of wood adopted in calculations

Young's modulus	Shear modulus	Poisson's ratio
E_t = 500 N/mm2	G_{tr} = 60 N/mm2	ν_{tr} = 0.3
E_r = 800 N/mm2	G_{tl} = 700 N/mm2	ν_{tl} = 0.02
E_l = 14000 N/mm2	G_{rl} = 600 N/mm2	ν_{rl} = 0.02

The bond line was modelled by a non-linear model. In this model the performance of the material is basically defined by three curves. One curve defines the pure shear stress vs. shear deformation response, one curve defines the pure normal stress versus normal deformation response and one curve defines the interaction at combined states of deformation. Here the model is first described for a general case and then restrictions are made so that the properties of the bond layer can be defined by only four parameters: the strength and fracture energy for pure shear and for pure tension: τ_f, $G_{f,s}$, σ_f and $G_{f,n}$.

The model used is an extension of the model developed by Wernersson in [11]. The model of Wernersson was two-dimensional, involving one shear component and one normal component. For three-dimensional application the model is expanded into consideration of the two shear components plus one normal component needed for definition of the interaction between two surfaces.

The bond line properties at pure shear and at pure tension are given by two piece-wise linear curves. Figure 15 shows such curves for both shear stress (solid line) and normal stress (dashed line).

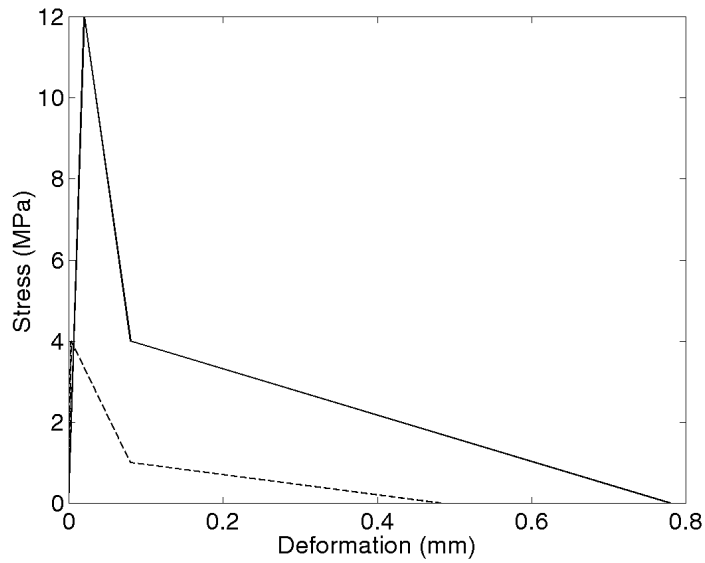

Figure 15. Stress-slip curve for bond layer in shear (solid line) and for normal stress (dashed line).

A general mixed mode state of deformation is described by the two shear slips, δ_{s1} and δ_{s2}, and by the normal deformation δ_n. The stress-deformation response is assumed to retain its piecewise linear shape for radial deformation paths (constant values of $(\delta_{s1}:\delta_{s2}:\delta_n)$), but vary smoothly with the degree of mixed mode, expressed by the mixed mode angles φ_{ss} and φ_{sn}:

$$\varphi_{ss} = \arctan(\delta_{s1}/\delta_{s2}) \tag{71}$$

$$\varphi_{sn} = \arctan(\delta_s/\delta_n) \tag{72}$$

where

$$\delta_s = \sqrt{\delta_{s1}^2 + \delta_{s2}^2} \tag{73}$$

The following criterion is used to determine whether the current state is in the linear elastic region:

$$\left(\frac{\delta_{s1}}{\delta_{s1,1}^0}\right)^m + \left(\frac{\delta_{s2}}{\delta_{s2,1}^0}\right)^n + \left(\frac{\delta_n}{\delta_{n,1}^0}\right)^p \le 1 \tag{74}$$

The second subscript, 1, refers to the first breakpoint in the piecewise linear curve and superscript 0 stands for uniaxial pure shear or normal loading properties. If the current state is linear elastic, the responses in the three directions are linear elastic and uncoupled. If not, new break point deformations $\delta_{s1,i}$, $\delta_{s2,i}$ and $\delta_{n,i}$ are calculated by means of an equation analogous to (74), using the

current values of the mixed mode ratios δ_{s1}/δ_{s2} and δ_s/δ_n. The stresses corresponding to a breakpoint, i, are then calculated according to

$$\tau_{1,i} = \tau^0_{1,i} \frac{\delta_{s1,1}}{\delta^0_{s1,1}} \tag{75}$$

$$\tau_{2,i} = \tau^0_{2,i} \frac{\delta_{s2,1}}{\delta^0_{s2,1}} \tag{76}$$

$$\sigma_i = \sigma^0_i \frac{\delta_{n,1}}{\delta^0_{n,1}} \tag{77}$$

Knowing the stresses at the breakpoints, the stress for the current deformation can be obtained by linear interpolation. In FE-analysis it is necessary not only to calculate the state of the stress for current deformation, but also the tangential stiffness of the material at the current state, i.e. the derivative of stress with respect to deformation. In the current FE-implementation this derivative is calculated numerically since it, for the present material model, is very difficult to find a general explicit equation for the derivative.

The FE-implementation is a so-called smeared crack implementation. This means that the above relations for stress versus relative displacement, or deformation, are transformed into relations for stress versus strain by dividing with the width of the continuum finite element used to model the bond layer.

In the present calculation the following has been assumed through out. In eq (74)

$$m=n=p=2 \tag{78}$$

and the basic pure loading stress-deformation curves have been defined by three linear parts, see Figure 15, where

$$\tau^0_{1,2} = \tau^0_{1,1} / 3 \quad \text{and} \quad \tau^0_{1,3} = 0 \tag{79}$$

and

$$\delta^0_{s1,2} = 4\,\delta^0_{s1,1} \quad \text{and} \quad \delta^0_{s1,3} = 39\,\delta^0_{s1,} \tag{80}$$

for shear in the s1-direction. The performance in the s2-direction was assumed to be the same as in the s1-direction. For the n-direction

$$\sigma^0_2 = \sigma^0_1 / 4 \quad \text{and} \quad \sigma^0_3 = 0 \tag{81}$$

and

$$\delta_{n,2} = 30\,\delta_{n,1} \quad \text{and} \quad \delta_{n,3} = 179\,\delta_{n,1} \tag{82}$$

Moreover

$$\tau^0_{1,1} = \tau^0_{2,1} = \tau_f \tag{83}$$

and

$$\sigma^0_1 = \sigma_f \tag{84}$$

which together with

$$G_{f,s} = \int \tau_1^0 \, d\delta_{s1}^0 = \int \tau_2^0 \, d\delta_{s2}^0 \tag{85}$$

and

$$G_{f,n} = \int \sigma^0 \, d\delta_n^0 \tag{86}$$

defines the bond layer properties for given numerical values of the four material parameters τ_f, $G_{f,s}$, σ_f and $G_{f,n}$.

The finite element subdivision used for most calculations is shown in Figure 16. Due to symmetry only one half of the length of the specimen as well as one half of the width was analysed. For cases with material properties like those analysed in studies I and III, having constant material direction in the wood, it would by principle have been possible to utilise additional symmetry properties. The model consists of approximately 14000 nodes, 42000 degrees of freedom and 12000 elements. The bond layer is modelled with 50 elements in the axial direction and 12 elements in the circumferential direction.

The elements representing the wood and the steel are standard, isoparametric 8 node brick elements. The bond layer was modelled by the same type of element, but with reduced integration with only 1 Gausspoint in order to avoid shear locking. Such locking can be a problem if the linear brick element has an extreme slenderness ratio.

For some calculations with brittle adhesive properties, giving a small length of active fracture process region, the element subdivision along the rod was refined so that the bond element length was halved by increasing the number element in the axial direction from 50 to 100.

In order to check if the finite element mesh in the plane of the cross section was fine enough, a mesh with about 65000 nodes and 195000 degrees of freedom was used in one calculation. Comparison with the load capacity calculated with the 14000 node mesh gave a difference of less than 1%.

Load was applied by increments in displacement, not force. Displacement controlled loading can make it possible to trace post peak-load behaviour.

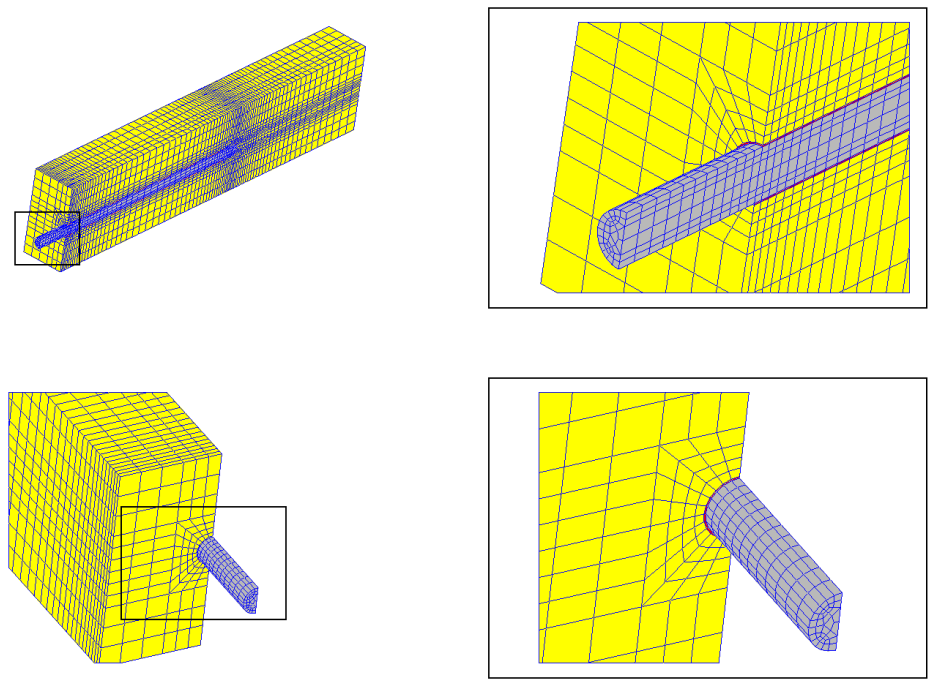

Figure 16. Finite element subdivision used in most simulations.

3.7.3 Parameter study 1: "pull-pull", constant material directions

In this study the joint load was "pull-pull" and the orientation of material directions of the wood was kept constant. The 22 simulations made are grouped into 6 groups, denoted A-F. Simulation A1 is the reference case, and each group refers to simulations where one parameter has been changed in relation to the value applied in simulation A1. In the groups the following parameters have been studied:

A. Variation of the fracture energies $G_{f,s}$ and $G_{f,n}$ at constant ratio $G_{f,s} / G_{f,n}=5$. The results obtained in this group also give information about the effect of a proportional change of τ_f and σ_f, about the effect of a proportional change of all stiffness parameters of the wood and the steel, and about the size effect, i.e. the effect of a proportional change of all geometrical dimensions.

B. Variation of the lengths l_g and l_w at constant ratio $l_g / l_w=1.4$.

C. Variation of the rod diameter, ϕ.

D. Variation of the length l_w.

E. Variation of the shear strength τ_f in simulations E1 and E2, and variation of the tensile strength σ_f in simulations E3 and E4.

F. Variation of the cross section dimensions b and h at constant ratio b/h=1.0.

The load displacement curves from simulations A1, B1 and B2 are shown in Figure 17, where the dots indicate the instance of fracture initiation. From the simulations it is also possible to obtain e.g. the stress distribution in the bond layer at different load levels. This is shown for simulations A1, B1 and B2 in Figure 18–23. In Table 3 the input parameter values are given together with

the computational result in terms the failure loads P_f. In the table also the nominal glued in rod shear strength $P_f/(\pi\phi l)$ and the nominal tensile stress in the rods $P_f/(\pi\phi^2/4)$ are indicated. In all calculations the distances l_v and t_g were kept constant: l_v=3 mm and t_g=0.5 mm.

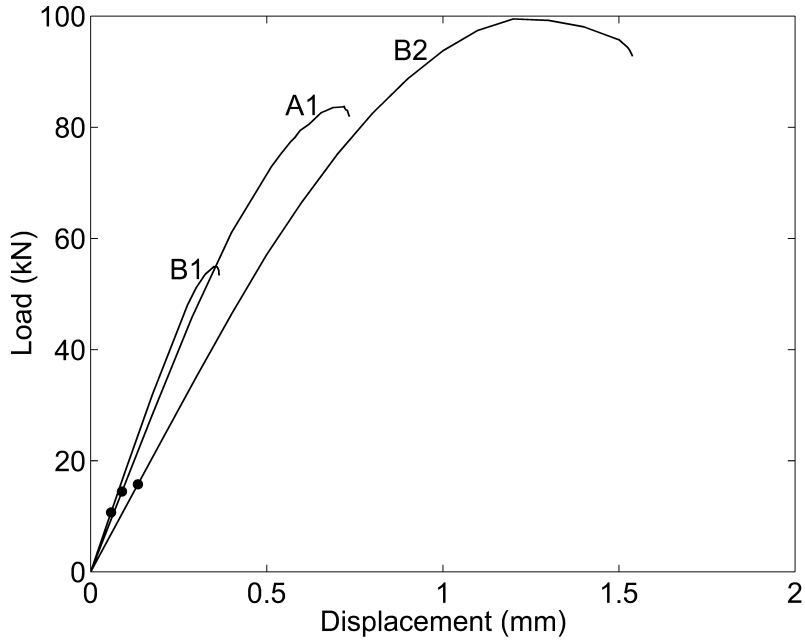

Figure 17. Load displacement response for simulations A1, B1 and B2.

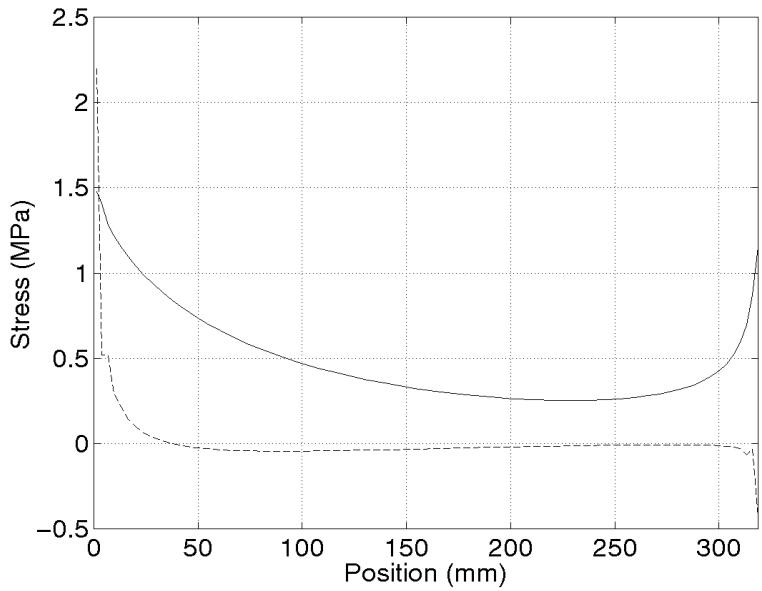

Figure 18. Linear elastic stress distribution. τ solid line and σ dashed line. Simulation A1.

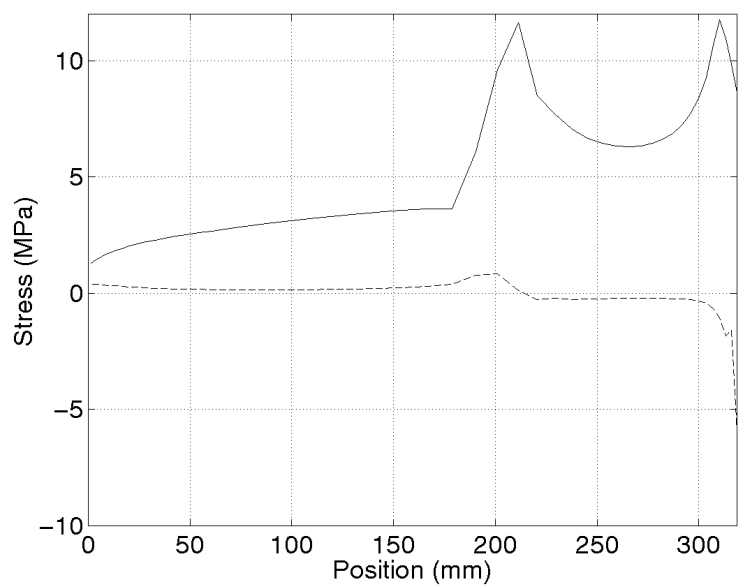

Figure 19. Stress distribution at maximum load. τ solid line and σ dashed line. Simulation A1.

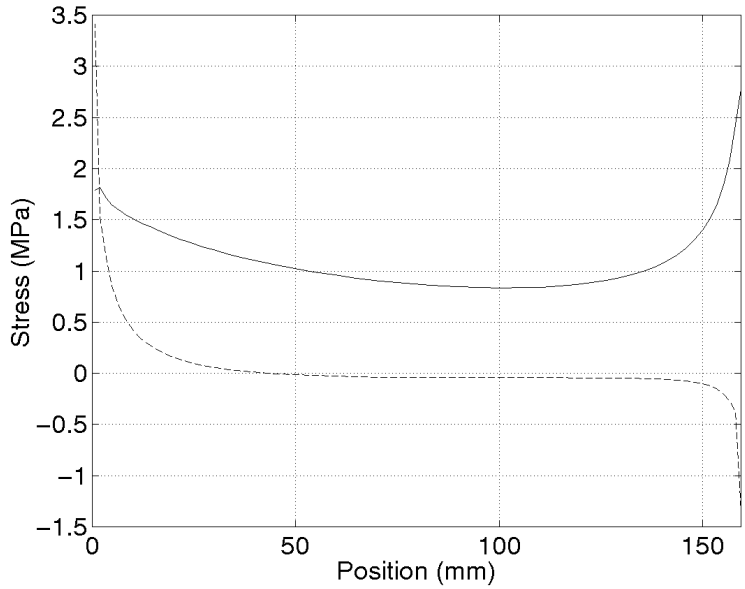

Figure 20. Linear elastic stress distribution. τ solid line and σ dashed line. Simulation B1.

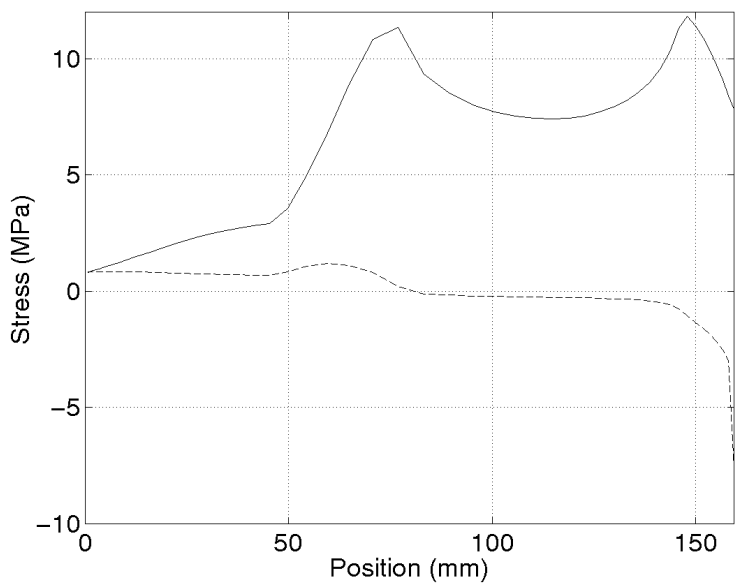

Figure 21. Stress distribution at maximum load. τ solid line and σ dashed line. Simulation B1.

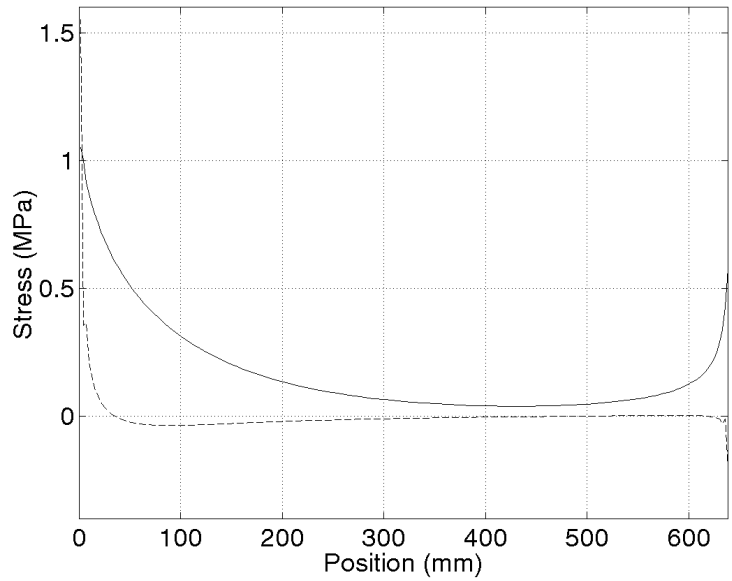

Figure 22. Linear elastic stress distribution. τ solid line and σ dashed line. Simulation B2.

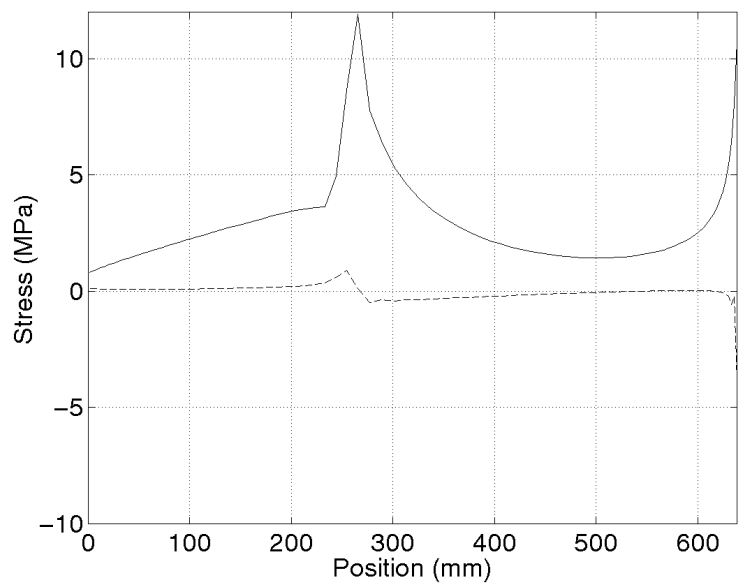

Figure 23. Stress distribution at maximum load. τ solid line and σ dashed line. Simulation B2.

Table 3. Input data and calculated pullout strength, P_f. All parameters are in unit mm, N/mm^2 or Nmm/mm^2, except P_f, which is given in kN. $\tau_{bond}=P_f/(\pi\phi l)$ and $\sigma_{steel}=P_f/(\pi\phi^2/4)$

Nr	ϕ	l_g	l_w	b=h	τ_f	σ_f	$G_{f,s}$	$G_{f,n}$	P_f kN	τ_{bond}	σ_{steel}
A1	**16**	**320**	**230**	**120**	**12**	**4**	**2.0**	**0.5**	**83.8**	**5.21**	**417**
A2	16	320	230	120	12	4	**4.0**	**1.0**	101.4	6.30	504
A3	16	320	230	120	12	4	**1.0**	**0.25**	65.9	4.09	327
A4	16	320	230	120	12	4	**8.0**	**2.0**	121.4	7.55	604
A5	16	320	230	120	12	4	**0.5**	**0.125**	45.8	2.85	228
A6	16	320	230	120	12	4	**16.0**	**4.0**	147.0	9.14	731
A7	16	320	230	120	12	4	**0.25**	**0.0625**	33.6	2.09	167
A8	16	320	230	120	12	4	**32.0**	**8.0**	171.6	10.7	853
A9	16	320	230	120	12	4	**64.0**	**16.0**	184.1	11.4	916
B1	16	**160**	**115**	120	12	4	2.0	0.5	54.9	6.83	273
B2	16	**640**	**460**	120	12	4	2.0	0.5	99.2	3.08	493
C1	**8**	320	230	120	12	4	2.0	0.5	33.0	4.10	657
C2	**32**	320	230	120	12	4	2.0	0.5	186.0	5.78	231
C3	**4**	320	230	120	12	4	2.0	0.5	12.1	3.02	963
D1	16	320	**115**	120	12	4	2.0	0.5	82.1	5.10	408
D2	16	320	**57.5**	120	12	4	2.0	0.5	84.4	5.24	420
E1	16	320	230	120	**6**	4	2.0	0.5	60.7	3.78	302
E2	16	320	230	120	**24**	4	2.0	0.5	97.2	6.04	483
E3	16	320	230	120	12	**2**	2.0	0.5	83.7	5.21	416
E4	16	320	230	120	12	**8**	2.0	0.5	84.5	5.25	420
F1	16	320	230	**60**	12	4	2.0	0.5	91.9	5.71	457
F2	16	320	230	**240**	12	4	2.0	0.5	81.8	5.08	407

3.7.4 Parameter study II: varying annual ring orientation and stresses in wood

In study II, varying (cylindrical) material orientation and the magnitude of the stresses in the wood were studied. Eight simulations were made. They are denoted G1-G4 and H1-H4. Input data and computational results are given in Table 5. The material orientations, G1-G4, in the glulam lamella are defined in Figure 24. The orientations are cylindrical with various locations of the pith. The middle lamella is somewhat thicker than the outer lamella, 0.375h and 0.3125h, respectively. This corresponds to middle lamella thickness 45 mm if h=120 mm. Input data and type of loading are according to those used in simulation A1 of study I, except for the material orientation and cross section size. The latter is varied in simulations H1-H4 at constant cylindrical material orientation in order to investigate the effect of cross section size on the magnitude of maximum stresses in the wood.

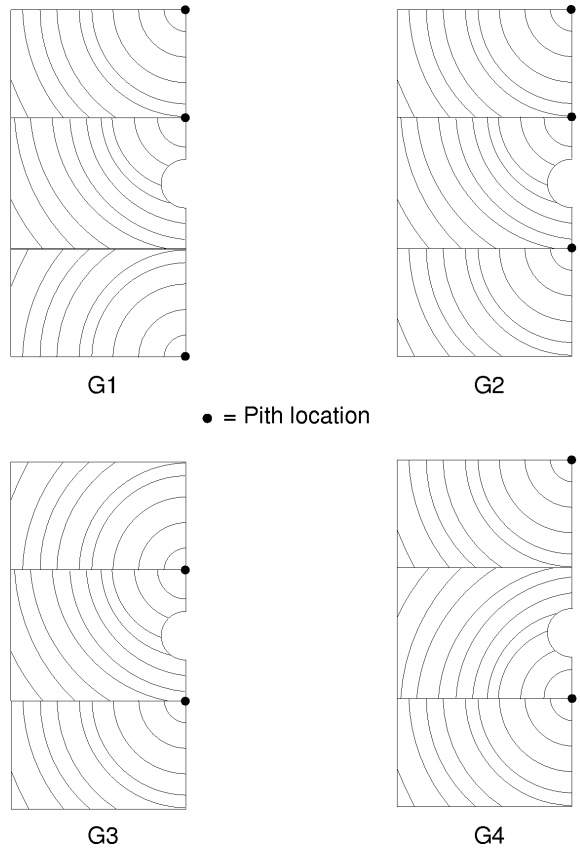

Figure 24. Annual ring orientations used in the simulations.

In order to estimate the risk of failure in the wood an effective stress in the wood is calculated according to a failure criterion of Norris, [10]. According to this criterion a dimensionless effective stress $\bar{\sigma}_{wood}$ is defined as

$$\bar{\sigma}_{wood} = \max (\bar{\sigma}_{wood,rt} , \bar{\sigma}_{wood,tl} , \bar{\sigma}_{wood,rl}) \tag{87}$$

where

$$\bar{\sigma}^2_{wood,rt} = (\sigma_r/f_r)^2 + (\sigma_t/f_t)^2 - \sigma_r\sigma_t/(f_r/f_t) + (\tau_{rt}/f_{rt})^2 \tag{88}$$

$$\bar{\sigma}^2_{wood,tl} = (\sigma_t/f_t)^2 + (\sigma_l/f_l)^2 - \sigma_t\sigma_l/(f_t/f_l) + (\tau_{tl}/f_{tl})^2 \tag{89}$$

$$\bar{\sigma}^2_{wood,rl} = (\sigma_r/f_r)^2 + (\sigma_l/f_l)^2 - \sigma_r\sigma_l/(f_r/f_l) + (\tau_{rl}/f_{rl})^2 \tag{90}$$

In these equations the normal strength values are assigned different values for tension and compression. According to the criterion of Norris failure develops in a point of the material if

$$\bar{\sigma}_{wood} = 1.0 \tag{91}$$

in that point. This may, or may not, lead to global failure. Table 4 gives the wood strength values chosen from literature [4, 8, 9].

Table 4. Adopted strength values.

Tensile or compressive strength			Shear strength
f_r = 5 N/mm^2	or	-6 N/mm^2	f_{rr} = 4 N/mm^2
f_t = 4 N/mm^2	or	-6 N/mm^2	f_{tl} = 10 N/mm^2
f_l = 90 N/mm^2	or	-45 N/mm^2	f_{tl} = 10 N/mm^2

In the present finite element simulations $\overline{\sigma}_{wood}$ has been calculated for the Gaussian points in each element representing wood. The values of $\overline{\sigma}_{wood}$ given in Table 5 are the maximum values found during the course of loading up to pull out failure of the rod. The spatial maximums of $\overline{\sigma}_{wood}$ versus the magnitude of the pull out load are shown in Figure 25 for the eight simulations. It is evident that maximum $\overline{\sigma}_{wood}$ is not found for P=P_f, but at about 0.7 P_f. This is because of favourable redistribution of stress when damage gradually develops in the bond layer. The results also show, somewhat surprising, that $\overline{\sigma}_{wood}$ is somewhat higher for the larger cross sections. Variation of material direction was not found to have any major effect, neither on P_f nor on $\overline{\sigma}_{wood}$.

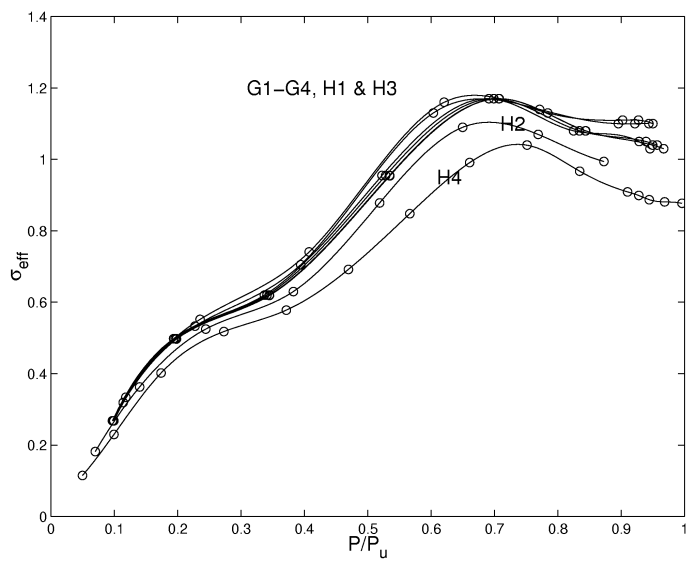

Figure 25. The spatial maximum of $\overline{\sigma}_{wood}$ versus the magnitude of the pull out load.

Table 5. Input data and calculated pullout strength, P_f, and max effective normalised stress in wood, $\bar{\sigma}_{wood}$. Input data as for A1, unless otherwise given in the table. All parameters are in unit mm, N/mm^2 or Nmm/mm^2, except P_f, which is given in kN and $\bar{\sigma}_{wood}$ which is dimensionless. $\tau_{bond}=P_f/(\pi\phi l)$ and $\sigma_{steel}=P_f/(\pi\phi^2/4)$

Nr	Material orientation of wood in glulam	b=h	P_f kN	τ_{bond}	σ_{steel}	$\bar{\sigma}_{wood}$
G1	Cylindrical "G1"	120	82.1	5.10	408	1.17
G2	Cylindrical "G2"	120	82.1	5.10	408	1.17
G3	Cylindrical "G3"	120	83.0	5.16	413	1.17
G4	Cylindrical "G4"	120	84.0	5.22	418	1.17
H1	Cylindrical "G1"	180	81.2	5.05	404	1.14
H2	Cylindrical "G1"	80	88.0	5.47	438	1.09
H3	Cylindrical "G1"	240	81.2	5.05	404	1.16
H4	Cylindrical "G1"	60	91.8	5.71	457	1.04

3.7.5 Parameter study III: influence of method of load application

In this study the influence of loading of the glued in rod joint by pull-compression versus loading by pull-pull was studied. In the case of pull-compression loading the method of load application was also studied. Application of the compressive load was modelled by means of the contact modelling facilities in ABAQUS. The modelling corresponds to application of the load by a stiff plate. The coefficient of friction between the plate and the wood was set equal to 0.6. Three sizes of the stiff plate were studied: a 120 by 120 mm square plate, a 100 mm diameter circular plate and a 40 mm diameter circular plate. In all plates was a hole for the rod. The diameter of the hole was made equal to the diameter of the hole in the wood plus 1 mm, i.e. 16+0.5+0.5+1=18.0 mm.

Input data and the calculated pull out strengths are indicated in Table 6. Input parameters not defined in Table 6 are according to the data used in simulation A1 in study I, see Table 2. Ratio l_w/l_g is slightly different in the different simulations. Comparison of simulations A1 and t1 suggests that this variation is of minor significance. In the simulations marked *) a finer element mesh with more nodes and elements in the contact area was used. In addition to results regarding effect of load application Table 6 also give additional information about the effect of rod length and fracture energy.

*Table 6. Input data and calculated pull out strength, P_f. Input data as for A1, unless otherwise given in the table. All parameters are in unit mm, N/mm^2 or Nmm/mm^2, except P_f, which is given in kN. $\tau_{bond}=P_f/(\pi\phi l)$ and $\sigma_{steel}=P_f/(\pi\phi^2/4)$ *) indicates refined finite element contact modelling.*

Nr	Load	Plate for application of compression	l_g	l_w	$G_{f,s}$	$G_{f,n}$	P_f kN	τ_{bond}	σ_{steel}
cs1	Pull-com.	120 mm square	320	256	2.0	0.5	73.3	4.56	365
t1	Pull-pull	-	320	256	2.0	0.5	83.8	5.21	417
cc1	Pull-com.	100 mm circular	320	256	2.0	0.5	72.9	4.53	363
cs2	Pull-com.	120 mm square	160	126	2.0	0.5	50.3	6.25	250
t2 = B1	Pull-pull	-	160	115	2.0	0.5	54.9	6.83	272
cs3	Pull-com.	120 mm square	320	256	4.0	1.0	90.9	5.65	452
t3 = A2	Pull-pull	-	320	230	4.0	1.0	101.4	6.30	504
cs4	Pull-com.	120 mm square	160	126	4.0	1.0	60.8	7.56	302
t4	Pull-pull	-	160	126	4.0	1.0	66.8	8.31	332
cs5	Pull-com.	120 mm square	320	259	1.0	0.25	53.4	3.32	266
t5 = A3	Pull-pull	-	320	230	1.0	0.25	65.9	4.10	328
cs6	Pull-com.	120 mm square	160	126	1.0	0.25	41.3	5.14	205
t6	Pull-pull	-	160	126	1.0	0.25	45.2	5.62	225
rcs1*)=cs1	Pull-com.	120 mm square	320	256	2.0	0.5	73.5	4.57	366
rcc1*)=cc1	Pull-com.	100 mm circular	320	256	2.0	0.5	72.7	4.52	362
rcc1-40*)	Pull-com.	40 mm circular	320	256	2.0	0.5	67.3	4.18	335

3.7.6 Parameter study IV: influence of load-to-grain angle

In order to examine the influence of the load-to-grain angle, two different FE-models were employed. Firstly the geometry of the pull-pull specimen as reported above was used in a series of simulations varying the slope of the grain from 0° to 90°. Although such a specimen has not been used in the GIROD-project, it is useful for comparison with the results from parameter study I. The difference in results as compared with parameter study I will then be due to the slope of grain only. In Figure 26 the response of the reference geometry (A1) for different load-to-grain angles is shown. Figure 27 shows the corresponding results for the B1 geometry (l_g=160mm). The corresponding numerical values are summarised in Table 7.

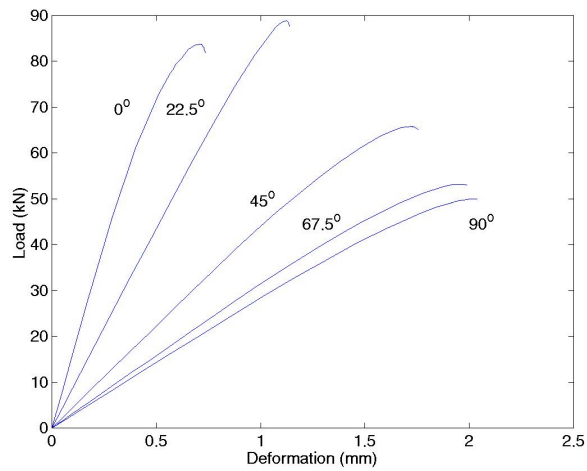

Figure 26. Load-displacement response for different load-to-grain angles. Loading by pull-pull. Geometry and bondline properties according to simulation A1.

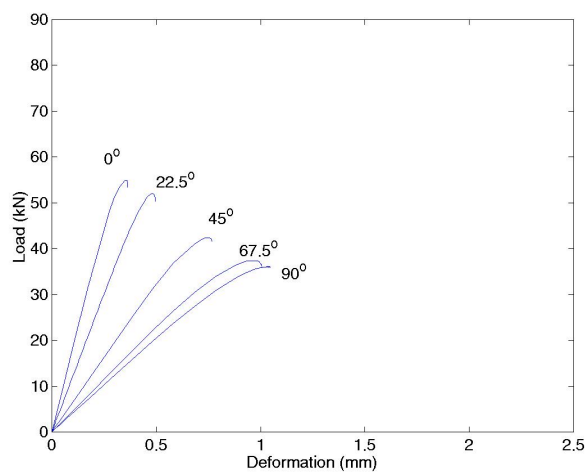

Figure 27. Load-displacement response for different load-to-grain angles. Loading by pull-pull. Geometry and bondline properties according to simulation B1.

Table 7. Pull-out load (pull-pull loading) for different load-to-grain angles. Specimen geometry according to simulation A1(l_g=320 mm) and B1(l_g=160 mm).

Load-to-grain angle	0°	22.5°	45°	67.5°	90°
l_g=320 mm	83.8	88.9	65.8	53.2	50.0
l_g=160 mm	54.9	52.1	42.3	37.4	36.1

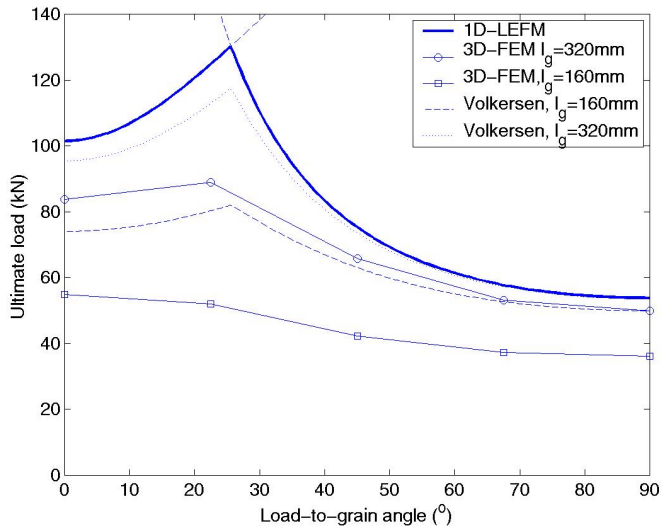

Figure 28. Comparison of different calculation models for the prediction of pull-out load for various load-to-grain angles. Loading in pull-pull.

3.7.7 Parameter study V: influence of load application – 3P-bending

In the GIROD-project tests were performed using a three-point bending specimen with the rod glued in at different angles. In order to analyse the possible influence of this different geometry, FE-simulations were also performed for 3P-bending with 90° load-to-grain angle. Two different geometries were analysed, 160 and 320 mm bolt (glued-in length) in a 60×120×1800 mm beam subjected to 3 point bending by pulling of the rod in the midspan. The FE-mesh used for the 320 mm bolt is shown in Figure 29. The results from this study are shown in Table 8. It turns out that the predicted pull-out strength is very much influenced by loading in bending as compared with loading in pull-pull. As an example, the FE-simulations predict a pull-out load of 50 kN for the pull-pull case (Table 7, 90°) and a pull-out load of 71.8 kN for the three-point bending case. The reason for this difference is that the three point bending set-up gives a more uniform shear stress distribution along the rod. For the three point bending, at least for the case where the rod length is not small in comparison with the beam depth, the shear stresses are transferred along the entire rod. For the pull-pull case there are more pronounced shear stress concentrations at the ends of the rod. For comparison, the linear elastic shear stress distribution along the rod is shown in Figure 30 for the pull-pull case and the three point bending case.

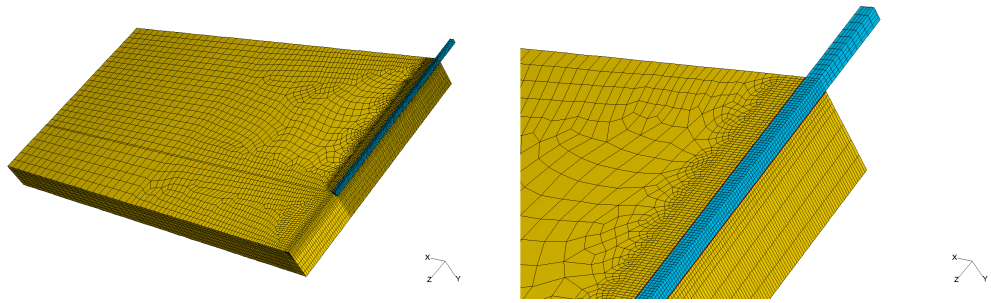

Figure 29. FE-mesh of the 3P bending specimen (only ¼ considered due to symmetry).

Table 8. Influence of load application on pull-out load (kN) for 90° load-to-grain angle.

Length	Pull-pull	3P-bending
320 mm	50.0	71.8
160 mm	36.1	44.0

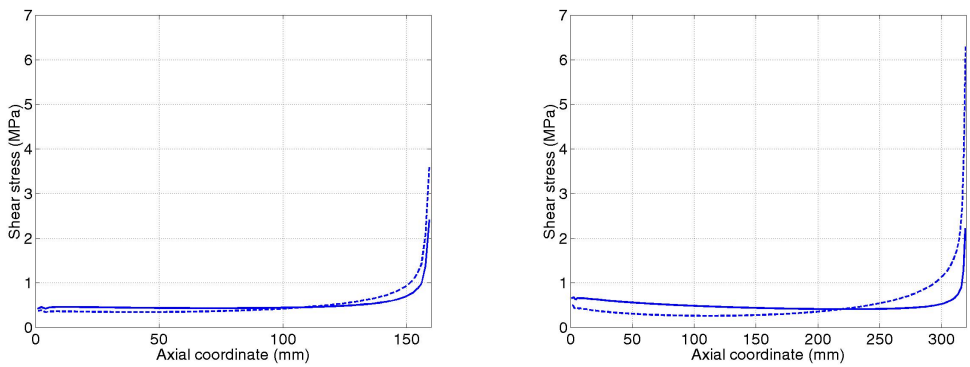

Figure 30. Linear elastic shear stress distributions for 3P-bending (solid) and for pull-pull(dashed). All curves correspond to an average shear stress of 0.5 MPa. l_g=160 mm (left) and l_g=320 mm (right). 90° load-to-grain angle.

4 RESULTS OF THE WORK CARRIED OUT – WP1.2

4.1 Remarks on testing for fracture mechanical properties

In WP1.2, one of the goals is to perform stable tests of small glued-in rods. For the test performance to be stable, i.e. a test including a possibly descending branch of the stress-slip relation, the test set-up needs to fulfil certain requirements. When the strength of the material tested is reached, softening begins and a localised failure develops. In order to achieve stability, the relaxation of the material surrounding the fracture process zone must correspond to the deformation developing during cracking. Stable test performance of softening materials thus requires displacement control as well as considerable stiffnesses outside the fracture process zone. The stiffness outside the fracture process zone includes the test specimen, its attachment to the testing machine, and the testing machine itself, including the load cells, grips, etc. Another way of expressing the stability requirement is to state that when the material softens, i.e. when the force applied by the testing machine decreases during the increase in deformation, the strain energy released outside the fracture process zone needs to be smaller than the energy required to extend the fracture zone.

4.2 Goals

The goals of "WP1.2 – Bondline tests of mechanical properties", are to perform stable tests on small bondlines and record their strength, stiffness, work to failure and the shape of the stress–displacement curve (including its descending branch after peak stress). If these goals are met the results can be fitted into a constitutive model based on nonlinear fracture mechanics theory. This model will be used to perform numerical simulations by the finite element method. Such simulations are necessary to check and calibrate the analytical expressions for the pull out strength being derived in WP1.1.

4.3 Test series

The original testing plan for WP1.2 contains a total of 50 tests on different combinations of glue (PRF, PUR and EPX), timber quality (C35 and C24), grain to load angle (0°, 22.5°, 45° and 90°), and adherents (steel and glass fibre). For all 3 glues the following combinations of these are tested: steel-wood (C35), 0°; steel-wood (C24), 0° (2×3 series). In addition to this, one of the adhesives was to be tested for the other load to grain angles (wood C35) and also a series with a glass-fibre reinforced polyester (FRP) rod (wood C35, 0°) (4 series). It was decided to change the adhesive type regarded as reference case from the PRF, which turned out to behave somewhat unexpected with no adhesion to the steel, to the EPX. In total the main tests includes 10 series of different test configurations. Each such series consists of five nominally equal tests–a total of 50 tests. The test series to be performed in WP1.2 are summarised in Table 9.

Table 9. Test series in WP1.2.

Description	PRF	PUR	EPX
steel/wood, C35, 0°	×	×	×
steel/wood, C24, 0°	×	×	×
steel/wood, C35, 22.5°	(×)		×
steel/wood, C35, 45°	(×)		×
steel/wood, C35, 90°	(×)		×
FRP/wood, C35, 0°	(×)		×

4.4 Sample preparation

4.4.1 General remarks

In testing for mechanical properties of e.g. an adhesive bond line, two markedly different approaches can be used:

- take the structure for which the properties are to be determined, and cut out a representative test specimen of appropriate size and shape, or
- prepare a test specimen of the size required in the test.

The two approaches have their respective advantages and disadvantages. The first approach is appealing since a test specimen is cut from a larger structure, which has been manufactured in the same way as in practice. For the present application this approach would mean that a long full-length rod is glued into a glulam beam and then cut (sliced) into pieces of appropriate size. If this approach is used the gluing in of the rod and the curing of the adhesive will take place under circumstances which are the same as those for all other specimens in the project. The major drawback of this method is that the sample preparation following the initial gluing in of the rod might damage the specimen in such a way that the subsequent testing gives results that are not representative for uncut glued-in rods. Another drawback, not so serious though, is that the sample preparation i.e. the cutting of the specimens can be somewhat difficult to perform since it requires special sawing facilities.

The second approach is a more standard approach, at least for pure mechanical testing of materials. In the present context this approach would mean that a "rod" of small length is glued into a small wood piece. Producing a specimen using this approach can cause several problems. Firstly the question arises whether the gluing and curing conditions of the adhesive are the same as for full-length rods. Using a short glued in length it is impossible to obtain a high pressure in the bondline during curing. It is also difficult to ensure a centrally placed rod. The gluing of a short rod means also that boundary effects in the curing might have an impact on the result (forming of CO_2-bubbles in PUR).

4.4.2 Materials and climate conditions

Both the above-described methods of producing test specimens have been used. These two methods are here after termed I and II.

All samples were prepared using wood pieces cut from glulam beams taken from the same shipment as the rest of the glulam used in GIROD. The glulam beams were stored in standard climate 20°C, 65%RH. The gluing and curing as well as the storing of the finished specimens was also done in this climate. All specimens were cured for at least 7 days prior to testing.

4.4.3 Pre-tests - series I

In the first pre-test series the approach of type I was tested. The cutting of the wood/rod into slices results in high temperatures in the steel, which in turn might affect the bondline. Therefore it was decided to use threaded glued-in tubes instead which proved to reduce the heat development considerably. A glulam beam of 120×120 mm^2 cross section was used. In this three holes with a diameter of ϕ=17 mm and a length of 165 mm were drilled parallel to the grain. The three adhesives to be tested were mixed according to the manufacturers instructions and the adhesives were poured into the holes using syringes. Three threaded (M16) tubes (inner diameter of 12 mm) were plugged (to avoid the glue to fill the tubes) and then pressed into the holes, letting the excessive amount of glue flow out of the hole. The specimens were left to cure for at least 7 days prior to any further processing. After curing the glulam beam with the glued-in tubes

was placed in a sawing machine, which is originally used to cut steel of large dimensions. The glulam beam with the rods was then sliced into 10mm thick slices of 120×120 mm^2. From this slice three specimens (48×48mm^2) were cut using an ordinary wood band saw. The sample preparation is schematically shown in Figure 31. Due to low accuracy of the sawing it was found that it was necessary to machine the slices to get smooth surfaces.

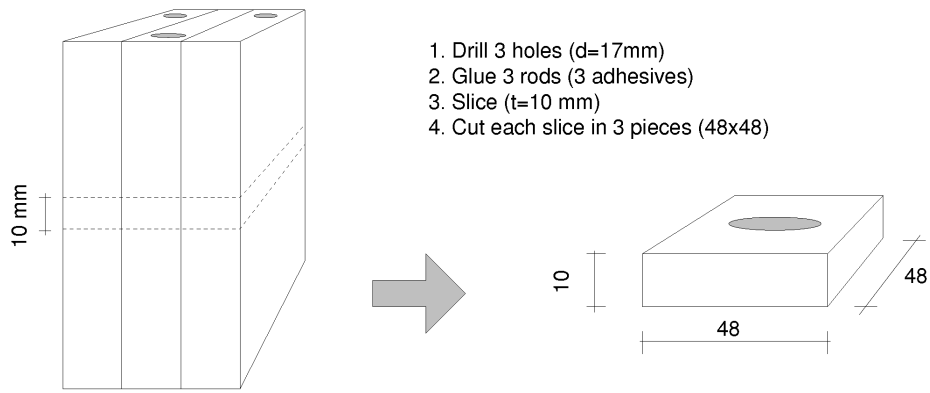

Figure 31. Preparation of specimens type I.

4.4.4 Pre-tests - series II

Due to the results obtained with the type I specimens it was decided to perform a test series with type II specimens. The glulam beam of cross section 120×120mm^2 was split into four pieces of 48×48 mm^2. Each such piece was then cut to a thickness of 20 mm (test series IIa) or 40 mm (test series IIb). In each test piece a hole of ϕ=17 mm was then drilled through the entire piece. From a threaded rod (M16), strength class 8.8, 90 mm long specimens with a threaded length of 8 mm were cut. In Figure 32 a schematic of the bolt and the way the wood pieces were cut is shown. After drilling the holes in the wood pieces, the holes were partially filled with "Tack-It" (kind of synthetic clay used to fix posters etc.) and a 0.5 mm Teflon film. An 8 mm deep hole was left for the threaded rod. Adhesive was poured into the holes and the rods placed in the holes. To ensure a good filling out of the cavities of the threads, glue was also spread on the bolts' thread. All specimens were cured for at least 7 days prior to testing. After curing of the adhesive the synthetic clay and the Teflon film was removed from the hole.

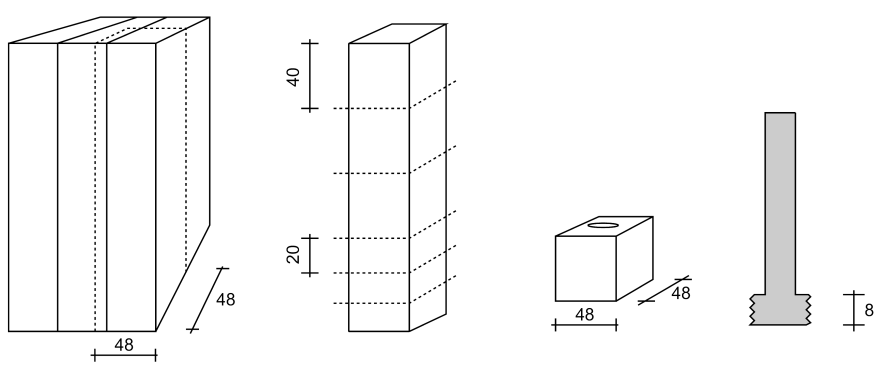

Figure 32. Preparation of specimens type II.

4.4.5 Main series

Since the results from the pre-tests using the type II specimens turned out promising, the main test series was performed using this specimen type, with minor changes. A fixing and guiding device was manufactured to make the gluing of the specimens more accurate and less time-consuming. In order to assure a centrally placed bolt in the drilled hole three metal clips were pressed into the synthetic clay so that the bolt was securely fixed in the center of the hole. The same principle for sample preparation was used for the tests performed on the FRP rod. The nominally 16 mm diameter rods were cut in 90 mm long pieces and were then machined to 12 mm diameter except for the 8 mm at one end. The FRP rods have a smooth surface and to improve the adhesion of the glue, they were lightly sanded by hand and then wiped clean using a cloth soaked with alcohol.

Three additional load to grain angles were tested for the material combination of EPX-adhesive and steel rod. These specimens were cut out so that the load to grain angle was 22.5°,45° and 90° respectively. In order to obtain specimens with uniform properties, each group of nominally equal specimens were cut from a single glulam lamination. This means that the 90° specimens, for instance, were cut almost in the radial direction, cf. Figure 33.

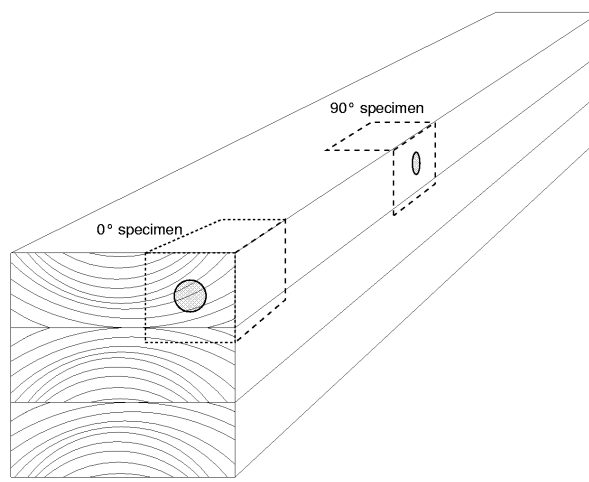

Figure 33. Schematic of specimen cut-out for two load to grain angles.

4.5 Test set-ups and testing conditions

4.5.1 General remarks

All tests were performed using displacement control so that the softening behaviour of the bondline could be recorded.

The pre-test series were performed with various speed to find a suitable testing speed, so that the peak stress was obtained within a few minutes and the total time for a test was approximately 7-10 minutes. This resulted in the tests being performed using an initial cross-head speed of 0.001-0.005 mm/s. The speed of the cross-head was manually increased after peak stress so that the final cross head speed was 0.01-0.05 mm/s.

The testing machine used is a hydraulic MTS closed loop system. The force applied and the displacement of the crosshead of the machine was measured in all cases.

The testing took place in normal room climate, and the specimens were kept in plastic bags, to avoid them from drying.

4.5.2 Pre-test series I

In Figure 34, a schematic of the set-up used in the pre-tests series I is shown. The set-up consists of a specimen holder made of steel with two grips, which prevents the specimen edges from lifting when load is applied. A steel cylinder was mounted in the hydraulic grips of the testing machine. The cylinder has a smaller diameter at the one end, allowing the edge of the steel tube glued into the wood to come in contact with the cylinder (Figure 34–left).

4.5.3 Pre-test series II

For pre-test series II the glued-in bolt was mounted directly in the hydraulic grips (Figure 34–right). For some of the tests, the deformation was measured using an LVDT. This was mounted inside the specimen holder, cf. Figure 34. However, it turned out that the difference in measured displacement was negligible, and the LVDT was not used in the main test series.

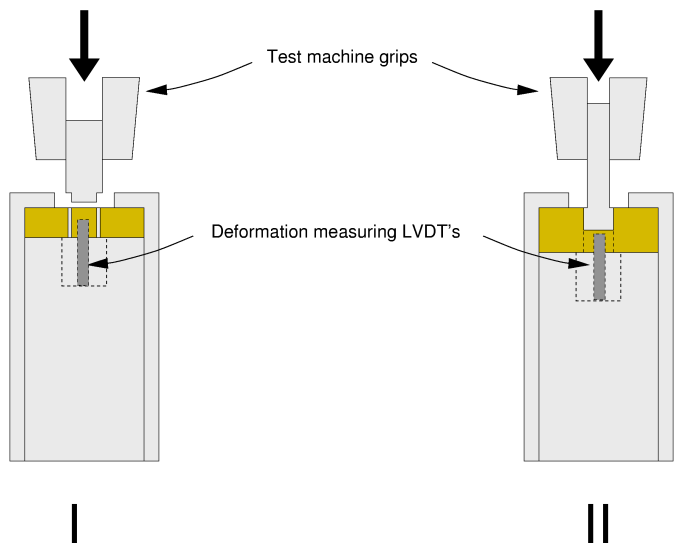

Figure 34. Test set-ups used in pre-test series I and II.

4.5.4 Main series

For the main series it was decided not to use the specimen holder, since the pre-test series II showed that the LVDT measurements gave the same result as measuring the displacement of the crosshead of the testing machine. The test specimens were instead placed on a self-aligning plate which in turn was fitted into the lower hydraulic grips of the testing machine. The self-aligning plate was used in order to achieve a more uniform stress distribution at the contact surface. A schematic of this set-up is shown in Figure 35.

The initial speed of the loading was set to 0.003 mm/s (cross-head speed). After a 40% load drop after peak load the loading speed was gradually increased so that each test was completed after 7-10 minutes. The final speed was set to be 0.03 mm/s.

In addition to the original plan, including five nominally equal test for every material combination, it was decided to investigate the characteristics at unloading after peak stress for one

specimen. Here, unloading means decreasing deformation. The unloading sequence of these tests was automatically initiated by the software of the test system. The unloading was set to take place after a 20% load drop. After the unloading sequence was completed a new loading sequence was run until complete failure of the specimen was achieved.

The density and the moisture content was also determined for the specimens. This was done by cutting small pieces of the wood, in the vicinity of the bondline, and weighing them in air and under water. This was done after the specimens had been stored at standard climate 20°C/65% RH. Following this the specimens were dried at 105°C for 24 hours and then weighed. The density values reported are calculated as (dry mass)/(volume at 20°C, 65RH).

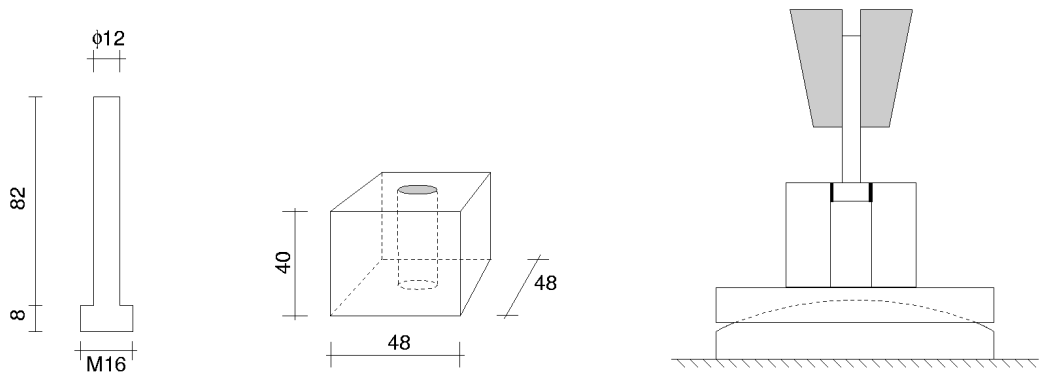

Figure 35. Specimens and set-up used in main test series.

4.6 Methods for the evaluation of test results

4.6.1 Strength and work to failure

From the tests it was straightforward to evaluate the strength of the bond (load divided by nominal area), and to integrate the stress-displacement curve to obtain the work to failure. Doing so it was assumed that the fracture area was equal to the area of a cylinder of 16 mm diameter. In the main series, the length of the fracture surface was measured after the tests were completed. For the pre-test, however, the length of the fracture surface was estimated from the nominal bondline length aimed at the manufacturing of the specimens.

The parameters obtained in this way are not likely to represent the local strength and fracture energy of the bond. Firstly, although a small glued in length has been used, the stress distribution is not completely uniform and there is also possibly peel stress present during the test. Secondly, the work to failure is mainly due to friction, after local fracture has taken place. The PRF bonded specimens failed at the thread-adhesive interface and, bearing in mind that the pitch of the used thread is 2 mm, it is obvious that the PRF-bondline has fractured completely after a deformation in the range of 0.5–1.0 mm. The remaining load-bearing capacity is therefore completely due to friction.

To overcome the difficulties in test evaluation a trial and error approach using nonlinear FE-simulations of the tests can be used. This is performed by fitting local bond strength (shear *and* peel strength) and fracture energies until the test results (strength, energy and shape of curve) can be reproduced numerically.

4.6.2 Brittleness and initial stiffness of the bondline

Instead of using the area below the stress displacement curve as a measure of the fracture energy of the bond, the initial slope of the descending branch can be used. This slope is the critical one for stable response. Furthermore, for structural-sized bonds, the total deformation before collapse is rather in the range of 1–2 mm than 8–10 mm, which was the typical total deformation at complete failure for most specimens. The remaining energy "consumed" during the small specimen tests is due to friction after the fracture has taken place and is therefore not a parameter needed for a structural sized specimen. The approach of using the initial negative slope of the descending branch is shown in Figure 36. Note that the initial elastic response of this curve has been subtracted, so that the displacement now corresponds to the relative slip across a bond interface of zero initial width.

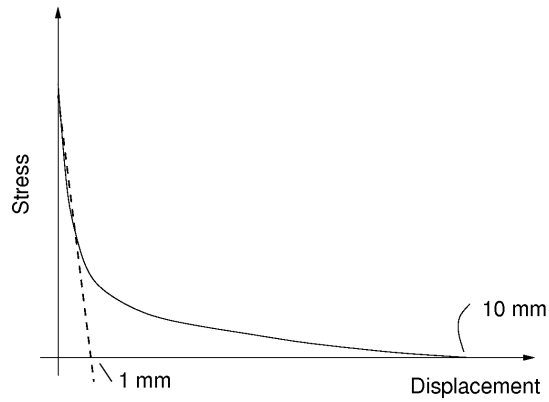

Figure 36. An example of how to evaluate the test results.

To estimate the initial stiffness, all slopes from zero to maximum load were calculated using least square fits, for intervals including approximately 25% of the maximum load. As initial stiffness, the steepest slope was taken. Figure 37 shows the results from the evaluation process for one of the PRF specimens. Three curves are shown. One represents the recorded test data with the load divided by the nominal shear area. It can be seen that, initially, the slope of the curve increases, probably due rough contact surfaces and initial movement of the self aligning plate of the test set-up. Following this initial nonlinear region, an almost perfectly linear part is found, followed by nonlinearities close to peak stress, probably due to an initiating fracture and possibly plasticity.

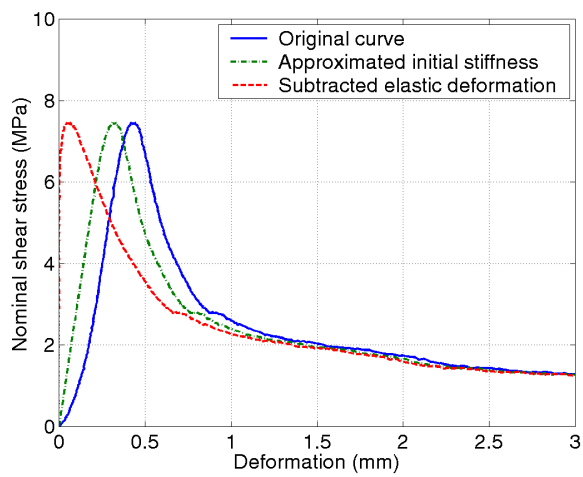

Figure 37. An example of the evaluation of the initial stiffness.

After the elastic deformations have been subtracted, the same algorithm was used for the descending part of the curve and the corresponding steepest slope was used as a measure of the softening characteristics.

4.7 Test results - pre-tests

4.7.1 General remarks

The pre-tests were performed on wood of both strength class C35 and C24, referred to as A and B in the following. The different adhesives are termed PR, PU and EP for the phenol-resorcinol, polyurethane and epoxy respectively. Each specimen is also given a number representing its original position (along grain) in the glulam beam. In the following tables the strength and the work to failure is given for every specimen tested. The work to failure is calculated as the area below the stress-displacement curve.

4.7.2 Pre-test series I

A total of 29 tests were performed in this series of which 21 are reported here and 8 were rejected. The 2 first tests were performed with a different test set-up involving a steel ball, which unfortunately gave a rotation of the bolt. 6 tests with PUR-adhesive and the low-density wood gave wood failures due to punching shear of the specimen at the edge of the hole in the test set-up.

The results are summarised in Table 10. The failure modes reported correspond to: 1–mainly failure in the adhesive (crushing of the threads in the adhesive layer) and 2–failure in the interface region of the wood-adhesive layer. The type 1 failure was only seen for the PRF-adhesive. For type 2 failures no significant difference between the PUR and EP-adhesives was found. The remarks U and (U) represent unstable and partially unstable response (i.e. an instantaneous drop in load) respectively. The remark P means that the peak stress was recorded at a plateau value. As an example of the test response and remarks in the table, the response from the test AEP07 is shown in Figure 38.

Table 10. Test results for series I.

Name	Strength (MPa)	Work to failure (kJ/m^2)	Failure mode
APR04	4.9	13.2	1
APR05	5.1	7.1	1
APR06	7.0	7.0	1
APR07	7.0	8.9	1
APR08	6.9	8.9	1
APR10	6.8	12.0	1
Mean	*6.3*	*9.5*	–
COV	*16%*	*27%*	–
APU02	6.4	7.1	2,U
APU03	4.9	5.0	2, (U)
APU04	6.6	6.4	2, (U)
APU05	4.4	7.3	2,P
APU06	3.7	6.4	2, P
BPU02	4.6	4.6	2
Mean	*5.1*	*6.1*	–
COV	*23%*	*18%*	–
AEP02	6.6	8.5	2, U
AEP03	5.3	6.2	2
AEP04	5.7	10.8	2, U
AEP05	7.8	7.0	2
AEP06	6.2	6.7	2
AEP07	4.0	7.6	2, P, (U)
AEP08	6.5	5.2	2
AEP09	7.3	6.2	2, (U)
Mean	*6.2*	*7.3*	–
COV	*19%*	*24%*	–

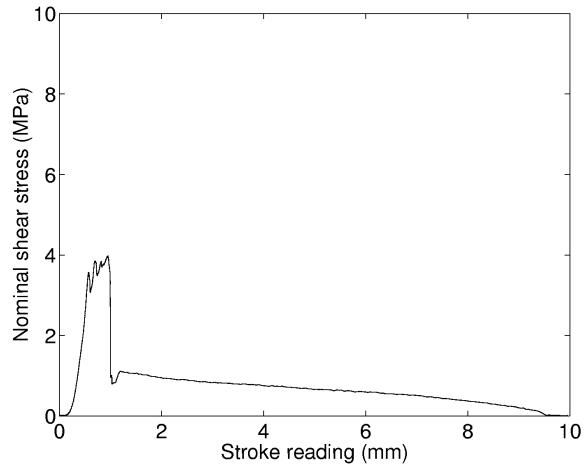

Figure 38. An example of test response for series I, showing cut off of peak stress (plateau value) and unstable response (the sudden drop at 1 mm deformation).

4.7.3 Pre-test series II

A total of 12 tests were performed, all with the PRF-adhesive. Of these tests, 6 were performed using the specimen thickness 20 mm (series IIa) and 6 with the specimen thickness 40 mm (series IIb). Two test were rejected in series IIa due to the bolt not being glued into the wood piece perfectly parallel to the loading direction. These test specimens also showed considerably lower strength than the others did. One test in series IIb was rejected due to unstable test performance during loading.

In Table 11 the results are summarised following the convention of names and remarks of above. As a typical example from these tests, the response curve of specimen APR21 is shown in Figure 39.

Table 11. Test results for series II.

Name	Strength (MPa)	Work to failure (kJ/m^2)	Failure mode
APR11	8.4	13.8	1
APR12	9.2	13.5	1
APR14	8.3	12.8	1
APR15	8.4	11.6	1
APR17	10.2	15.6	1
APR18	9.5	16.1	1
APR19	8.7	14.2	1
APR20	9.3	14.7	1
APR21	8.5	15.2	1
Mean	*8.9*	*14.2*	–
COV	*7.3%*	*9.9%*	–

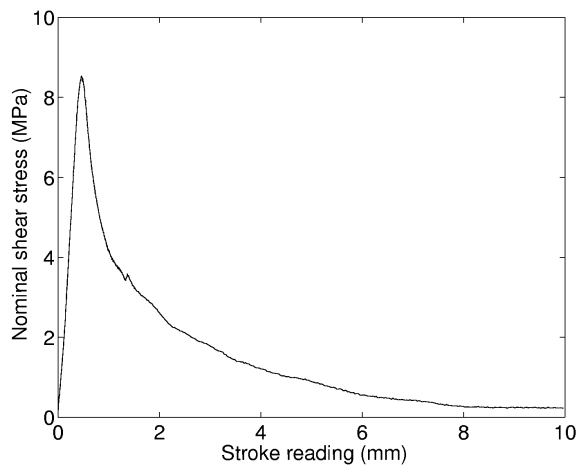

Figure 39. An example of test response in test series IIb.

4.8 Test results - main test series

4.8.1 General remarks

A total of 62 test were performed of which 61 are reported here. The test rejected was one of the FRP-specimens which failed in the rod itself, probably due to damage caused to the rod in the manufacturing of the specimen. The tests are named according to

A: Steel/timber C35/0º load to grain angle/three adhesives,

B: Steel/timber C24/0º load to grain angle/three adhesives,

C: Steel/timber C35/various load to grain angles/epoxy, and

D: FRP/timberC35/0º load to grain angle/epoxy

The different combinations and their corresponding names are shown in Table 12. For each nominally equal material combination, 5 replicates were performed with monotonically increasing deformation of the testing machine's crosshead. In addition, for each material combination, one test was performed with unloading of the specimen in the softening region, after peak stress.

Table 12. Main test series. Tests performed and naming convention.

Rod / timber/angle	Phenol resorcinol	Polyurethane	Epoxy
Steel/C35/0º	APR	APU	AEP
Steel/C24/0º	BPR	BPU	BEP
Steel/C35/22.5º	-	-	CEP
Steel/C35/45º	-	-	CEP
Steel/C35/90º	-	-	CEP
FRP/C35/0º	-	-	DEP

4.8.2 Test results

The test results are summarised in Table 13 and given in detail in Appendix A. The table gives the average density, strength, initial elastic slope, negative slope after peak stress and work to failure.The strength and initial elastic slope statistics are all based on 6 replicates, while the other statistics are based on 5 replicates since the unloading part of the curve complicates the evaluation of these quantities. The statistics from the FRP-rod tests are based on 7 and 6 tests respectively.

The work to failure can be regarded as an attempt to assess a measure of the ductility of the specimen. However, the load displacement response reveals that a large amount of the work to failure is due to friction in the fracture zone and therefore this work to failure is not a good measure of the bondline fracture energy. Instead the slope of the initial descending part of the stress-displacement curve is used as a ductility measure. The reason for this is discussed in more detail in Section 4.6, where also the methods for evaluating the slopes are described.

In Appendix A, the results from individual tests are reported, and in Appendix B the stress-displacement curves are given, for clarity in two different scales.

Table 13. Test results from main series, average values.

Rod/timber/ adhesive/angle	Density (kg/m^3)	Moisture content (%)	Strength (MPa)	Elastic stiffness (MPa/mm)	Negative stiffness (MPa/mm)	Work to failure (kJ/m^2)
Steel/C35/PRF/0°	449	14.4	7.1	24	9	11.8
Steel/C35/PUR/0°	492	13.2	10.5	72	62	9.6
Steel/C35/EPX/0°	462	12.8	13.1	74	60	22.0
Steel/C24/PRF/0°	348	12.8	6.2	21	7	14.4
Steel/C24/PUR/0°	368	13.1	10.6	70	62	8.0
Steel/C24/EPX/0°	341	12.7	11.0	55	52	21.4
Steel/C35/EPX/22.5°	454	13.8	12.8	55	48	23.5
Steel/C35/EPX/45°	429	13.3	10.7	35	28	24.9
Steel/C35/EPX/90°	461	13.5	7.1	12	3	24.9
FRP/C35/EPX/0°	451	13.5	11.8	48	44	28.1

4.8.3 Failure modes

The failure modes obtained in the main test series are of three types, each typical for one type of adhesive:

1. Failure in the adhesive at the threading of the bolt. This failure mode was obtained only for the PRF adhesive at about 75-100% of the fracture area. The remaining fracture area showed a wood interface failure.
2. Failure in the adhesive close to the wood. This failure was obtained only for the PUR specimens at 100% of the fracture area.
3. Failure in the wood in the vicinity of the adhesive. Note that this wood failure is not characterised by a large plug being pushed out, but rather by a wood interface failure due to a weak boundary layer. This failure type was obtained only for the EPX specimens. For the 0° load to grain angle tests there was a fairly large amount of wood fibres visible on the adhesive after failure. For the other load to grain angles the fracture surface was almost free from fibres.

In Appendix C, some photos of different specimens show examples of the three failure modes. As opposed to the results in the pre-tests there was a consistent difference in failure modes for the three adhesive types. The reason for these distinctively different failure modes can be explained as follows.

For the PRF adhesive the bad adhesion to the steel in combination with a tendency of shrinkage at curing, leads to an initial lack of fit between the adhesive and the threads of the bolt. This results in stress concentrations at the thread/adhesive interface and also a low initial stiffness of the joint. The large stress concentrations lead to the failure at the bolt/adhesive interface region. From the stress-displacement curves it can also be seen that there is a considerable amount of frictional work performed during the test. The pitch of the threads used (M16) is 2 mm and since the failure takes place at the tip of the threads, an approximately 1 mm deformation implies that the bond line has come to a complete failure.

The curing of the PUR adhesive relies on the possibility of taking up moisture from the adherents and the surrounding air. The chemical reaction forms CO_2 which causes some bubbles to form in

the bondline. In the case of low or no pressure at all during curing this bubble formation becomes intense. The failure surfaces of the PUR specimens had bubbles of sizes in the order of 0.1-0.5 mm. The bubble formation can be expected to be more intense at the free surface of the adhesive and at the wood interface were there is more moisture available. Thus the fracture surface would be located close to the wood/adhesive interface.

The EPX adhesive gives strong bondlines with good adhesion to both the steel, the wood and the FRP-rods. Therefore the failure is located in the wood which in this case is the weakest link.

4.8.4 Influence of adhesive type on strength and stress-displacement response

Based on the above discussion of the failure modes the strength of the adhesives should form a sequence showing increasing strength in the order of PRF, PUR and EPX. The mean strength as reported above also confirms this. In Figure 40 hand-drawn mean curves, one for each adhesive type shows the influence on the stress-displacement response of the adhesive type. The curves show the response with the elastic deformation subtracted.

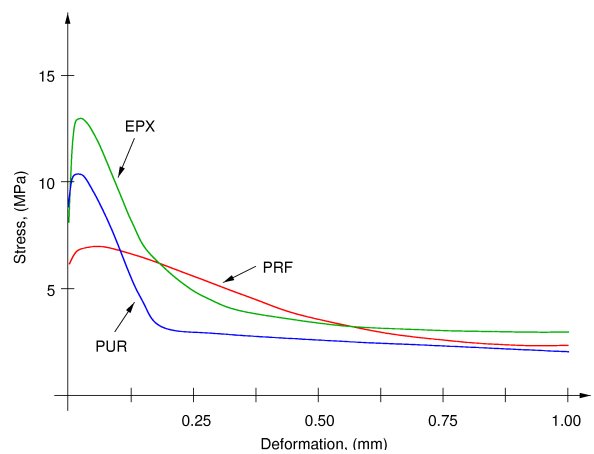

Figure 40. Mean stress-displacement curves showing influence of adhesive type.

4.8.5 Influence of wood density on strength

The influence of the wood density on the strength is complicated to assess, since the density of the wood can be expected to influence in at least three ways. Firstly it is often assumed that the density and the strength of wood are positively correlated, secondly a change in density could mean a change in adhesion to the wood, and finally a change of density can result in different modulus of elasticity which in turn can affect the strength of a glued-in rod due to change in stress-distribution. The influence of the density on the strength can be viewed in Figure 41, showing the strength of three groups of adhesives for the two groups of timber density tested. There is a statistically significant (0.05) difference in density between the two timber qualities, but this difference does only result in a significant (0.05) difference for the PRF and EPX adhesives. The mean densities were found to be 457.9 and 352.4 kg/m^3 for the C35 and C24 timber respectively,

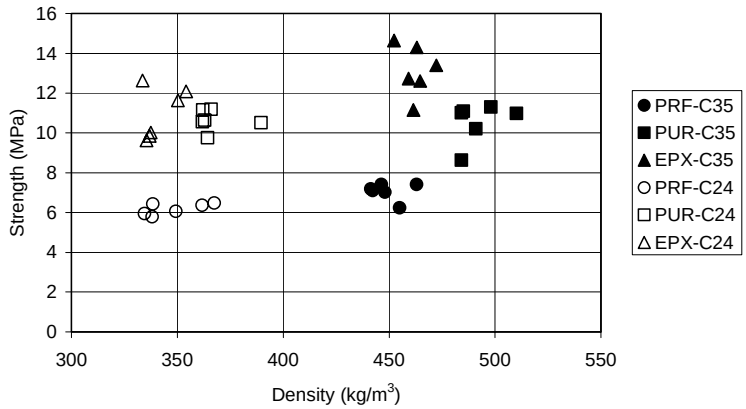

Figure 41. Influence of density on nominal shear strength.

4.8.6 Influence of load to grain angle on strength and stress-displacement response

The influence of the load to grain angle on the performance of the rod is of several different types. Changing the load to grain angle will affect the effective modulus of elasticity of the adherent, in terms of one dimensional theory. It is also probable that the adhesion of the glue the wood is different for different orientations. Finally it should be emphasised that a load to grain angle different from 0º will always result in parts of the wood being stressed in longitudinal shear (τ_{rl}) and some parts in rolling shear (τ_{rr}). Therefore the results from such a test will be some kind of average taken in the circumferential direction, both shearing modes being included. If the strength in longitudinal shear is much different from the strength in rolling shear, the fracture will be a propagating one (in the circumferential direction). Such a propagating failure will lead to an apparently ductile behaviour at a larger scale, i.e. at the scale at which the present tests are being monitored. Figure 42 shows the influence on the average strength for the four angles investigated for the EPX adhesive. Finally Figure 43 shows the influence on the stress-displacement response, with the elastic deformations subtracted.

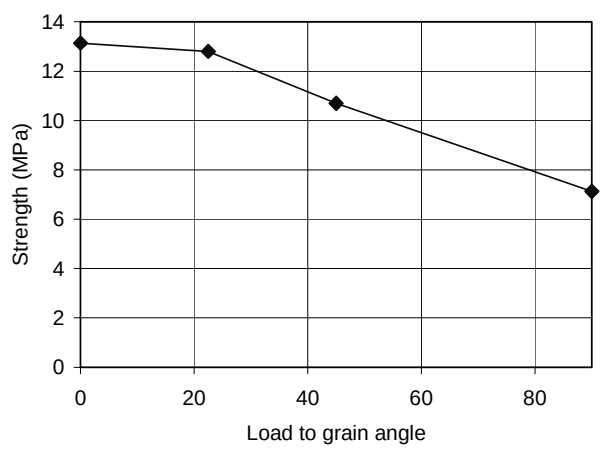

Figure 42. Influence of load to grain angle on strength (average values) . Epoxy adhesive.

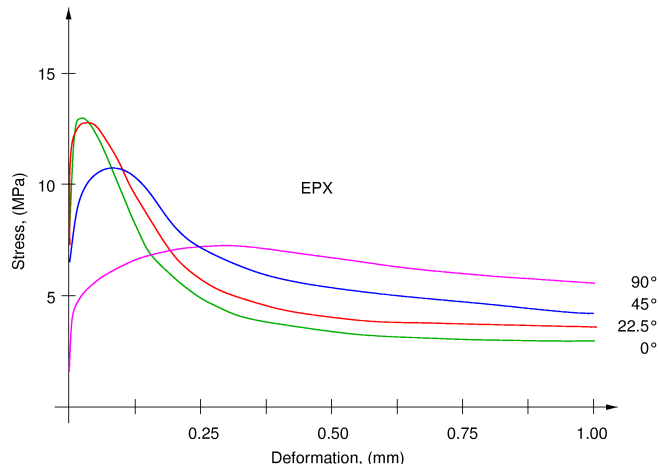

Figure 43. Influence of load to grain angle on stress-displacement response. Epoxy adhesive.

4.9 Test result summary

The results from the main series can be summarised as follows:

- The mean strength was found to be 7.1 MPa for the PRF, 10.5 MPa for the PUR and 13.1 MPa for the EP adhesive at 0º load to grain angle.
- The wood density was found to have a small effect on the strength of the PRF and EPX, but no effect on the strength of the PUR adhesive.
- The mean work to failure was found to be 11.8, 9.6 and 22.0 kJ/m^2 for the PRF, PUR and EPX adhesives respectively.
- The negative slope of the descending part of the stress-displacement curve, which is a measure of the brittleness of the bondline was evaluated for the three adhesives. It was found that the EPX and the PUR were the more brittle ones and that the PRF was more ductile.
- The load to grain angle was found to have a major influence on both the strength and the ductility. At 0º the average shear strength was 13.1 MPa and the other load to grain angles resulted in shear strengths of 12.8, 10.7 and 7.1 MPa for 22.5º, 45º and 90º respectively. The more ductile behaviour of the cross grain specimens is explained in part by a propagating (in the circumferential direction) failure mode.

5 RESULTS OF THE WORK CARRIED OUT – WP1.3

WP1.3 concerns short term ramp loading testing of glued-in rods conditioned at 65% RH. Some tests of WP1.3 are common with references tests of WP4 and WP5. Many of the tests results of WP7 [7], obtained by partner SP, may be used together with the test results of WP1.3 for verification and calibration purposes.

Project partner FMPA has co-ordinated the work of WP1.3 and a detailed Technical Report has been provided by FMPA, including, empirical equations for the influence rod length and diameter. Partner FMPA has also carried a large number of additional tests outside the GIROD project, but very closely related to the GIROD tests [1, 2].

The dimension of the glulam specimens are indicated in Table 14, where l_g is the glued-in length. The centric tensile load applied to the rod was for the specimens loaded parallel to grain counteracted by a tensile loading of a rod glued-into the opposite end of the specimen. The counteracting rod had glued-in length of 1.2 l_g and its diameter was 1.5 times the diameter of the tested rod. The rods were glued in the centre of the specimens.

In Table 15 the characteristics of the specimens are given together with mean and COV of the pullout strengths. Please note that the nominal shear strengths are calculated as $P_f/(\pi d l_g)$. They could alternatively be calculated for a cylinder with the diameter of the hole, i.e. for the diameter d+1mm. The number of tests in each series was 7.

Table 15 shows for the 0 degree specimens also the density of the wood in the lamella, or in the two lamella, in which the rod was placed. The density was determined for a piece of length 1.2 l_g, cut after the ramp load testing from the middle of the specimen. In case of a finger joint in the test piece, its length was reduced so that the joint became excluded. The mean moisture content was 11.7% and the standard deviation of the moisture content was 0.7%.

The mean value of the COV from 24 test series is 9%. For the PRF-series with the rod along grain the mean COV is 8%, for the PUR-series with the rod along grain it is 10%, for the Epoxy-series with the rod along grain it is 13% and for test series with the rod at some angle to grain it was 7%.

Table 14. Dimensions of glulam.

Specimens	Dimensions of glulam (b×h×l) [mm^3]	Number of lamellae	Thickness of lamella [mm]
d=8mm, rod angle 0^0	70×70×3.6l_g	2	35+35
d=6mm, rod angle 0^0	120×120×3.6l_g	3	37.5+45+37.5
d=30mm, rod angle 0^0	210×210×3.6l_g	5	37.5+3×45+37.5
Rod to grain angle > 0^0	120×450×2400	10	10×45

Table 15. Results of WP1.3. Pull-out strength test results obtained at ramp loading of specimens conditioned at 65%RH.

Series	Partner that did the testing	d [mm]	l_g [mm]	Glue	Wood	Density,ρ_{12} [kg/m^3]	Rod	Angle	P_f [kN]	$\tau_{bond}=P_f/(\pi d l_g)$ [N/mm^2]	
										Average	COV(%)
2.1/r	SP	16	320	PRF	C35	-	ste	22.5	94.5±7.8	5.88	8.3
2.2/r	TTL	16	320	PRF	C35	-	ste	45	103.6±7.3	6.44	7.0
2.3/r	TTL	16	320	PRF	C35	-	ste	90	103.4±5.1	6.43	4.9
2.4/r	TTL	16	160	PRF	C35	-	ste	90	50.9±6.3	6.33	12.4
2.5/r	FMPA	8	80	PRF	C35	483±27	ste	0	12.7±1.7	6.32	13.4
2.6/r	FMPA	8	160	PRF	C35	447±12	ste	0	31.3±1.6	7.78	5.1
2.7/r	FMPA	8	320	PRF	C35	476±22	ste	0	40.5±1.5	5.04	3.7
2.8/r	FMPA	16	80	PRF	C35	451±13	ste	0	24.1±2.4	5.99	10.0
2.9/r	FMPA	16	160	PRF	C35	468±37	ste	0	55.3±2.8	6.88	5.1
2.10/r	FMPA	16	320	PRF	C35	470±17	ste	0	101.7±5.1	6.32	5.0
2.11/r	FMPA	16	640	PRF	C35	473±59	ste	0	144.1±10.99	4.48	7.6
2.12/r	FMPA	30	150	PRF	C35	446±25	ste	0	60.5±4.6	4.28	7.6
2.13/r	FMPA	30	300	PRF	C35	451±56	ste	0	142.3±20.2	5.03	14.2
2.14/r	FMPA	30	600	PRF	C35	427±52	ste	0	280.4±17.1	4.96	6.1
2.15/r	FMPA	16	320	PUR	C35	511±41	ste	0	92.7±5.8	5.76	6.3
2.16/r	FMPA	16	320	EP	C35	517±40	ste	0	103.6±11.7	6.44	11.3
2.17/r	FMPA	16	320	PRF	C24	487±28	ste	0	102.3±8.2	6.36	8.0
2.18/r	FMPA	16	320	PUR	C24	492±34	ste	0	93.3±22.5	5.80	24.1
2.19/r	FMPA	16	320	EP	C24	520±28	ste	0	96.6±9.8	6.01	10.1
2.20/r	TTL	16	160	PUR	C35	-	gla	0	-	-	-
2.21/r	TTL	16	160	PUR	C35	-	ste	90	63.9±2.9	7.95	4.5
2.22/r	FMPA	16	160	PUR	C35	488±45	ste	0	68.3±6.5	8.49	9.5
2.23/r	FMPA	8	160	PUR	C35	480±23	ste	0	31.4±3.4	7.81	10.8
2.24/r	FMPA	16	160	EP	C35	437±37	ste	0	57.3±10.8	7.12	18.8
2.25/r	FMPA	8	160	EP	C35	478±21	ste	0	28.5±2.9	7.09	10.2

6 RESULTS OF THE WORK CARRIED OUT – WP1.4

6.1 Introduction

In section 6.2 a design method and equation for the basic short-term ramp loading pull-out strength is proposed. In section 6.3 that proposal is compared with test results. The proposal given in 6.2 is just one example of a possible rational design equation. In section 6.4 modifications that give alternative design equations are briefly discussed.

Section 6.5 presents results of FE-analysis of the particular specimens tested. Both the small size bond line test specimen and some of the full scale glued-in rod specimens are analysed. The FE-results are compared with the corresponding test results.

6.2 A proposal of design method and design equation

6.2.1 Basic goals

The idea before proposal of a strength design method for the basic pull-out strength at short time ramp loading at constant climate was to find some method such that:

- The method is both general and simple, preferably just one or a few explicit equations.
- The equations should have a rational theoretical and physical basis.
- The method should give reasonably accurate strength predictions, and in average and in general give predictions on the safe side.

6.2.2 Outline of proposal

The combined Volkersen-Fracture mechanics theory is used as the basis. The pullout strength is according this theory determined by the geometry of the joint and by two material property parameters[1] that depend on the properties of the materials involved: the rod material and its surface texture, the adhesive and its thickness, and the wood and its orientation.

It is proposed that the two material parameters are determined by testing the pullout strength of two sets of full-scale joints with different geometry. The joints tested should be loaded in "pull-compression".

Given the two material parameters, the equation for the "pull-compression" loading is used also for "pull-pull" and "pull-distributed", the later type of loading (combined with other loading) referring to a rod being glued perpendicular into a beam. This gives a single and simple design equation, which according to theory gives "exact" predictions for the first type of loading and predictions on the safe side for the other two types of loading.

The above proposal is intended for adhesives that have some bond also to the rod. It is probable that some such bond is achieved as long as the shrinkage of the glue is reasonably small. For other adhesives, like the PRF tested in the GIROD-project, no equation that fulfils the above basic goals has yet been found. For such adhesives it is proposed that testing is made as for the common adhesives, but no design equation is given, only a design rule saying that the load

[1] To be accurate there are three material property parameters, the third being E_f/E_w, i.e. the ratio of modulus of elasticity of the rod material and the wood. According to the theory adopted here, the value of this ratio is however of minor significance for joint strength and assigning it a constant value makes it possible to separate the joint geometry parameters from the joint material parameters. In this proposal ratio E_f/E_w is throughout set equal to 18 for loading along grain and 540 for loading perpendicular to grain.

bearing capacity of joints with greater or equal rod diameter or greater or equal length may be assigned the same load bearing capacity as the tested joint.

6.2.3 Basic equation for design and test result evaluation

For the loading case pull-compression, from eq (29) in section 3.3.6

$$\frac{P_f}{\pi d l} = \tau_f \frac{\tanh \varpi}{\varpi} \tag{92}$$

where

P_f is the pullout strength [e.g. in N],

πdl is the bond area [e.g. in mm^2],

τ_f is the local bond line shear strength [e.g. in N/mm^2]

and

$$\varpi = \sqrt{\frac{l_{geo}}{l_m}} \tag{93}$$

where l_{geo} is a length parameter, which, apart from the influence of ratio E_r/E_w, is defined by the geometry of the joint:

$$l_{geo} = \frac{\pi d l^2}{2}\left(\frac{1}{A_r} + \frac{E_r / E_w}{A_w}\right) \tag{94}$$

and l_m is a material property length parameter, which can be expressed as:

$$l_m = \frac{E_r G_f}{\tau_f^2} \tag{95}$$

The two parameter to be determined from tests are τ_f and l_m. (It is thus no necessary to separate l_m into E_r, G_f and τ_f, although this in general is simple since E_r in general is known). Ratio E_r/E_w may in general be estimated without having to test the adherend materials. In the present

evaluation of test result obtained for steel rods glued-in along the grain direction of the wood ratio E_r/E_w is throughout made equal to 18.

6.2.4 Further notations used in this proposal

d is the diameter of the fracture surface area

d_r is the nominal diameter of the rod

l is the glued-in length of the rod

A_r is the cross section area of the rod

A_w is the cross section area of the wood as defined in the below section.

E_r is the elastic modulus of the rod material in the direction of the rod (e.g. in N/mm^2)

(information about E_r is not needed)

E_w is the elastic modulus of wood in the direction of the rod (e.g. in N/mm^2).

(information about E_w is not needed)

G_f is the glued-in-rod bondline fracture energy (e.g. in Nmm/mm^2)

(information about G_f is not needed)

f_v is short for $P_f/(\pi dl)$

6.2.5 Definition of A_w

For a square shaped cross section with a centric location of the rod $A_w = a^2$, where a is the side length of the square. For other geometry $A_w = a^2$, where $a/2$ is the shortest distance from the centre of the rod to an edge of the cross section. (The effect of reduction of the cross section area due to the hole is negligible as a result of rules for minimum edge distance.)

This shortest edge distance, $a/2$, may not be less than a distance determined in WP3, presumably $4d_r$.

Rod spacing and the calculation of A_w in the case of several glued-in rods in a joint will given in other part of code.

6.2.6 Limitation of the glued-in length, l

The minimum anchorage length (the minimum glued in length) should be taken as

$$\boldsymbol{l}_{\min} = \max\begin{cases} \boldsymbol{d_r}^2 / \boldsymbol{d_o} \\ 8\boldsymbol{d_r} \end{cases} \qquad (96)$$

where $d_0 = 2.5\ mm$.

(This rule for l_{min} is from ENV 1995-2:1997, page 35. The exact basis of the rule is not clear. The only difference between ENV 1995-2:1997 and equation (96) is that d_o is introduced, so that the equation won't require the use of certain units.)

6.2.7 Effect of orientation of rod

$P_f /(\pi dl)$ for arbitrary inclination, α, of the rod relative to grain may be determined by interpolation according to the Hankinson equation:

$$f_{v\alpha} = \frac{f_{v90}\ f_{v0}}{f_{v0}\sin^2(\alpha) + f_{v90}\cos^2(\alpha)} \tag{97}$$

where $f_v = P_f/(\pi dl)$ for α=0° and α=90° is from equation (92) with material parameters τ_f and l_m as valid for α=0° and α=90°, respectively.

6.2.8 Effect of wood density (strength class of timber)

Having determined parameters τ_f and l_m for joints with timber of any certain strength class, these values may be used also for joints with timber of any higher class.

6.2.9 Tests for determination of τ_f and l_m

The joint testing should be made in pull-compression loading, with details of the test setup according to, for instance, the GIROD project tests carried out at S.P. denoted "method A with circle plates" or the method proposed in section N.9.2 of "GIROD: WP8: VO3 (1999) – Draft Design Rules (WP8) – Draft, 2nd Revision".

One set of tests should be made with

$$\begin{cases} l_{geo} \le 3500\,mm \\ 8 \le a/d \le 10 \end{cases} \tag{98}$$

and one set of tests with

$$\begin{cases} l_{geo} \ge 17500\,mm \\ 8 \le a/d \le 10 \end{cases} \tag{99}$$

For design of a rod glued-in at arbitrary rod to grain angle, tests must in general be carried out both for rods parallel to grain and for rods perpendicular to grain. The specific limits of l_{geo} proposed above may be regarded as preliminary.

The wood cross section should be square, a times a, in the case of testing parallel to grain, and rectangular, a times $4a$, in the case of testing perpendicular to grain. The rod material must be such that yielding does not start in the rod before joint failure.

Knowing $P_f/(\pi dl)$ for the two sets of tests, τ_f and l_m can be obtained from equation (92). In such calculation it is convenient first to consider the ratio of the failure loads of the two sets of joints. By this, τ_f is eliminated from the equation and then l_m can be found by simple iterations or trials. Knowing l_m, also τ_f is found and, if so desired, then from equation (95) also G_f can be calculated provided that E_r is known.

Number of tests and statistical treatment of test results will be discussed within WP8.

6.3 Evaluation of material parameters and verification of design equation

6.3.1 Introduction

In this evaluation and verification, the fracture surface diameter d is throughout taken as the nominal diameter of the rod, d_r. The rod cross-section area A_r is throughout calculated as $\pi d^2/4$.

6.3.2 Test result evaluation

Test results on the pullout strength at pull-compression loading are presented by project partner SP in "GIROD – Glued in rods for timber structures. WP 7 – Test methods for production control. Technical Report Nr SP-TR-1". These tests are shown in Table 16, where the failure load indicated is the average value of 10 tests in each set of tests. The test results shown are those of "Test series 1 – circle shape of steel plate". Parameters τ_f and l_m (and G_f) determined from test results for the three adhesives by use of the method described in the above are also indicated. Figure 44 shows $P_f/(\pi dl)$ versus $l_{geo}^{1/2}$ according to the test results and according to equation (92) with the parameters determined from the tests. Here also parameters for the PRF are given although the theory of equation (92) may not be suitable for adhesives that don't bond to the rod. The values of G_f obtained for epoxy and PUR are of a magnitude that could have been expected from values that can be found in literature for other types of glued timber joints

Table 16. Test results for determination of material property parameters τ_f and l_m.

Adhesive	d mm	l mm	a mm	l_{geo} mm	Failure load, P_f kN	$P_f/(\pi d\, l)$ N/mm^2	τ_f N/mm^2	l_m mm	G_f [1)] Nmm/mm^2
EPX	16	160	115	4070	62.61	7.79	10.5	3600	1.89
	16	320	115	16300	77.36	4.81			
PRF	16	160	115	4070	63.83	7.94	8.9	11000	4.15
	16	320	115	16300	98.43	6.12			
PUR	16	160	115	4070	58.98	7.33	9.7	3960	1.77
	16	320	115	16300	74.09	4.61			

1) G_f calculated from l_m at the assumption E_r=205000 N/mm^2.

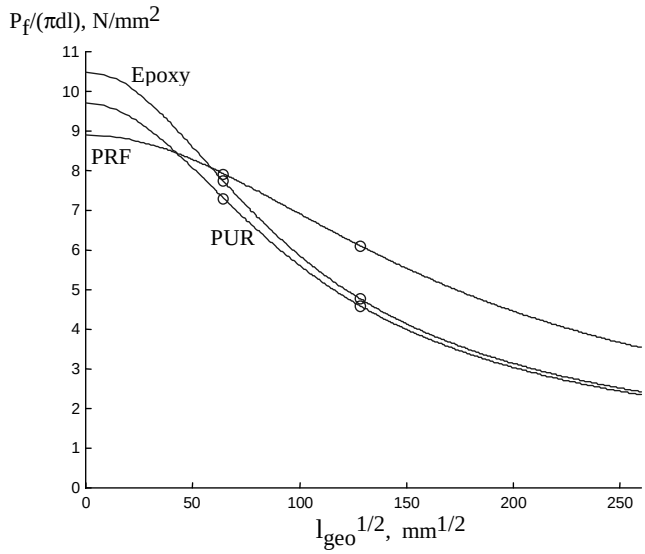

Figure 44. Pull-compression joints strength results obtained at SP for three adhesives and 2-parameter theoretical model with parameter values according to the tests. The diagram shows $P_f/(\pi dl)$, N/mm^2, versus square root of l_{geo} , $l_{geo}^{1/2}$, mm$^{1/2}$.

6.3.3 Verification of design equation

The material combinations for which the material parameters were determined have been used in several other joints, with other geometry and other type of loading. In Figure 45-Figure 47 are the design equation compared with those other test results. Each mark in the diagrams represent mean values obtained in series with 6-10 tests in each series. The diagrams include the tests at SP of pull-pull loading and the SP-tests at pull-compression using a square plate. The diagram also includes the tests made at FMPA at pull-pull of joints of varying size and shape. Both the results for timber strength class C35 and the three series with timber of strength class C24 are included. For epoxy and PUR are in addition three previous series by Aicher and Herr and a test series of Deng, Moss and Buchanan, see [3], included.

For the PRF does not only the test results not comply with the theoretical curve, but the diagram also shows a scattered picture, indicating that $P_f/(\pi dl)$ may hardly be described as a function of l_{geo}. (l_{geo} is in most cases very close to being proportional to l^2/d.) Although the results as indicated in Figure 45 appear scattered, some consistency with respect the influence of parameters d and l can be found.

The results found for PUR and epoxy are more appealing. The design equation gives reasonable predictions and the predictions are in most cases on the safe side. The results found for PUR are especially satisfying.

The various results found for the three adhesives are most probably related to the different ways in which the bond lines act. For PUR and epoxy there is in the critical region tensile stress (and very small deformation) normal to the bond area. For the PRF there is most probably compressive stress (and significant deformation) normal to the bond area. Comparing the epoxy and the PUR, the epoxy adhesive tends to give fracture of the wood along the bond line, while the PUR appear to be affected more by failure within the bond line.

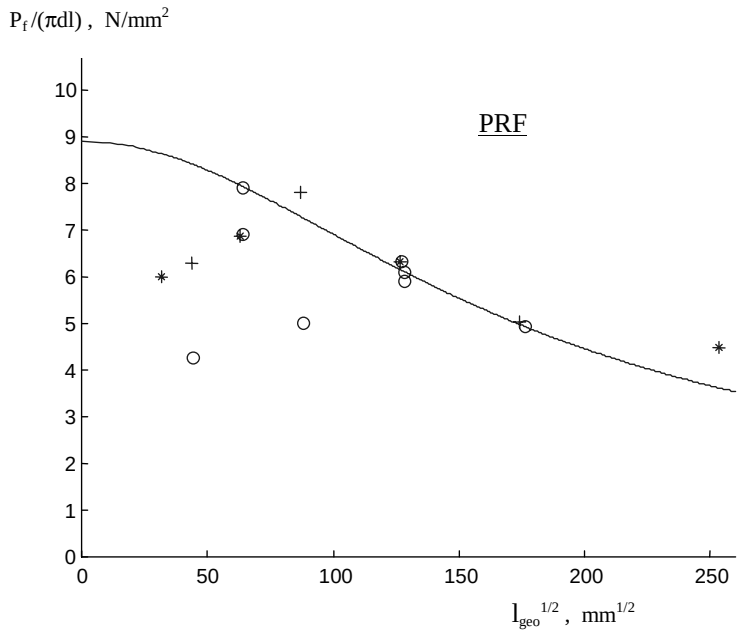

Figure 45. PRF: $P_f/(\pi dl)$, N/mm^2, versus square root of l_{geo} , $l_{geo}^{1/2}$, mm$^{1/2}$.

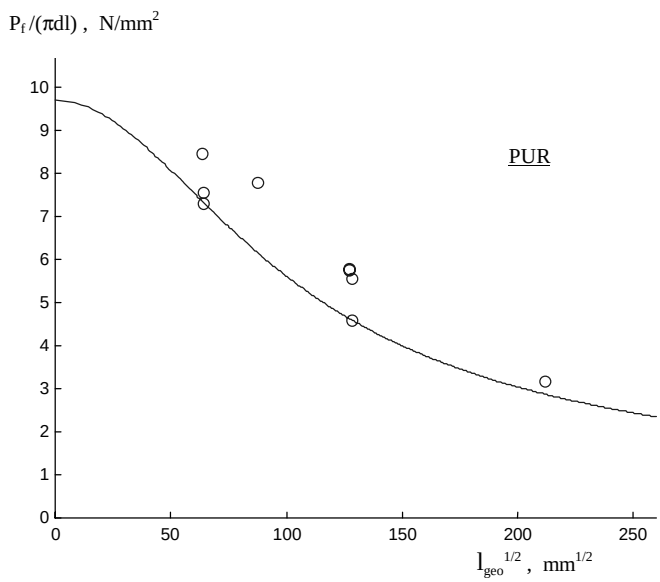

Figure 46. PUR: $P_f/(\pi dl)$, N/mm^2, versus square root of l_{geo} , $l_{geo}^{1/2}$, mm$^{1/2}$

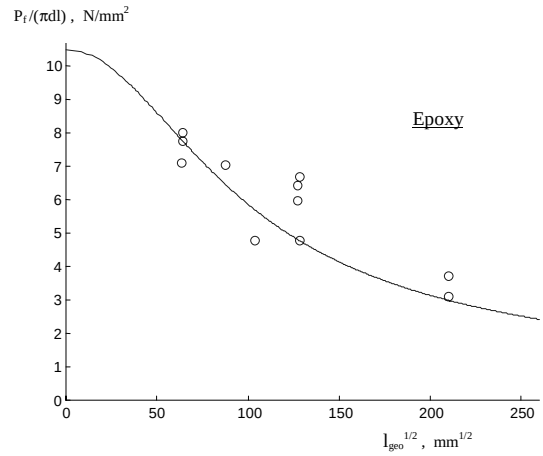

Figure 47. Epoxy: $P_f/(\pi dl)$, N/mm^2, versus square root of l_{geo} , $l_{geo}^{1/2}$, $mm^{1/2}$

6.3.4 Conclusion

It seems that equation (92) and the design method proposed may be useful for the adhesives that don't shrink too much and accordingly have some bond to the rod. For adhesives without bond a very simple design approach has been proposed, but this approach does not comply with the goal of a design equation with a rational theoretical basis and may give design unnecessary much on the safe side or require testing as a part of the design.

For the PRF does not only the test results not comply with the theoretical curve, but the diagram also shows a scattered picture, indicating that $P_f/(\pi dl)$ may hardly be described as a function of l_{geo}. (l_{geo} is in most cases very close to being proportional to l^2/d.) The results found for PUR and epoxy are more appealing: the design equation gives reasonable predictions and the predictions are in most cases on the safe side.

The different results found for the three adhesives are probably related to different ways in which the bond lines act. For PUR and epoxy there can in the critical region be tensile stress (and very small deformation) normal to the bond area. For the PRF there may be compressive stress (and significant deformation) normal to the bond area. Compressive stress might be due not only to the over-all stress distribution in the joint, but also due to the inclination of the individual threads of the rod.

6.4 Alternative proposals by modifications

Above one single design proposal has been discussed. Possible modifications giving alternative, yet similar, proposals include:

1. No consideration to grain to rod angle. Testing and all design made as for parallel orientation.
2. No consideration to different loading conditions (pull-pull, pull-compression, pull perpendicular to beam). Testing and all design made as for pull-pull.

The first modification implies less testing and more simple design calculation: tests for loading perpendicular to grain would not be needed and for rods orientated at some inclination to the grain there wouldn't be any need to use some interpolation formula, e.g. like the Hankinson equation. The second modification implies determination of the parameters τ_f and l_m by testing pull-pull loading instead of pull-compression loading and replacement of eq (92) as design equation by the corresponding pull-pull equation from section 3.3.6.

The simplifying modifications are reasonable if it can be assumed that pull-compression loading is not used in practical design and provided that rods are glued-in perpendicular to grain only in beams. The stress distribution for a rod glued-in perpendicular to a beam is beneficial as compared to the stress distribution for the pull-pull kind of joint, see Table 7 and 8 and also the test result in Table 15. Since the simplifications exclude consideration to pull-compression loading, better agreement between tests results and a design equation can be expected, also for the PRF glue. On the other hand it may, or may not, be easier to test glued-in rod joints in pull-compression than in pull-pull.

If leaving rational design equations for purely empirical equations, several proposals can be found in literature. A compilation of such equations can be found in [3] and applications to the present tests results can be found in [2].

6.5 Verification by finite element analyses

6.5.1 Introduction

A number of FE-simulations were performed in order to verify the "material" properties obtained in the small specimen tests of WP1.2. The verification consisted of finite element simulations of the test set-up used in the small specimen tests (WP1.2) and the test set-up used in the full-size specimen tests (pull-pull).

6.5.2 Simulation of small specimen tests

From WP1.2 the strengths and the negative slope of the descending part (post peak stress) of the recorded force vs. displacement curve were known. These values were used as input in a series of FE-analyses. The FE-analyses were performed in an iterative manner, changing slightly the input values of material parameters, until the response of the tests could be obtained, using the same methods of evaluation as for the laboratory tests. The input curves used for the adhesive bond lines are shown in Figure 48. The response of the small specimen tests is compared with the respective FE-simulation in Figure 49. Note that in this figure the curves shown correspond to the nominal shear stress versus inelastic deformation according to the description given in section 4.6. For the PRF a slightly modified version of the bond line model was used which allowed the peel strength to be zero, with no coupling between the shear and peel stress behaviour. In compression perpendicular to the bond line, the PRF was assumed to behave linear elastic with unlimited strength.

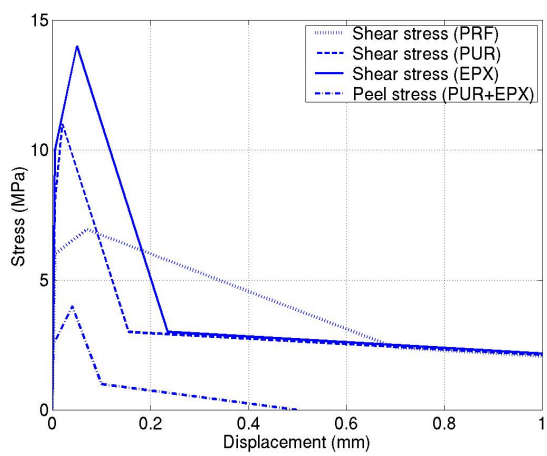

Figure 48. Input data curves used for the bondline model.

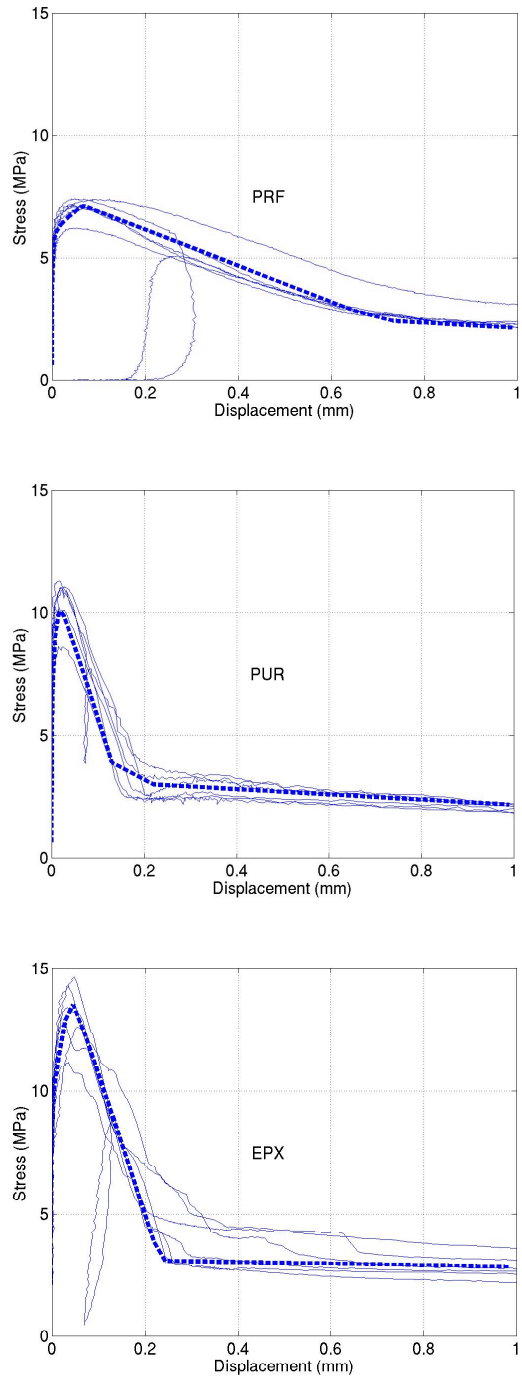

Figure 49. Response of the small specimen tests compared with the respective FE-simulation.

6.5.3 Simulation of large specimen tests

The tests used for comparison in this section are those performed and reported in WP1.3 and in WP7. All test results and FE-simulations are for loading in pull-pull. The input values obtained for the bond line constitutive model as described above, were used for calculating the load-bearing capacity in pull-pull for different glued-in lengths for the three adhesives. The results from these simulations are given in Table 17.

Table 17. Simulated and tested pull-out loads.

	PRF			PUR		EPX	
Glued-in length (mm)	160	320	640	160	320	160	320
Pull-out load, test (kN)	55.3	101.7	144.1	64.4	91.0	61.6	106.3
Pull-out load, FEM (kN)	53.9	104.1	151.6	67.1	93.8	89.2	118.7

Also, bond line shear stress vs. displacement-curves for the simulations of the PRF adhesive were calculated. These are compared with test results in Figure 50. Here it can be seen that the simulations show a good correlation to the tests, although the initial stiffness is overestimated, especially for the shorter glued-in length. The initially low stiffness and progressive behaviour recorded in the tests is probably due to the test set up aligning during increase of load, and this effect has not been taken into account in the simulations.

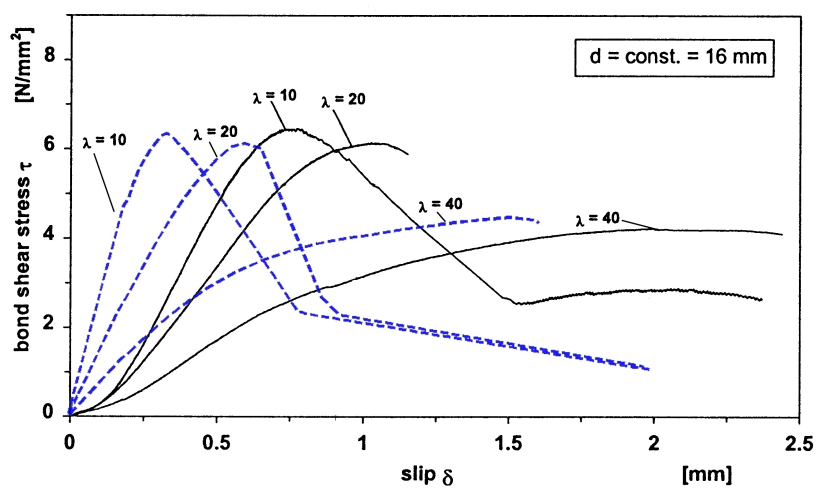

Figure 50. Comparison of the shear stress vs. slip response for PRF-bonded rods. Dashed curves are FE-results and solid curves are test results from [3].

6.5.4 Conclusions

The verification from the small scale tests (8 mm glued-in length) to the large specimen tests (320/640 mm glued-in length) was successful for the PRF and the PUR adhesive. For the EPX however the result is not satisfactory. One possible explanation is that the simulations assume the failure to take place in or in the vicinity of the adhesive bond line. In the tests however, this was not always the case

7 CONCLUSIONS

7.1 WP 1.1

Theoretical models based on fracture mechanics for prediction of pull out strength of glued-in rods have been developed. In Figure 51 is shown a comparison of predicted pull out strengths, for the loading case pull-pull, using the different models dealt with. Material data is according to simulation A1, Table 3, section 3.7.3

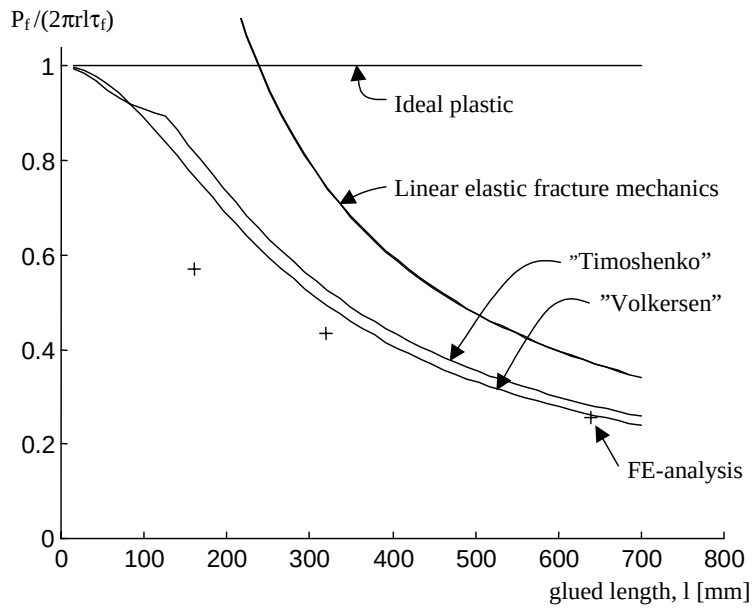

Figure 51. Comparison of different models proposed.

7.2 WP 1.2

The following conclusions can be drawn from the work conducted in WP1.2:

- Test methods:
  - Testing for fracture mechanical properties is very demanding, and several pre-tests to determine a proper test set-up was needed.
  - Using the set-up of type I, the test results were unreliable and not useful for further evaluation.
  - The set-up of type II was reliable and also the one used for the main series.
- Test results:
  - It is possible to obtain the complete shear-stress versus shear-slip response of small glued-in rods specimens.
- Methods of test result evaluation:

– A method of evaluating the test results in terms of strength and fracture energy has been proposed. The fracture energy is evaluated by the initial slope of the stress-displacement response of the specimen tested.

The results of WP1.2 was used in WP1.4. In that work package, tests are simulated using the finite element method.

7.3 WP 1.3

The test results on the strength of full size glued-in rod joints from WP1.3 [1, 3] together with the test results of WP 7 [7] and the results of complementary tests for the GIROD project [2] forms a significant database on the pull out strength of glued-in rods.

7.4 WP 1.4

It seems that the proposed design equation and method for determination of the two required bond property parameters are useful for adhesives that have some bond to the rod. The equation is simple and reasonably general, based on a rational theoretical and physical basis, and produce predictions that in general are somewhat on the safe side. Alternatives to the design method discussed are mentioned.

For adhesives like the PRF, which shrinks significantly and has no bond to the rod, a very simple design approach has been proposed, but this approach does not comply with the goal of a design equation with a rational theoretical basis and may give design unnecessary much on the safe side or require testing as a part the design.

FE analysis of full-size glued-in rod joints were conducted with the small specimen bond property test results of WP1.2 as input. These analyses suggest that it is difficult to predict with high accuracy the strength of a full size joint from the basic small-scale bond property tests for the EPX adhesive, for the PRF and PUR-adhesives however the prediction of the full-size joint strength was accurate.

8 REFERENCES

[1] Aicher, S.: *WP1.3 – Tests for calibration and verification*. Technical report, Otto Graf Institute, University of Stuttgart, 2001.

[2] Aicher, S.: *Characteristic axial resistance of threaded rods glued-in spruce dependent on adhesive typ. A complementary database for the GIROD projec.* Otto Graf Institute, University of Stuttgart, 2001.

[3] Aicher,S., Gustafsson, P.J. and Wolf, M.: *Load-displacement and bond strength of glued-in rods in timber influenced by adhesive, wood density, rod slenderness and diameter.* In Proceedings of the 1st RILEM symposium on Timber Engineering, September 1999, Stockholm, Sweden, pp 369-378.

[4] Boström, L. *Method for determination of the softening behaviour of wood and the applicability of a nonlinear fracture mechanics model.* Report TVBM–1012, Lund University, Division of Building Materials 1992.

[5] Gustafsson, P. J. *Analysis of generalized Volkersen-joints in terms of non-linear fracture mechanics*. In Mechanical Behaviour of Adhesive Joints, PLURALIS 1987, pp. 323-328.

[6] Hibbitt, Karlsson & Sorensen Inc. *ABAQUS, Version 5.7.* Pawtucket, RI, USA 1997.

[7] Johansson, C.J.*: GIROD – Glued in rods for timber structures. WP 7 – Test methods for production control.* Technical Report Nr SP-TR-1, SP, Borås, Sweden.

[8] Kollmann, F. F. P., Côté, W. A. *Principles of wood science and technology. Vol. 1.* Springer Verlag. Berlin 1968.

[9] Larsen, H. J., Riberholt, H. *SBI-anvisning 135: Trækonstruktioner. Beregninger. 3.udgave. (SBI-directions 135: Timber structures. Calculations. 3:d edition.)*. ISSN 0106-6757. Danish Building Research Institute 1994. (In Danish).

[10] Norris, C. B: *Strength of orthotropic materials subjected to combined stresses.* Forest Products Laboratory, Rep. no. 1816, 1962.

[11] Wernersson, H. *Fracture characterization of wood adhesive joints.* Report TVSM–1006, Lund University, Division of Structural Mechanics 1994.

APPENDIX A - Detailed test results

Below, the test results from the main test series are given in detail. The volume is the wet volume at 20ºC 65%RH, while the weight is the dry weight after 24 hours of drying at 105ºC. The density is calculated as dry weight/wet volume. MC is moisture content and G_f is the total work to failure.

NAME	VOLUME (cm^3)	WEIGHT (g)	MC (%)	DENSITY (kg/m^3)	STRENGTH (MPa)	E.STIFFNESS (MPa/mm)	NEG.STIFFF (MPa/mm)	G_f (kJ/m^2)
APR23	9.55	4.264	14.4	446	7.40	22.26	6.88	15.85
APR24	7.49	3.407	14.5	455	6.22	19.10	6.82	10.23
APR25	7.08	3.170	14.5	448	7.01	25.80	9.07	10.97
APR26	7.02	3.099	14.6	441	7.19	24.67	9.50	10.46
APR27	10.63	4.703	14.4	442	7.10	26.79	10.83	11.57
APR28	4.98	2.306	14.1	463	7.40	27.15	-	-
MEAN	7.79	3.49	14.40	449	7.05	24.29	8.62	11.82
COV	0.26	0.25	0.01	0.02	0.06	0.13	0.20	0.20
APU16	5.84	2.826	12.9	484	11.01	75.39	57.59	9.17
APU17	5.53	2.716	13.4	491	10.20	67.31	57.71	9.49
APU18	6.05	2.931	13.3	484	8.63	63.03	52.12	8.84
APU19	6.05	2.933	13.5	485	11.08	73.49	55.87	11.09
APU20	5.81	2.964	13.4	510	10.98	80.62	87.64	9.21
APU21	6.15	3.062	13.0	498	11.31	72.43	-	-
MEAN	5.90	2.91	13.24	492	10.54	72.05	62.19	9.56
COV	0.04	0.04	0.02	0.02	0.10	0.09	0.23	0.09
AEP09	8.03	3.685	12.9	459	12.73	68.11	62.93	17.69
AEP10	7.92	3.665	13.0	463	14.30	74.73	65.76	21.30
AEP11	7.54	3.560	12.9	472	13.40	75.24	72.82	23.35
AEP12	12.28	5.666	12.8	461	11.16	74.93	46.56	21.43
AEP13	9.11	4.233	12.7	465	12.61	75.04	50.93	26.05
AEP14	10.05	4.546	12.6	452	14.64	78.85	-	-
MEAN	9.15	4.23	12.81	462.14	13.14	74.48	59.80	21.96
COV	0.20	0.19	0.01	0.01	0.10	0.05	0.18	0.14
BPR01	4.86	1.786	12.5	367	6.47	23.12	4.71	17.71
BPR02	3.43	1.239	13.0	362	6.37	23.52	7.80	12.20
BPR03	4.41	1.540	13.0	349	6.05	21.91	6.81	13.78
BPR04	5.18	1.752	13.0	338	5.79	16.56	7.36	14.57
BPR05	5.46	1.847	12.6	338	6.42	18.10	8.46	13.76
BPR06	5.92	1.979	12.7	335	5.95	20.48	-	-
MEAN	4.87	1.69	12.81	348	6.18	20.61	7.03	14.40
COV	0.18	0.16	0.02	0.04	0.05	0.14	0.20	0.14
BPU09	6.81	2.480	13.3	364	9.76	70.27	63.82	7.45
BPU11	7.30	2.644	13.1	362	11.15	68.13	60.35	8.60
BPU12	7.39	2.674	13.3	362	10.56	65.10	61.59	7.32
BPU13	6.45	2.361	13.1	366	11.19	72.67	59.08	8.86
BPU14	8.36	3.035	13.3	363	10.63	71.03	65.51	7.90
BPU15	8.16	3.179	12.6	390	10.52	73.33	-	-
MEAN	7.41	2.73	13.13	368	10.63	70.09	62.07	8.03
COV	0.10	0.12	0.02	0.03	0.05	0.04	0.04	0.09
BEP01	6.66	2.334	12.7	350	11.64	60.94	59.00	20.53
BEP02	7.77	2.620	13.0	337	10.02	54.63	50.56	17.30
BEP03	7.91	2.637	13.0	334	12.64	56.96	54.01	25.95
BEP04	6.20	2.196	12.0	354	12.09	50.88	47.18	24.50
BEP05	6.80	2.282	12.6	335	9.63	54.42	51.24	18.48
BEP06	7.50	2.527	12.8	337	9.85	51.35	-	-
MEAN	7.14	2.43	12.68	341	10.98	54.87	52.40	21.35
COV	0.10	0.08	0.03	0.03	0.12	0.07	0.08	0.18

NAME	VOLUME (cm^3)	WEIGHT (g)	MC (%)	DENSITY (kg/m^3)	STRENGTH (MPa)	E.STIFFNESS (MPa/mm)	NEG.STIFFF (MPa/mm)	G_f (kJ/m^2)
CEP01	7.61	3.517	13.7	462	12.53	54.27	50.06	23.05
CEP02	6.93	3.178	13.9	459	13.65	52.04	39.07	24.33
CEP03	7.56	3.428	13.8	453	11.97	57.64	53.82	22.06
CEP05	6.34	2.886	13.7	455	12.60	55.27	52.69	23.79
CEP06	8.66	3.874	13.8	448	13.01	56.15	44.30	24.05
CEP07	8.24	3.696	13.9	448	13.04	53.27	-	-
MEAN	7.56	3.43	13.80	454	12.80	54.77	47.99	23.46
COV	0.11	0.10	0.01	0.01	0.04	0.04	0.13	0.04
CEP10	8.79	3.983	13.0	453	10.47	37.70	22.41	22.58
CEP11	9.14	3.591	13.1	393	11.13	32.42	25.91	24.34
CEP12	6.79	3.273	13.0	482	11.34	38.03	36.58	22.70
CEP13	7.75	3.057	13.8	394	10.03	31.63	25.55	28.06
CEP14	6.62	3.055	13.3	462	11.37	39.69	29.04	26.63
CEP16	8.47	3.289	13.4	388	9.82	29.98	-	-
MEAN	7.93	3.37	13.26	429	10.69	34.91	27.90	24.86
COV	0.13	0.11	0.02	0.10	0.06	0.12	0.19	0.10
CEP19	9.64	4.320	13.9	448	6.49	10.90	1.84	23.32
CEP20	8.33	3.875	13.3	465	7.12	12.10	2.00	24.90
CEP21	8.85	3.916	13.6	443	7.75	12.49	5.00	26.01
CEP22	7.70	3.725	13.0	484	7.04	11.73	2.97	25.47
CEP23	4.62	2.381	13.4	516	7.47	13.61	3.82	24.78
CEP24	8.33	3.840	13.5	461	6.86	11.19	-	-
MEAN	7.91	3.68	13.46	469	7.12	12.00	3.13	24.90
COV	0.22	0.18	0.02	0.06	0.06	0.08	0.42	0.04
DEP01	7.50	3.355	13.3	447	12.41	45.27	41.19	32.02
DEP03	6.76	3.016	13.4	446	12.07	47.63	41.91	30.23
DEP04	6.69	2.965	14.0	443	12.74	46.93	41.28	27.35
DEP05	5.31	2.427	14.1	457	10.81	50.15	46.78	25.48
DEP06	6.84	3.064	13.9	448	11.84	49.09	-	-
DEP07	6.25	2.865	13.1	458	10.37	48.87	45.71	25.08
DEP08	6.13	2.780	12.9	454	12.07	49.81	48.98	28.53
MEAN	6.50	2.92	13.53	451	11.76	48.25	44.31	28.11
COV	0.11	0.10	0.03	0.01	0.07	0.04	0.07	0.10

APPENDIX B - Stress-displacement curves

The stress displacement curves, in two different scales, for the tests in the main series are given on this and the following nine pages. The curves shown on the upper half are the original curves and on the lower half the curves with the elastic deformation subtracted.

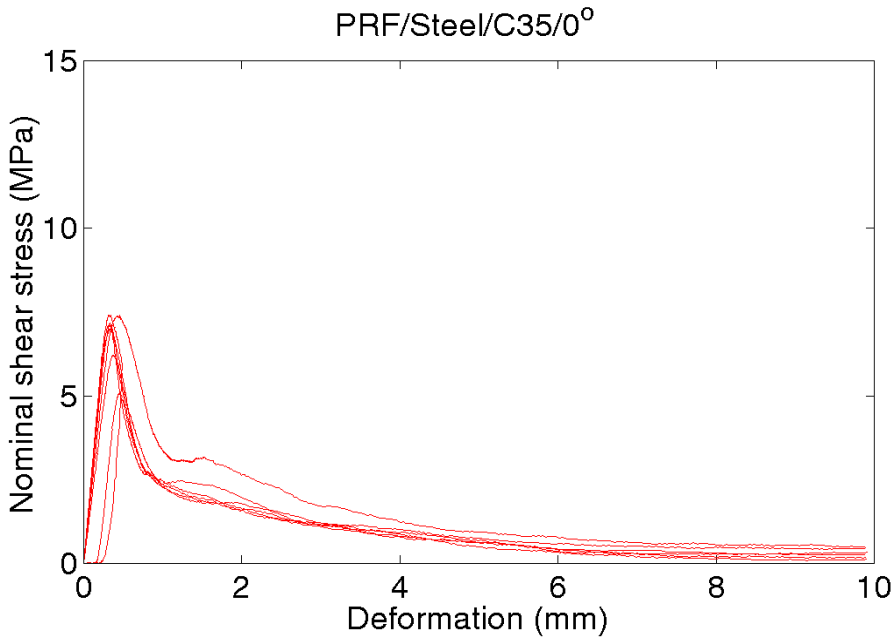

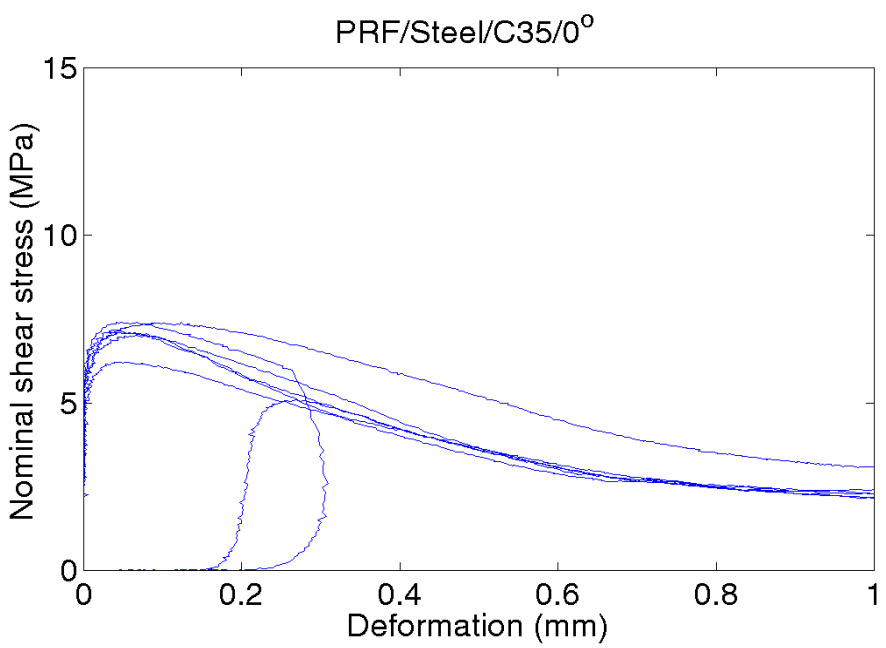

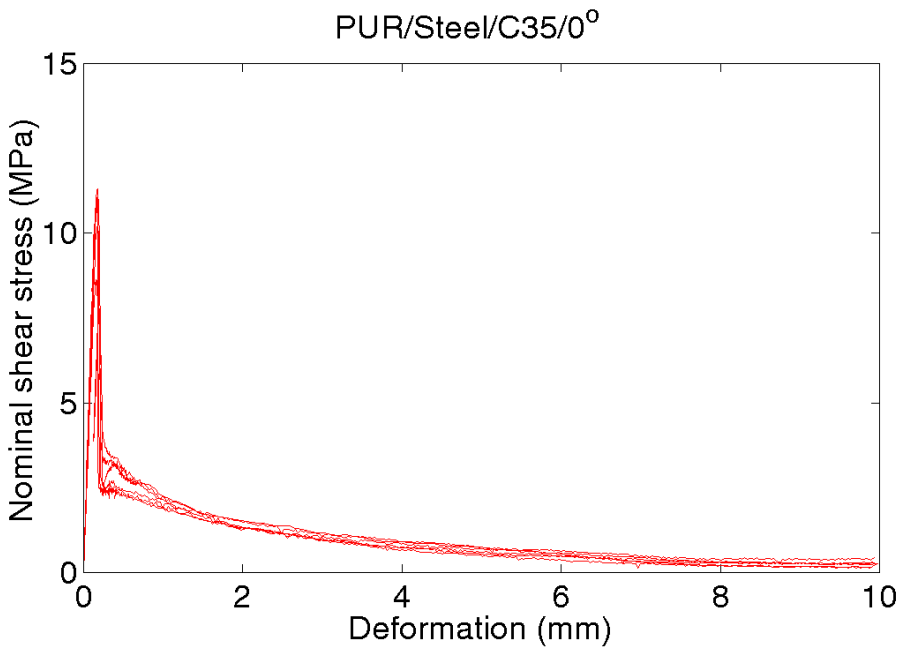
PUR/Steel/C35/0°
Nominal shear stress (MPa)
Deformation (mm)
0
5
10
15
0
2
4
6
8
10

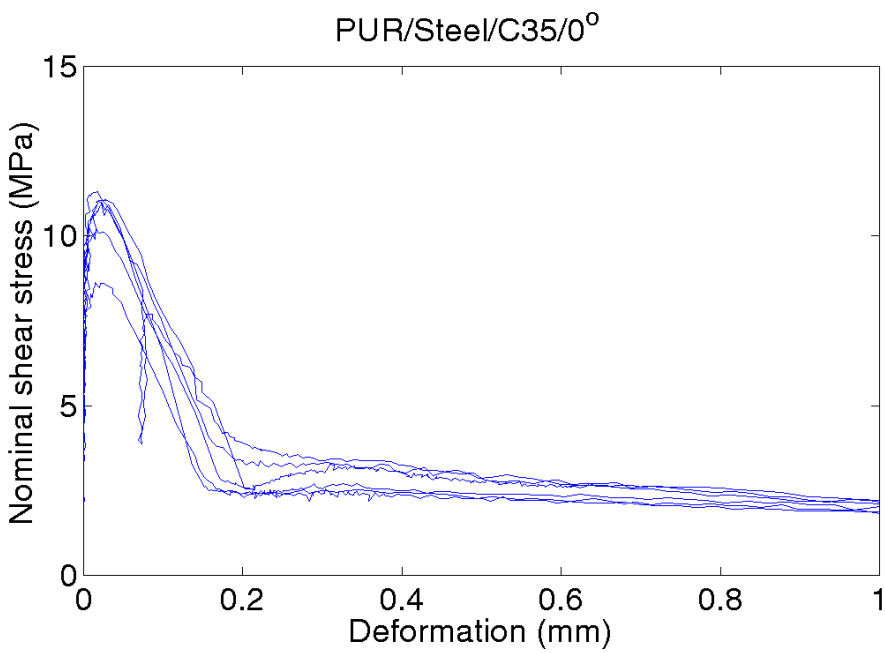
PUR/Steel/C35/0°
Nominal shear stress (MPa)
Deformation (mm)
0
5
10
15
0
0.2
0.4
0.6
0.8
1

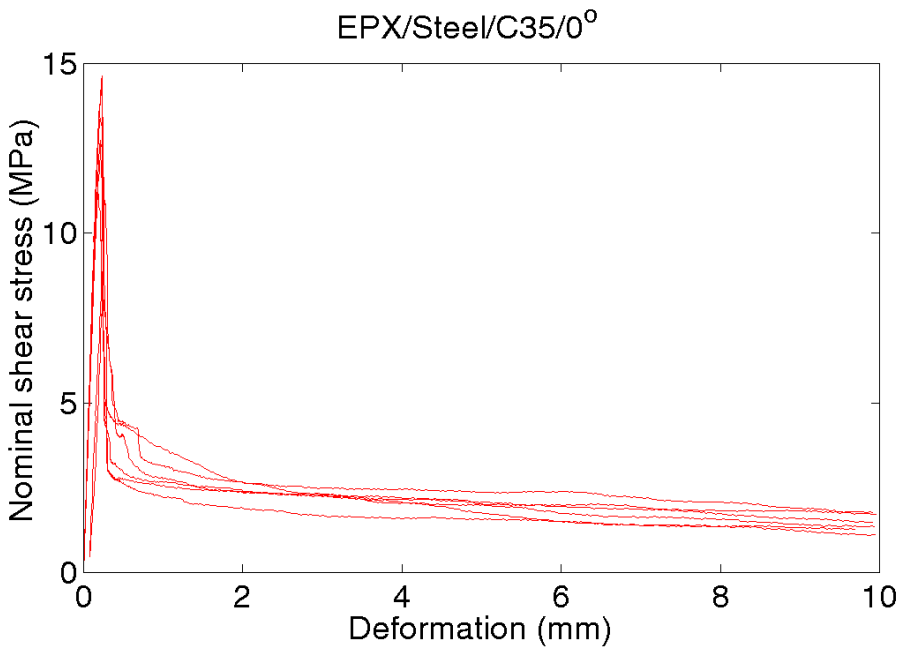
EPX/Steel/C35/0°
Nominal shear stress (MPa)
Deformation (mm)
0
5
10
15
0
2
4
6
8
10

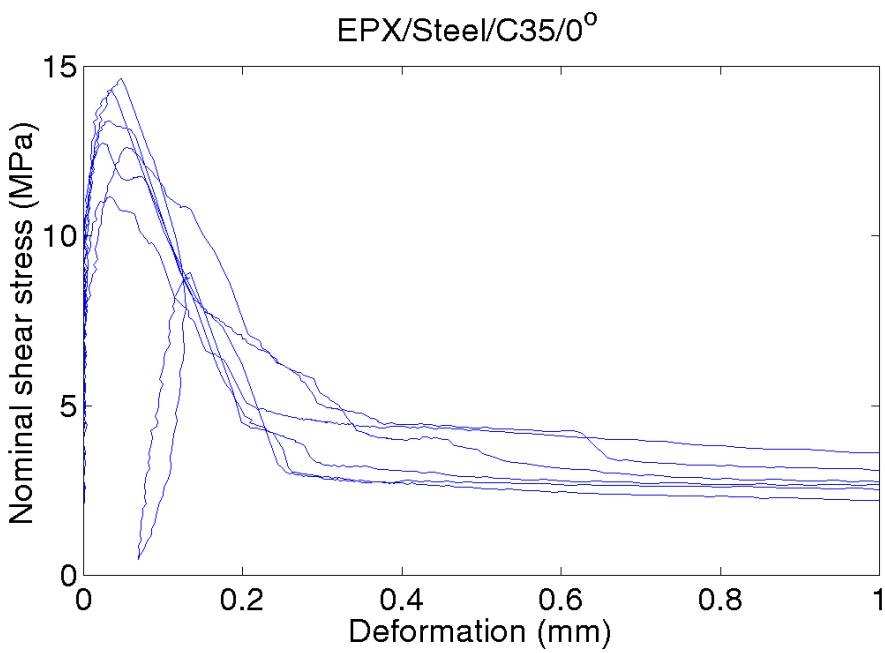
EPX/Steel/C35/0°
Nominal shear stress (MPa)
Deformation (mm)
0
5
10
15
0
0.2
0.4
0.6
0.8
1

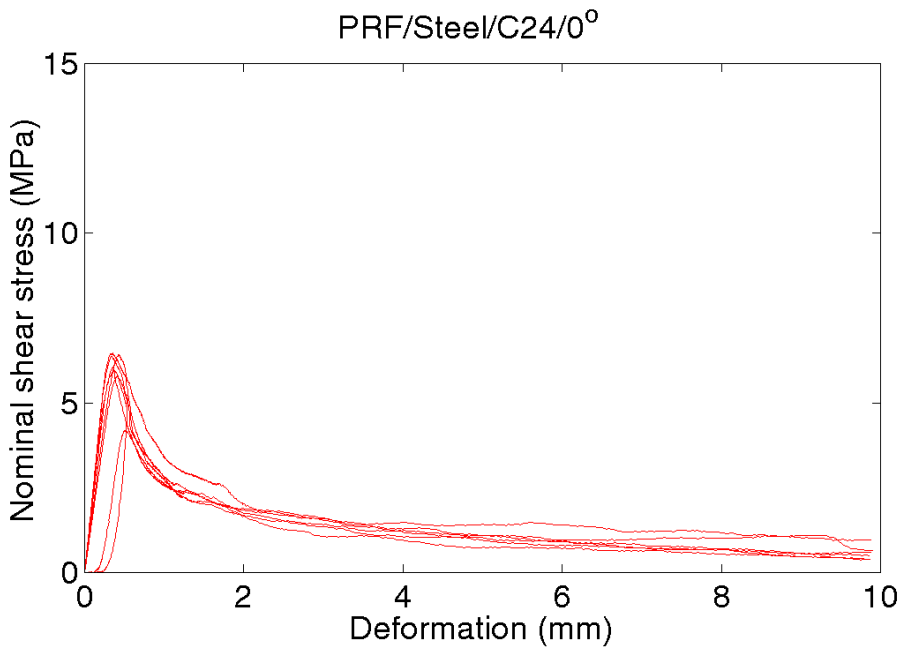
PRF/Steel/C24/0°
Nominal shear stress (MPa)
Deformation (mm)
0
5
10
15
0
2
4
6
8
10

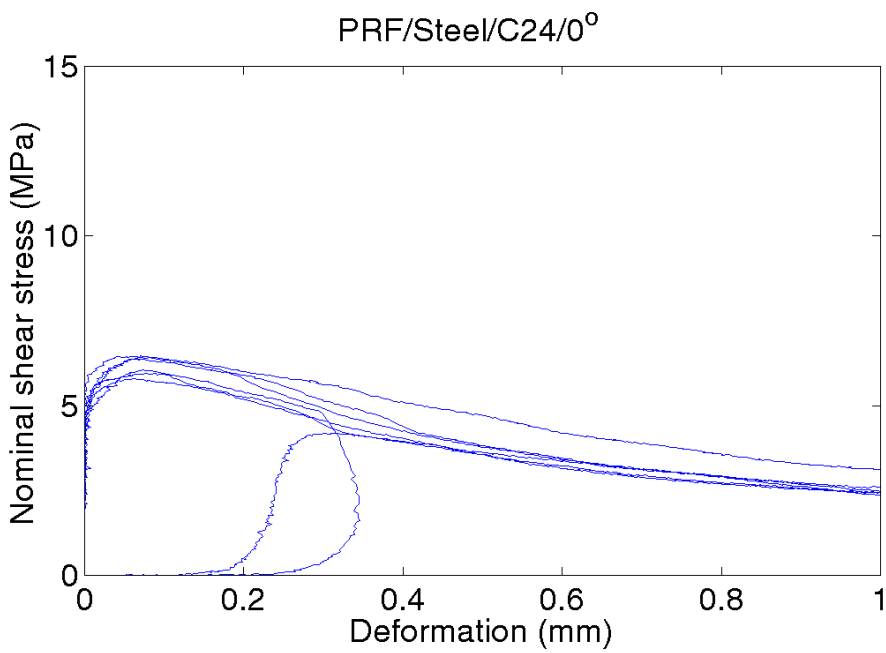
PRF/Steel/C24/0°
Nominal shear stress (MPa)
Deformation (mm)
0
5
10
15
0
0.2
0.4
0.6
0.8
1

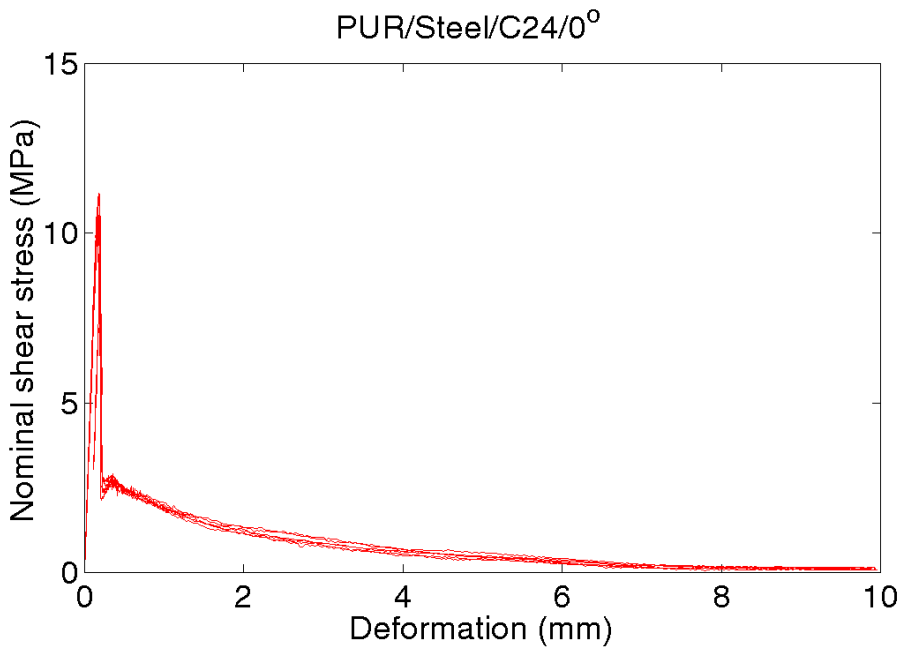
PUR/Steel/C24/0°
Nominal shear stress (MPa)
Deformation (mm)
0
5
10
15
0
2
4
6
8
10

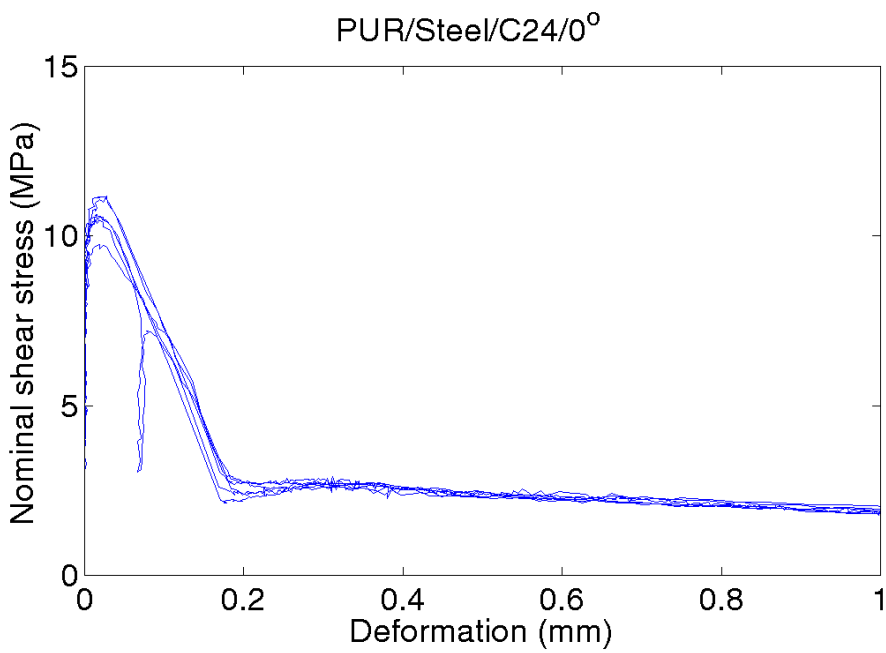
PUR/Steel/C24/0°
Nominal shear stress (MPa)
Deformation (mm)
0
5
10
15
0
0.2
0.4
0.6
0.8
1

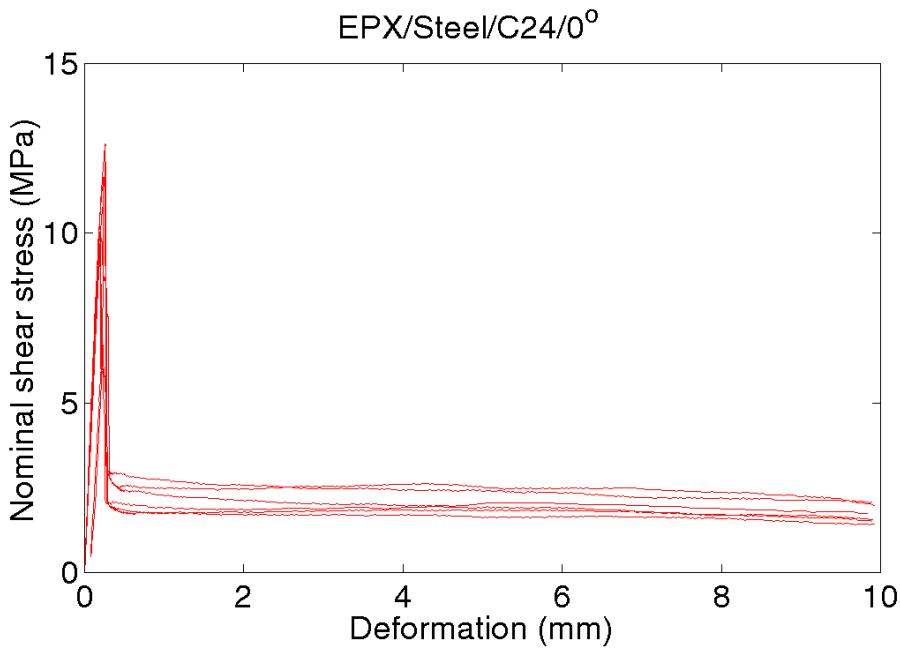
EPX/Steel/C24/0°
Nominal shear stress (MPa)
Deformation (mm)
0
5
10
15
0
2
4
6
8
10

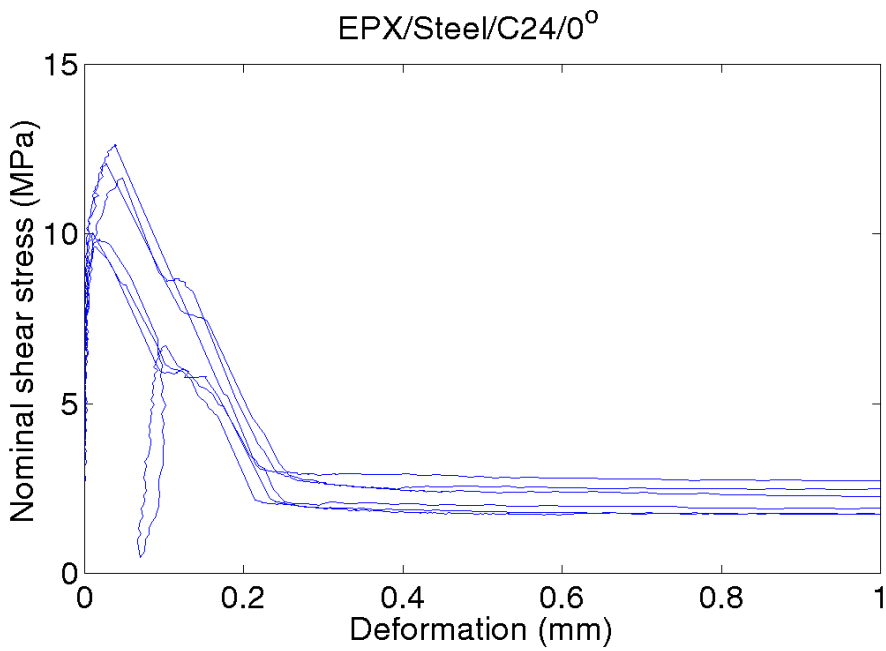
EPX/Steel/C24/0°
Nominal shear stress (MPa)
Deformation (mm)
0
5
10
15
0
0.2
0.4
0.6
0.8
1

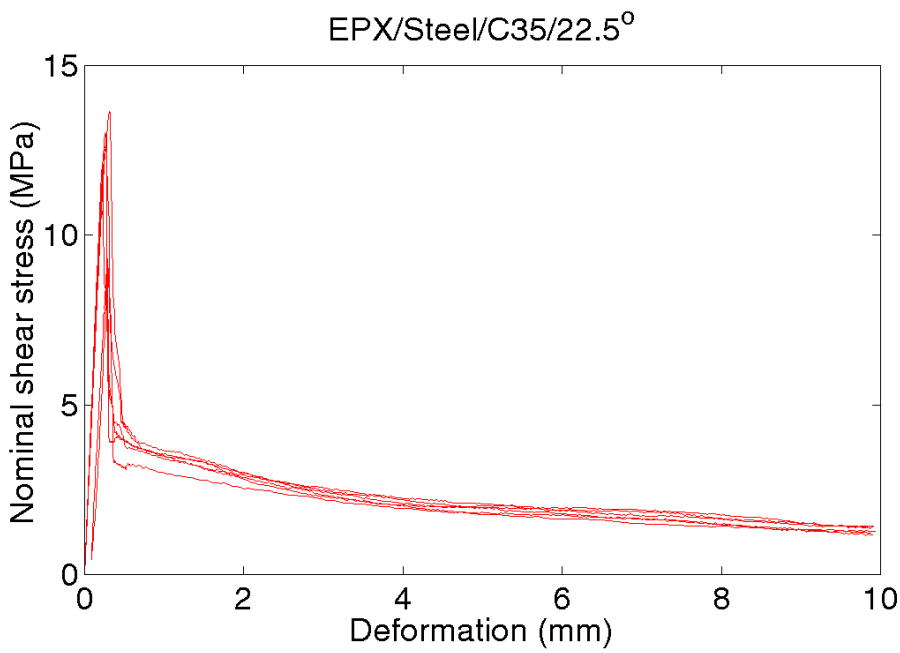
EPX/Steel/C35/22.5°
Nominal shear stress (MPa)
Deformation (mm)
0
5
10
15
0
2
4
6
8
10

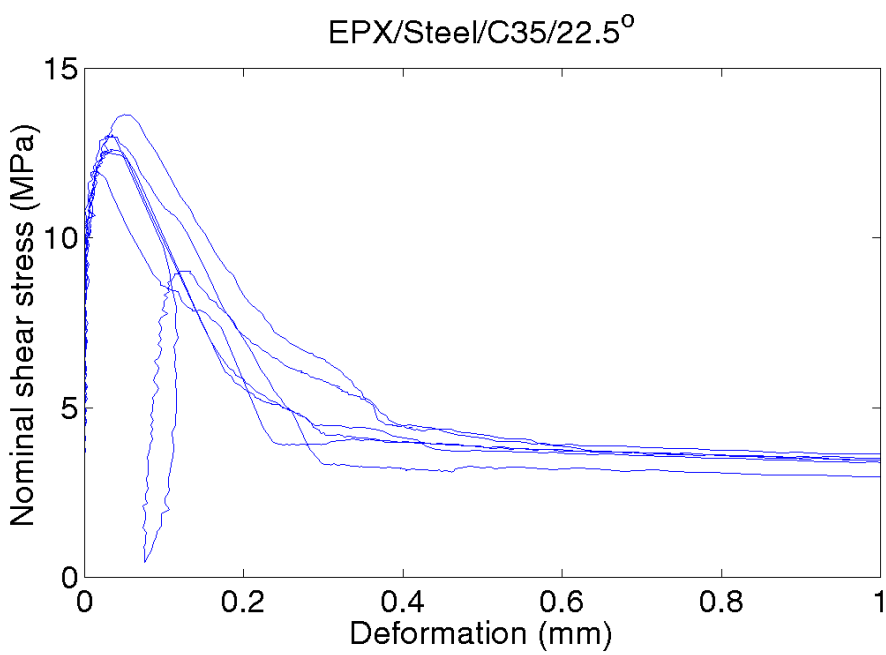
EPX/Steel/C35/22.5°
Nominal shear stress (MPa)
Deformation (mm)
0
5
10
15
0
0.2
0.4
0.6
0.8
1

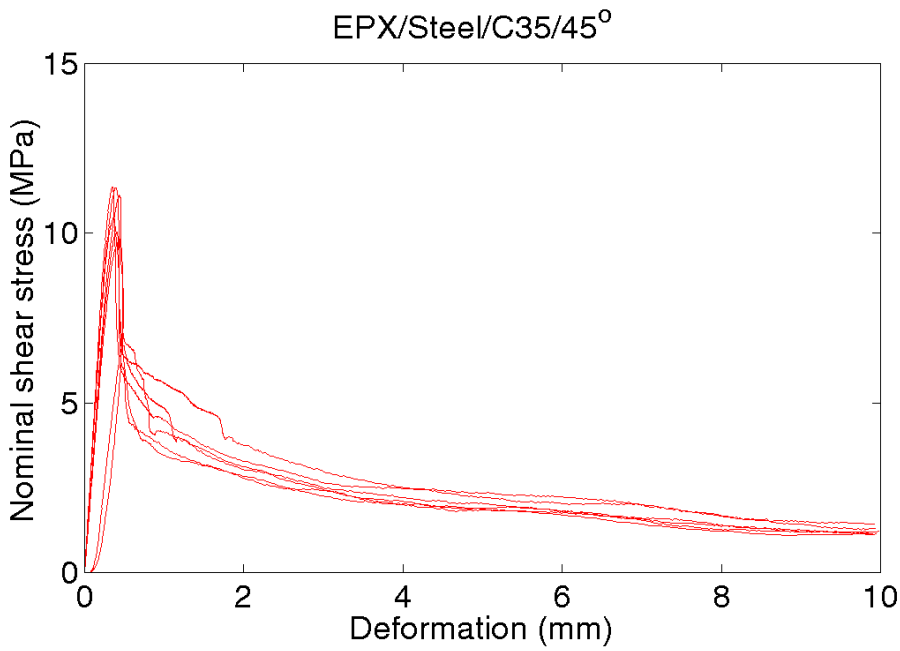
EPX/Steel/C35/45°
Nominal shear stress (MPa)
Deformation (mm)
0
5
10
15
0
2
4
6
8
10

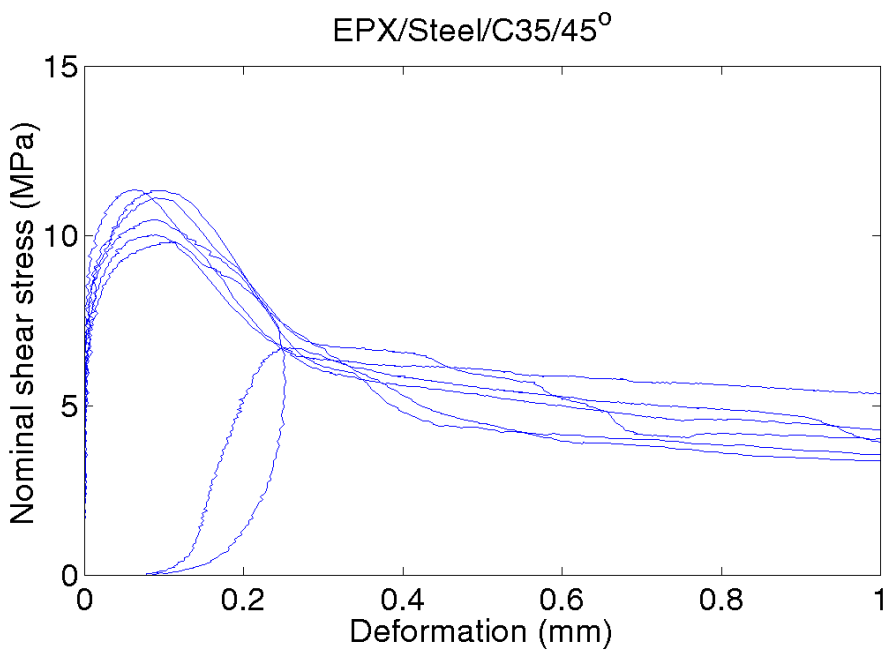
EPX/Steel/C35/45°
Nominal shear stress (MPa)
Deformation (mm)
0
5
10
15
0
0.2
0.4
0.6
0.8
1

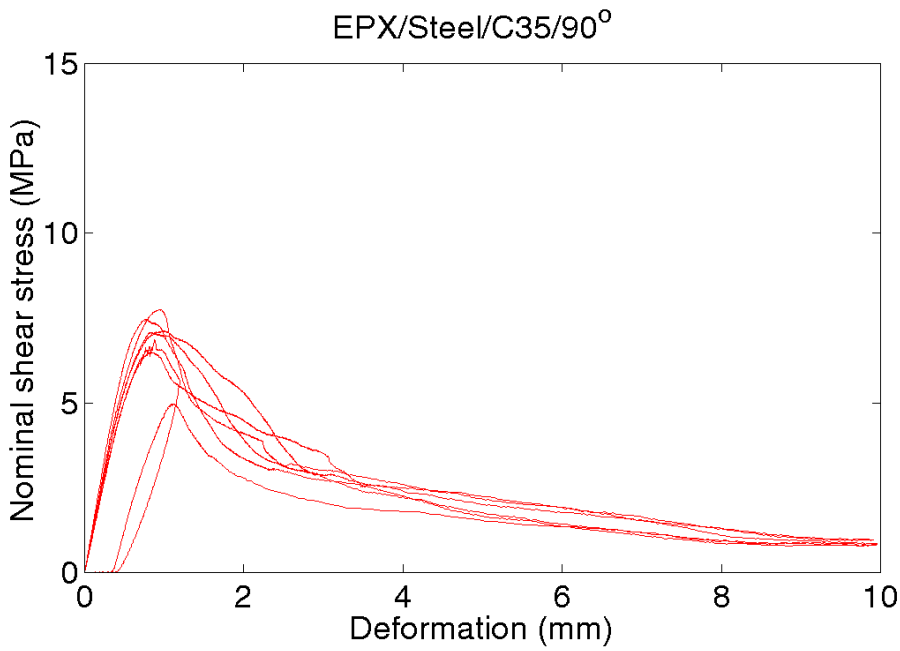
EPX/Steel/C35/90°
Nominal shear stress (MPa)
Deformation (mm)
0
5
10
15
0
2
4
6
8
10

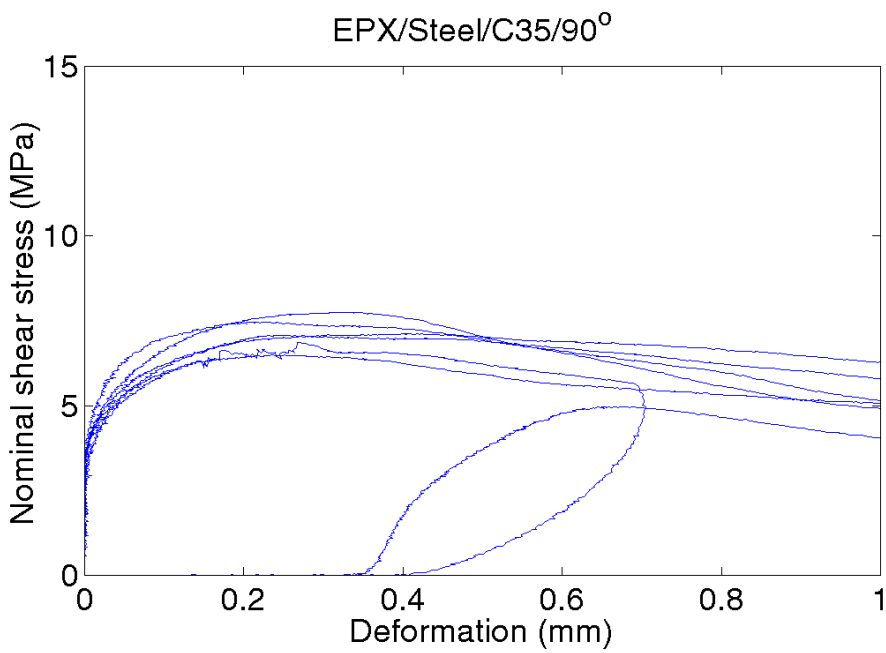
EPX/Steel/C35/90°
Nominal shear stress (MPa)
Deformation (mm)
0
5
10
15
0
0.2
0.4
0.6
0.8
1

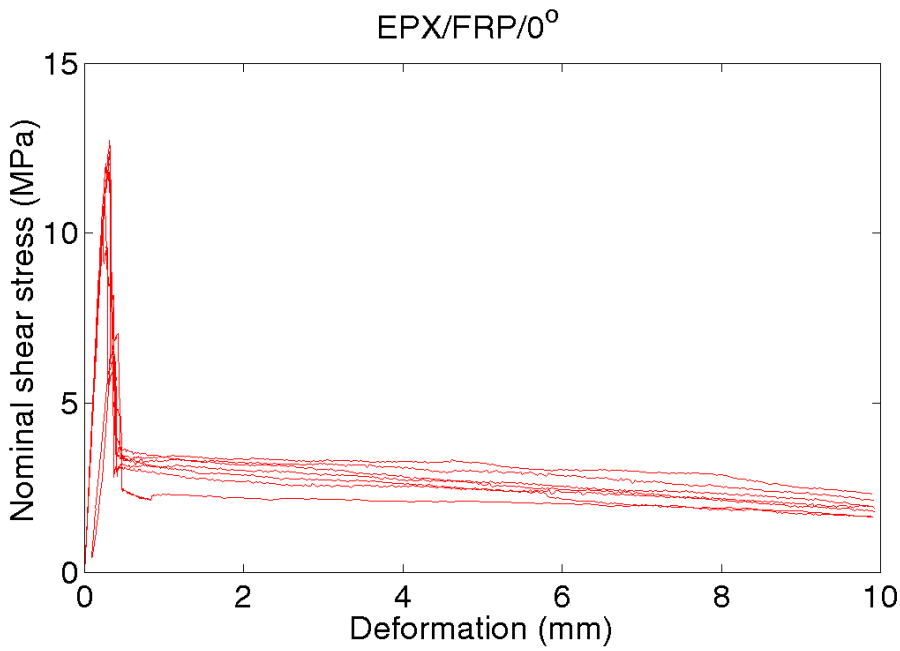
EPX/FRP/0°
Nominal shear stress (MPa)
Deformation (mm)
0
5
10
15
0
2
4
6
8
10

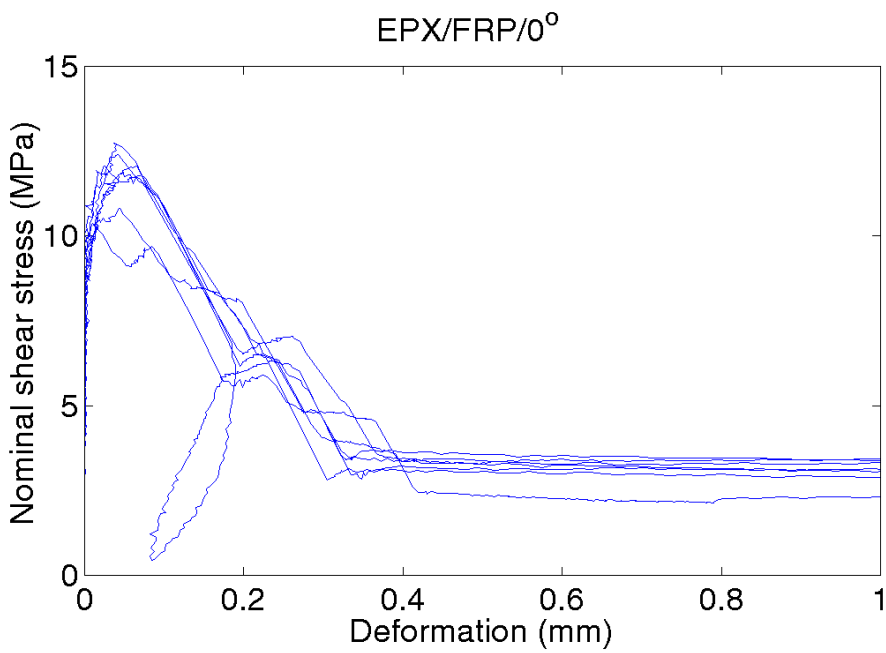
EPX/FRP/0°
Nominal shear stress (MPa)
Deformation (mm)
0
5
10
15
0
0.2
0.4
0.6
0.8
1

APPENDIX C - Examples of failure modes

On the following pages the failure surfaces from some of the different material combinations are shown. The photographs show the wood/adhesive interface and the rod surface after failure.

PRF/C35/0°

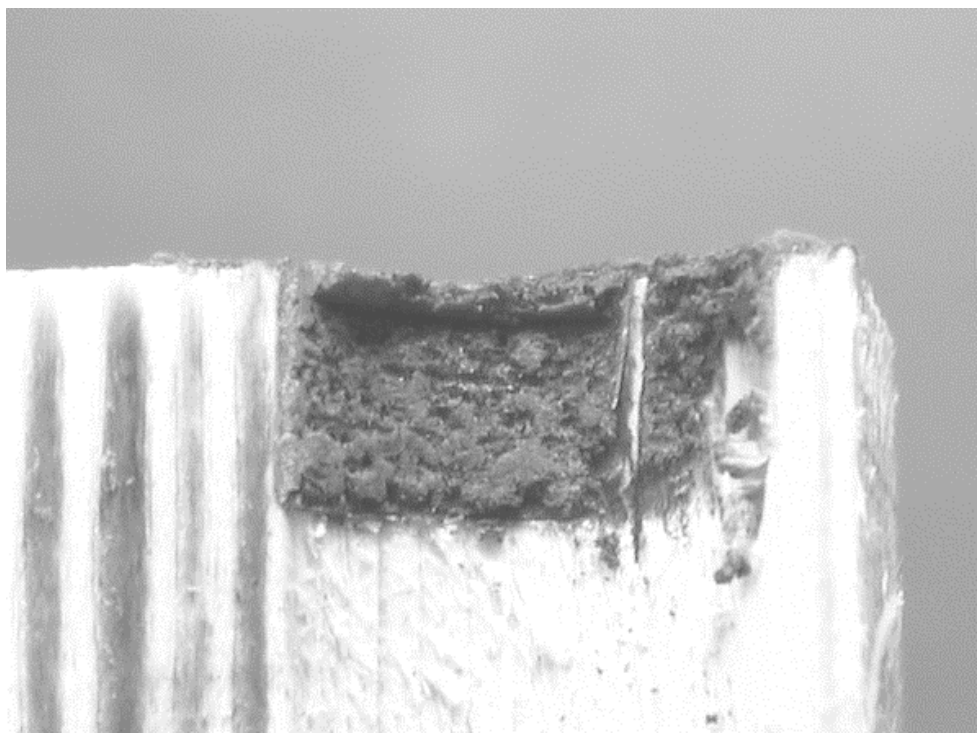

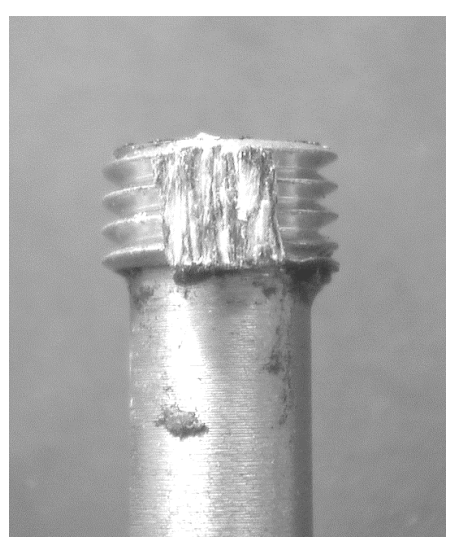

PUR/C35/0º

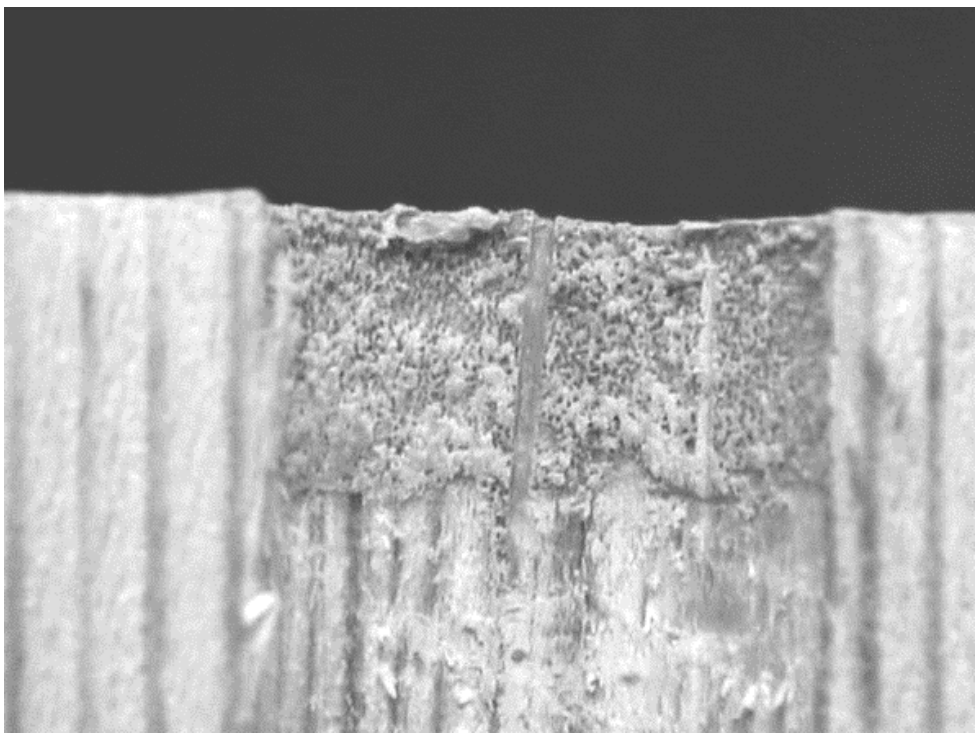

EPX/C35/0º

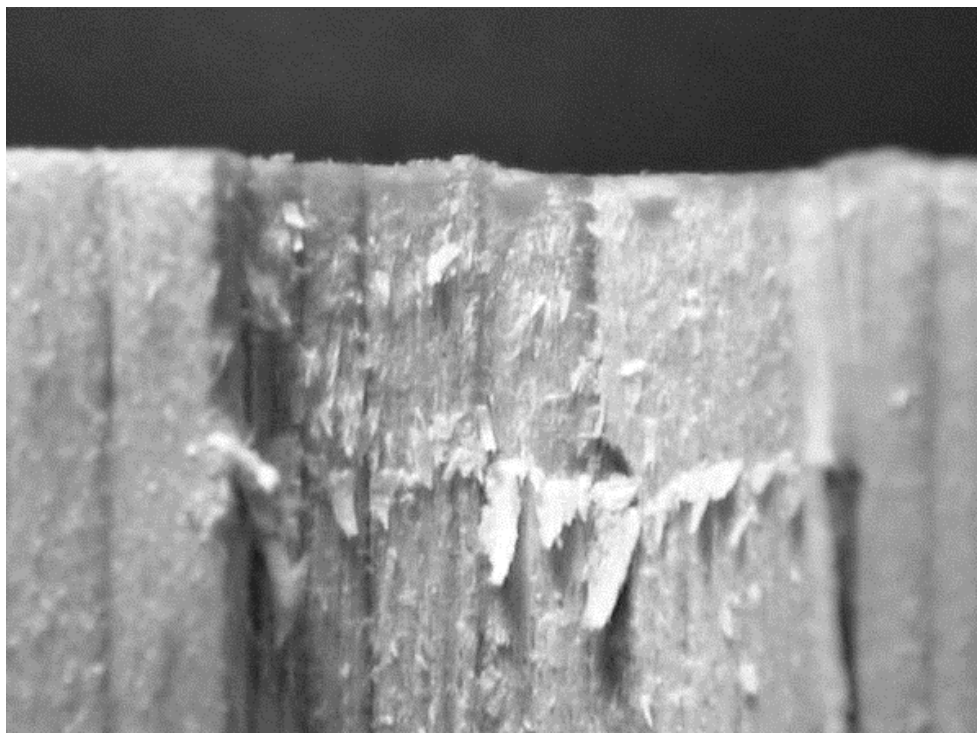

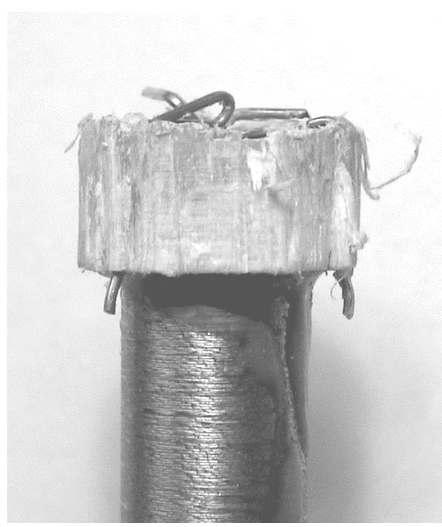

EPX/C35/90º

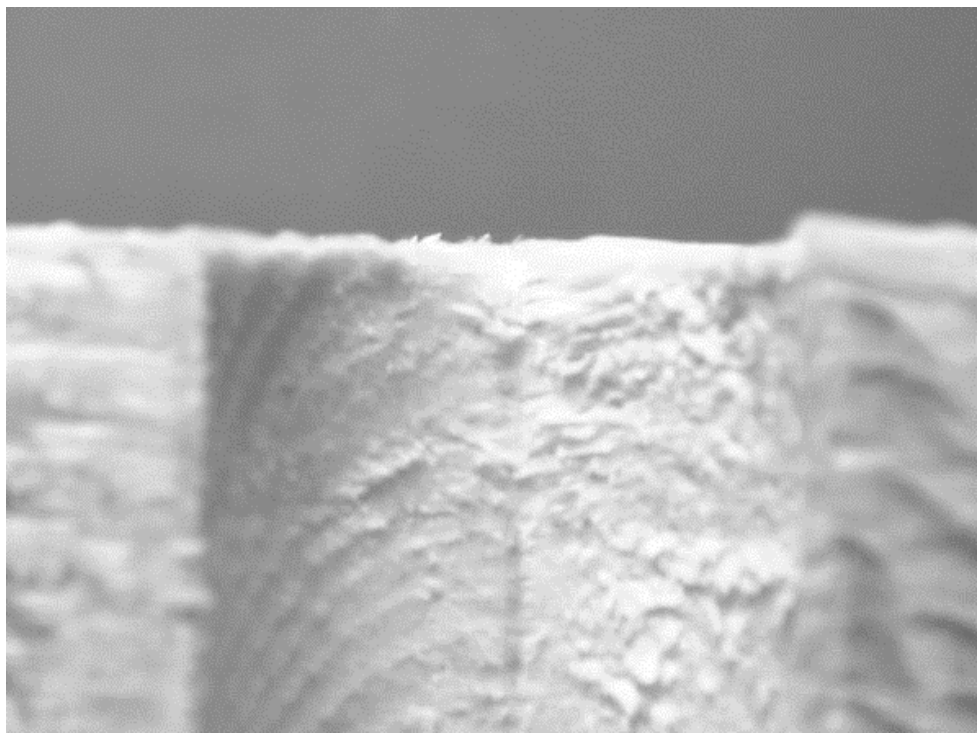

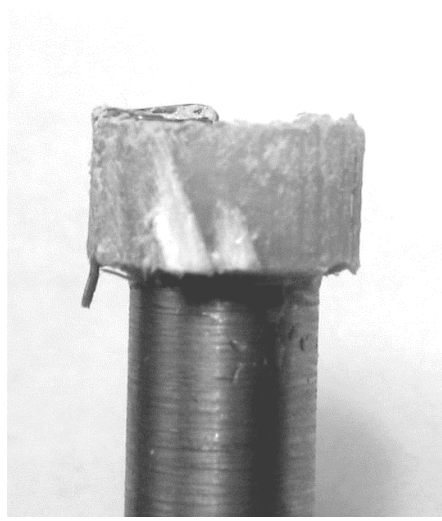

EPX/FRP/0º